

Characterization of Parkin, Tau, and Zinc Interactions  
with the Microtubule Network

by

Alison Nisbet Killilea

A dissertation submitted in partial satisfaction of the

requirements for the degree of

Doctor of Philosophy

in

Comparative Biochemistry

in the

Graduate Division

of the

University of California, Berkeley

Committee in charge:

Professor Kenneth H. Downing, Co-chair

Professor Tom Alber, Co-chair

Professor Eva Nogales

Professor George F. Sensabaugh

Fall 2009

The dissertation of Alison Nisbet Killilea, titled Characterization of Parkin, Tau and Zinc

Interactions with the Microtubule Network is approved:

Co-chair \_\_\_\_\_ Date \_\_\_\_\_

Co-chair \_\_\_\_\_ Date \_\_\_\_\_

\_\_\_\_\_ Date \_\_\_\_\_

\_\_\_\_\_ Date \_\_\_\_\_

University of California, Berkeley

Characterization of Parkin, Tau, and Zinc Interactions  
with the Microtubule Network

© 2009

Alison Nisbet Killilea

## Abstract

### Characterization of Parkin, Tau, and Zinc Interactions with the Microtubule Network by

Alison Nisbet Killilea

Doctor of Philosophy in Comparative Biochemistry

University of California, Berkeley

Professor Kenneth H. Downing, Co-chair

Professor Tom Alber, Co-chair

The microtubule cytoskeleton is essential for regulation of cell morphology, trafficking within the cell and cell cycle progression. These diverse functions involve complex microtubule dynamics and the interaction of microtubule-associated proteins (MAPs), molecular motors, and various small ligands. Here we investigate three distinct aspects of microtubule activity: the interactions of microtubules with parkin and tau which may be involved in Parkinson's disease and Alzheimer's disease, respectively, and effects on microtubule stability in prostate cancer.

Autosomal Recessive Juvenile Parkinson's disease (ARJP) is a degenerative disorder of the central nervous system. Over 50% of ARJP cases result from mutations that occur within the PARK2 gene that encodes the protein parkin. Recent evidence has suggested that parkin binds to microtubules and can stabilize microtubules against depolymerization. Visualization of the parkin-tubulin complex would help us understand the mechanism of this interaction and provide insights on the role of parkin in the cell. Parkin was expressed, purified and used to decorate microtubules for cryo-electron microscopy. Fourier transforms of images suggest that parkin binds specifically to the tubulin dimer. Further cryo microscopy of the interaction of parkin with microtubules will help define the etiology of ARJP and may reveal novel targets of therapeutic intervention.

Hyperphosphorylation of the microtubule-associated protein tau results in a pathological form of the protein found in plaques of patients with Alzheimers disease. Our work has been focused on clarification of the two current models proposed for tau binding along the outside and the inside of the microtubule.

Microtubule networks are also clinically important as targets of many chemotherapeutic drugs. Prostate cancer is commonly treated with the microtubule-targeted drug paclitaxel (taxol). A previous report indicated that supplemental zinc sensitized prostate cancer cells to taxol-induced apoptosis, suggesting that increased zinc levels might affect taxol efficacy. We tested taxol's effect in two prostate cancer cell lines maintained under moderately zinc deficient conditions. Taxol-induced apoptosis was reduced in LNCaP cells from zinc-deficient conditions. The IC50 for paclitaxel-induced cell cycle arrest was higher in LNCaP cells. Extracellular zinc levels were thus shown to be an important factor in paclitaxel activity in a prostate cell cancer line.

I dedicate this work to my parents Allister and Florence Nisbet who always encouraged me to follow my aspirations and approach challenges with patience and determination and to my husband David whose love and constant encouragement made this work possible.

## **Table of Contents**

LIST OF FIGURES	iv
LIST OF TABLES	v
LIST OF SYMBOLS	vi
ACKNOWLEDGMENTS	ix

### **CHAPTER ONE: TUBULIN AND MICROTUBULES: Structure, function, and interactions**

INTRODUCTION	1
Tubulin	1
Microtubule drugs	6
Microtubule binding proteins	9
MAPs	9
Microtubule motors	9
Tubulin isotypes and posttranslational modification	10
Zinc and microtubules	11

### **CHAPTER TWO: PARKIN INTERACTIONS WITH MICROTUBULES**

INTRODUCTION	12
Parkinson's Disease	12
Overall structure and function of parkin	13
Domain structure	13
Function	18
Substrates	18
Parkin-microtubule interactions	19
EXPERIMENTAL PROCEDURES	21
Cloning	21
Purification	22
Binding assay	23
Computational alignment	23
Cryo electron microscopy	23
Image processing and analysis	23
RESULTS	24
Purification	24
Binding assay	25
Electron microscopy	26
DISCUSSION	28

### **CHAPTER THREE: TAU-MICROTUBULE INTERACTIONS**

INTRODUCTION	31
Structure and function of tau	31
Alzheimer's disease	33
Microtubule-tau interaction	33
EXPERIMENTAL PROCEDURES	35
Binding assays	35
Computational alignment	35

Cryo electron microscopy	35
Image processing and analysis	36
RESULTS AND DISCUSSION	37
<b>CHAPTER FOUR: ZINC DEFICIENCY REDUCES TAXOL EFFICACY IN HUMAN PROSTATE CANCER CELLS</b>	
INTRODUCTION	40
EXPERIMENTAL PROCEDURES	41
Reagents	41
Cell culture	41
Zinc-deficient media	41
Cell viability assays	41
Elemental analysis	42
Immunocytochemistry	42
Cell cycle analysis	42
Statistical analysis	43
RESULTS	43
DISCUSSION	48
<b>CHAPTER FIVE: SUMMARY</b>	51
<b>CITED LITERATURE</b>	53

<b>List of Figures</b>	<b>page</b>
Figure 1: Schematic of tubulin heterodimer, protofilament and microtubule structures	2
Figure 2: Ribbon diagram of the functional domains of the tubulin heterodimer	2
Figure 3: Interprotofilament view of two heterodimers	3
Figure 4: Conservation of an internal residue in mammalian $\beta$ -tubulin	5
Figure 5: Schematic of classical and non-classical RING finger domains	14
Figure 6: Alignment of parkin protein sequences from representative eukaryotes	15
Figure 7: Domain structure of the mammalian PARK2 gene with PD mutations	15
Figure 8: Ubiquitin and the parkin ubiquitin like domain share a similar fold	16
Figure 9: Ribbon diagram of the IBR RING finger in parkin	17
Figure 10: Schematic of expression vectors	21
Figure 11: Aggregation levels differ between rat and human parkin	25
Figure 12: Parkin binds to microtubules in pelleting assays	26
Figure 13: Electron micrograph of parkin-decorated microtubules	27
Figure 14: Class average and power spectrum of parkin decorated microtubules	27
Figure 15: Alignment of parkin protein sequences from human and rat	29
Figure 16: Schematic of the six isoforms of tau	32
Figure 17: Alignment of tau microtubule-binding repeats	32
Figure 18: Three models for tau binding to microtubules	34
Figure 19: Co-sedimentation of tau and tubulin	35
Figure 20: Increasing concentrations of tau result in a PF number change	37
Figure 21: Tau increases distribution of 14-protofilaments	38
Figure 22: Reconstruction of a tau-decorated microtubule	39
Figure 23: Zinc deficiency did not reduce cellular growth rates	44
Figure 24: Zinc deficiency did not alter cell cycle distribution or intracellular zinc	45
Figure 25: Zinc deficiency was associated with reduced cell cycle arrest	46
Figure 26: Zinc deficiency reduced Taxol's efficacy to initiate apoptosis	47



## List of Tables

Table I: Chemical structure of microtubule stabilizing drugs	6
Table II: Chemical structure of microtubule destabilizing drugs	7
Table III: Extraction profile of commercial immobilized chelators in FBS	43

## List of Symbols and Abbreviations

1-D	1-dimensional
2-D	2-dimensional
3-D	3-dimensional
3R	3 repeat
4R	4 repeat
<sup>3</sup> H	tritium
Å	Angstrom
α	alpha
β	beta
°C	degrees Centigrade
AD	Alzheimer's disease
Amp	ampicillin
Arg	arginine
ARJP	autosomal recessive juvenile parkinsonism
ATP	Adenosine triphosphate
BamHI	Bacillus amyloliquefaciens HI
BCA	bicinchoninic acid
c-Cbl	Casitas B-lineage Lymphoma
C-terminal	carboxy-terminal
Ca	calcium
CDC-rel1	cell division control-related protein 1
cDNA	complementary deoxyribonucleic acid
cdk5	cyclin-dependent kinase 5
CHIP	carboxyl terminus of the Hsc70-interacting protein
CLASP	CLIP-Associated Protein
CV	correlation of variance
Da	dalton
DAPI	4',6-diamidino-2-phenylindole
DMSO	dimethyl sulfoxide
DNA	deoxyribonucleic acid
DRI	dietary reference intakes
DTPA	diethylenetriamine pentaacetic acid
DTT	dithiothreitol
DUB	deubiquitinating enzymes
EAR	estimated average requirement
E. coli	Escherichia coli
EcoRI	Escherichia coli R-factor I
eIF4e	eukaryotic translation initiation factor 4E
E6AP	E6-associated protein
EDTA	ethylenediaminetetraacetic acid
EM	electron microscopy
fPD	familial Parkinson's Disease
FBS	fetal bovine serum
FPLC	fast protein liquid chromatography
FRA6E	fragile site, aphidicolin type, common, fra(6)(q26)

FtsZ	filamenting temperature-sensitive mutant Z
g	gravity
G2/M	gap2/mitosis phase of the cell cycle
G-protein	guanine nucleotide-binding proteins
GDP	guanosine diphosphate
GMPCPP	Guanosine-5'-[( $\alpha$ , $\beta$ )-methylene]triphosphate
GST	glutathione-S-transferase
GTP	guanosine triphosphate
H	helix
HCl	hydrochloric acid
HECT	Homologous to E6AP carboxy terminus
HHARI	human homologue of <i>Drosophila ariadne</i>
HNO <sub>3</sub>	nitric acid
HRP	Horseradish peroxidase
HtrA2	high-temperature requirement factor A2
IBR	in between RING
IC <sub>50</sub>	inhibitory concentration at 50% response
ICP-AES	inductively coupled plasma-atomic emission spectrophotometry
IgG	immunoglobulin G
IHRSR	iterative helical real space reconstruction
IPTG	isopropyl $\beta$ -D-1-thiogalactopyranoside
KAP-1	KRAB domain-associated protein 1
kb	kilobase
KDa	kilodalton
kV	kilovolt
L-dopa	levodopa
LB	Luria broth
LNCaP	Lymph node cancer of prostate
LOH	loss of heterozygosity
LRRK1	leucine-rich repeat kinase 1
$\mu$ m	micrometer
$\mu$ M	micromolar
mM	millimolar
M	molar
MAP	microtubule associated protein
MAPK	microtubule associated protein kinase
MAPT	microtubule associated protein tau (gene)
MARK	MAP/MT affinity regulating kinase
Mbp	Mega base pair
MBP	maltose binding protein
MCF7	Michigan Cancer Foundation human breast adenocarcinoma line 7
Mdm	murine double minute oncogene
MPTP	1-methyl-4-phenyl- 1,2,3,6-tetrahydropyridine
mRNA	messenger ribonucleic acid
MS	mass spectrometry
MTT	3-(4,5-Dimethylthiazol-2-yl)-2,5-diphenyltetrazolium bromide

MW	molecular weight
N-terminal	NH <sub>2</sub> terminal
NaCl	sodium chloride
NFT	neurofibrillary tangles
NIST	National Institute of Standards and Technology
nm	nanometer
nM	nanomolar
NMR	nuclear magnetic resonance
NotI	<i>Nocardia otitidis-caviarum</i> I
OD	optical density
Pael-R	Parkin associated endothelin-receptor like receptor
PC3	prostate cancer 3
PCR	polymerase chain reaction
PD	Parkinson's Disease
PGGG	proline glycine glycine glycine
PHF	paired helical filaments
PINK1	PTEN induced putative kinase 1
PML	Promyelocytic leukemia protein
PVDF	polyvinylidene fluoride
RDA	recommended daily allowance
RIPL	arginine isoleucine proline leucine
RING	really interesting new gene
RIR	RING1 in between RING RING2
Rpn10	Regulatory Particle Non-ATPase 10
sPD	sporadic Parkinson's Disease
SAP	stress activated protein kinases
TAEA	Tris(2-aminoethyl)amine-agarose
TBS	Tris buffered saline
TBST	Tris buffered saline + Tween
TCEP	tris(2-carboxyethyl)phosphine
TEV	Tobacco Etch Virus
Thr	threonine
TIPs	microtubule plus-end tracking proteins
TMAO	trimethylamine N-oxide
tRNA	transfer ribonucleic acid
Tris	tris(hydroxymethyl)aminomethane
Ubc7	ubiquitin conjugating enzyme 7
Ubc8	ubiquitin conjugating enzyme 8
Ubl	ubiquitin like domain
UPR	unfolded protein response
w/v	weight/volume percent
XbaI	<i>Xanthomonas badrii</i> I
X-gal	bromo-chloro-indolyl-galactopyranoside
XMAP215	<i>Xenopus</i> microtubule associated protein 215
Zn	zinc
ZnSO <sub>4</sub>	zinc sulfate

## Acknowledgements

For invaluable help to me and this work over the past 6 years,  
I would like to specifically thank:

Professor Kenneth H. Downing for his incredible generosity, for nurturing both my scientific and personal growth, and for his insight and friendship,  
Professor Tom Alber, for thankfully acting as my co-chair and reminding me during my exam that it is good to be nervous,  
Professor Eva Nogales for graciously inviting me into her lab meetings, for her candid and thoughtful critiques, and for serving on my thesis committee,  
Professor George Sensabaugh for valuable insights and criticism, and for serving on my thesis committee,  
Chuck Sindelar, my 4000 sensei and microtubule cohort,  
Roseann Csencsits, who is not a biologist, but knows how to talk to them,  
Swan Lee, for her dedication to my projects and her willingness to learn,  
Lara Gundel, a wonderful role model, who made graduate school a possibility,  
The members of the Nogales and Alber labs for their technical assistance,  
Dr. Jap and Dr. Wailin, for whom without parkin would still be aggregated,  
Drs. Balczon and Goodman, who were patient yet demanding, and started my scientific journey,  
and to my closest friends that encouraged me, sympathized with me, and reminded me to laugh when I wanted to cry.

# Chapter 1.

## Tubulin and Microtubules: Structure, function, and interactions

### Introduction

#### Tubulin

Microtubules are major structural components of the cytoskeleton responsible for cellular division, movement and trafficking. They are polymers of repeating alpha- and beta-tubulin heterodimers that assemble head-to-tail to form longitudinal protofilaments that associate laterally to create the hollow tube of the microtubule with a diameter of about 25 nm (Figure 1). Most microtubules in mammalian cells have 13 protofilaments while microtubules made in vitro often have a range of protofilaments (11-16 protofilaments). Cellular microtubules are nucleated from complexes containing gamma-tubulin, which likely provide constraints regarding protofilaments number.

Humans express 6  $\alpha$ -tubulin and 7  $\beta$ -tubulin isotypes that have different tissue distribution and display different inherent properties. Alpha- and beta-tubulin are globular proteins of approximately 450 amino acids with a sequence homology of 40% and similar secondary structure. Each monomer can be divided into three structural domains: the N-terminal domain has a Rossmann fold with alternating parallel  $\beta$ -strands and  $\alpha$ -helices and is involved in GTP binding; an intermediate domain is composed of mixed  $\beta$ -sheets and  $\alpha$ -helices that are involved in lateral and longitudinal interactions between the subunits and also contains the majority of the hydrophobic pocket necessary for binding of the microtubule stabilizing drug paclitaxel (Taxol, a trademark of Bristol-Meyers Squibb); and the C-terminal domain is formed by two antiparallel helices that cross the N-terminal and intermediate domains and plays a role in microtubule regulation (Nogales et al. 1998). The last 15 residues of the C-terminal sequence contain the most heterogeneity, with around 85% variation among all isotypes, which lends to their unique characteristics (Sullivan and Cleveland 1986).

The  $\alpha\beta$ -tubulin heterodimer was solved to atomic resolution in a 3.7Å structure determined by electron crystallography (Nogales et al. 1998) with subsequent refinement to 3.5 Å (Figure 2) (Lowe et al. 2001). Zinc ions were used to form a 2D crystal of tubulin by inducing the formation of antiparallel protofilaments (zinc sheets). Building on this work, Li et al. used a combination of cryo EM and image processing to obtain a 3D reconstruction of the microtubule at a resolution of 8 Å (Li et al. 2002). Docking the crystal structure of tubulin into the microtubule density map revealed how the lateral interactions in the microtubule differed from those found in the zinc sheets. In zinc sheets, the protofilaments are anti-parallel to each other allowing the M loop to interact with helices H12 and H5. In the microtubule structure, where the protofilaments are parallel, the M loop interacts with the N-terminal H1-S2 loop (N loop) and to a lesser extent with helix 3 (Figure 3). Taxol appears to have the same effect in stabilizing the M loop to enhance interprotofilament interactions in the two different structures.

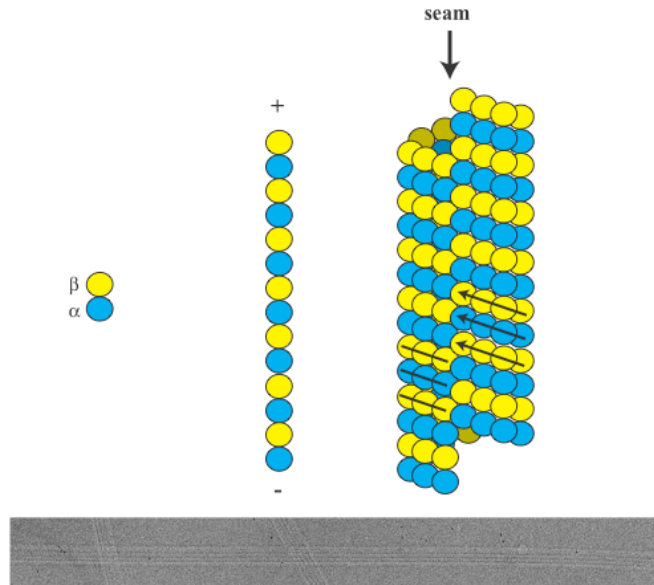


**Figure 1. Schematic of tubulin heterodimer, protofilament and microtubule structures.** The  $\alpha$ -tubulin (blue) and  $\beta$ -tubulin (blue) monomers assemble into stable heterodimers. Tubulin heterodimers assemble head-to-tail to form linear protofilaments. The protofilaments form lateral interactions with adjacent protofilaments to form the microtubule (13 protofilament shown). A typical image of a frozen hydrated microtubule image taken at a defocus of 4  $\mu\text{m}$ .

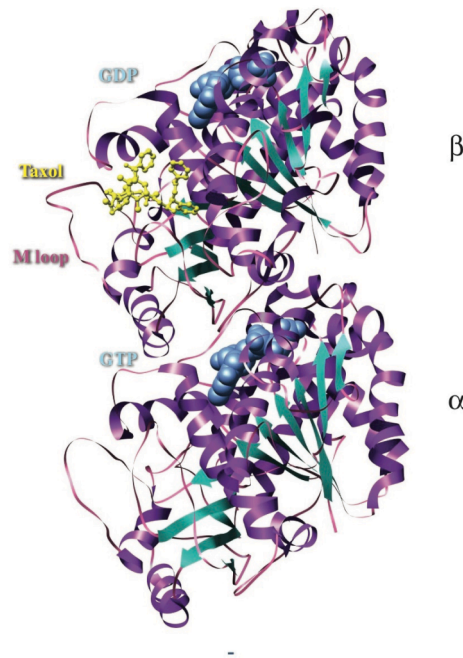


**Figure 2. Ribbon diagram of the functional domains of the tubulin heterodimer.** The nucleotide binding sites in the tubulin heterodimer are identified with bound GTP and GDP (blue spheres). The taxane binding site in the tubulin heterodimers is identified with a bound taxol molecule (yellow ball and stick structure). Polarity of the tubulin heterodimer ends is indicated with plus and minus symbols. The figure was made in Chimera (Pettersen et al. 2004) using the coordinates from the Protein Database file 1JFF (Löwe et al. 2001).

Both subunits of tubulin bind GTP, but hydrolysis of GTP to GDP only occurs in  $\beta$ -tubulin and usually only following polymerization. GTP hydrolysis by  $\beta$ -tubulin is an important step in the ability of microtubules to oscillate between the growing and shrinking phases of dynamic instability. Microtubule dynamics vary throughout the cell cycle. While interphase microtubules can have a half-life of 1.5-5 minutes, microtubules in the highly dynamic stage of mitosis can have a half-life of as little as 3-22 seconds (Saxton et al. 1984). The stable microtubule arrays found in interphase have the ability to completely disassemble and reorganize into the highly dynamic mitotic spindle. Microtubules in mitosis must be dynamic in order to search the cell for their attachment sites (kinetochores) on chromosomes and then with the help of microtubule motors and associated proteins pull the chromosomes to the poles in order for cellular division. Even more interesting are microtubules in differentiated neuronal cells. The microtubules found in axons are often associated with factors that influence their stability. Microtubule stability in both dividing and differentiated cells is promoted by a class of proteins called MAPs (microtubule-associated proteins). These proteins bind to, stabilize and promote the assembly of microtubules (Hyams and Lloyd 1994). Neuronal MAPs are unique in their ability to stabilize microtubules for long periods of time, and they do so by suppressing catastrophes (the transition from microtubule polymerization to depolymerization) and promoting rescues (the transition from microtubule depolymerization to polymerization) in the cell (Pryer et al. 1992). Many of the processes in which microtubules take part in the cell involve modulation of microtubule dynamics by accessory proteins that stabilize or destabilize the microtubule, which emphasizes why identifying other microtubule binding proteins and defining their function is so important.

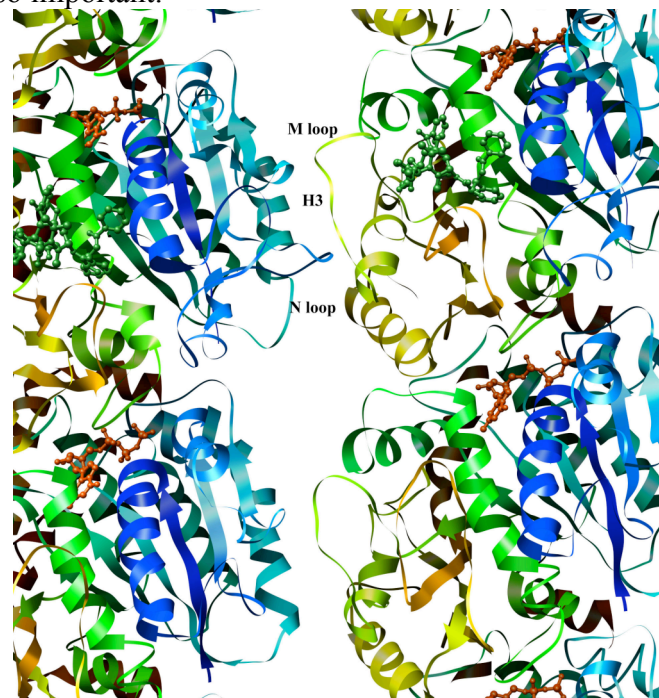


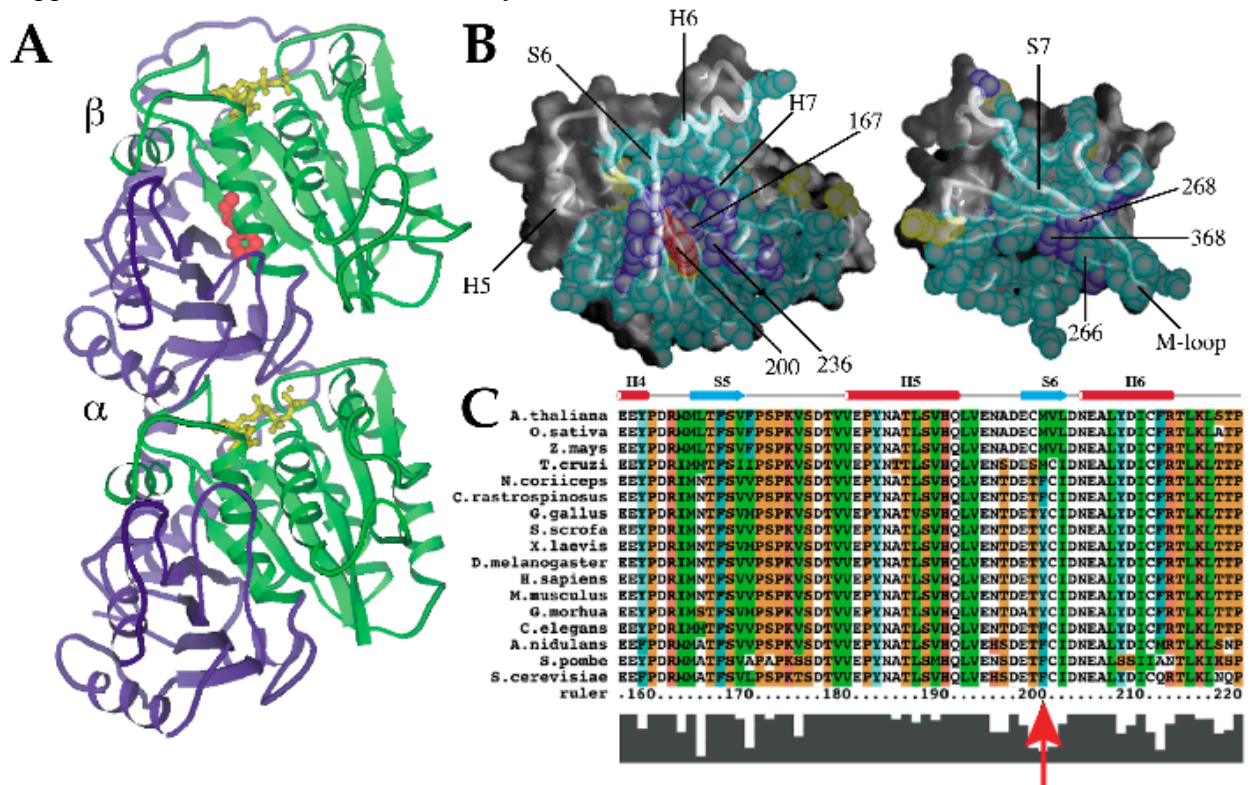
**Figure 3. Interprotofilament view of two heterodimers.** View from inside the microtubule showing two protofilaments.  $\beta$ -tubulin features are labeled (M loop, N loop, H3). The nucleotide (orange) and taxol (green) are shown as ball and stick models. The figure was made in Chimera using the coordinates from the Protein Database file 1JFF docket into microtubule density from (Li et al 2002).



When microtubules depolymerize the protofilaments peel back and form rings and spirals. The tubulin in these structures is bound by GDP. The tubulin that is added to the microtubule is bound by GTP and believed to be constrained in a straighter conformation. A model for microtubule polymerization describing the straight and curved conformations has recently come from the Nogales lab using atomic models from electron crystallography of zinc-induced sheets to model tubulin heterodimers in the straight conformation and tubulin heterodimers bound to RB3 (a stathmin homologue that depolymerizes microtubules) and the microtubule depolymerizing drug colchicine obtained by X-ray crystallography to represent the curved tubulin conformation. These models along with two other microtubule intermediates (GDP tubulin rings and ribbon structures stabilized with non-hydrolysable GTP analogue GMPCPP) were used to explain how GTP bound heterodimers are added to the growing microtubule lattice. Divalent cations were used to produce GDP rings in the absence of depolymerizing agents like stathmin or colchicine. Docking of the  $\beta$ -tubulin from the RB3 model and the  $\alpha$ -tubulin from the zinc sheet model into the 12 Å resolution map obtained by cryo EM for the GDP rings revealed that the bent conformation of GDP tubulin, specifically the bending of the intra-dimer and inter-dimer interfaces, would make addition to the growing microtubule unlikely due to absence of the lateral contacts (Wang and Nogales 2005). To investigate the GTP form, cryo EM and helical reconstruction were used to obtain an 18 Å resolution structure of ribbons that form in the presence of GMPCPP. This map depicts an intra-dimer bend of 5° versus 12° seen in the GDP ring structure. This confirmed that the interfaces straighten significantly but not completely upon GTP binding and the straighter conformation of the GTP tubulin is what allows for lateral contacts when the heterodimers is added to the growing microtubule. A final straightening is required in order to produce microtubule closure (Wang and Nogales 2005). The presence of a GTP cap at the growing end of the microtubule stabilizes the body of the microtubule that consists mainly of GDP tubulin since GTP is hydrolyzed after incorporation into the microtubule. Loss of the GTP cap results in protofilament peeling and catastrophe (Caplow and Shanks 1996, Mitchison and Kirschner 1984). When depolymerization occurs, protofilaments peel back from the tube of the microtubule indicating that depolymerization occurs by weakening of the lateral interactions versus the longitudinal interactions (Jánosi et al. 1998).

Precisely controlled dynamic properties are required for microtubule functions. To better understand how tubulin's dynamics are embedded in its primary sequence we investigated in vivo the consequences of altering a single, highly conserved residue in  $\beta$ -tubulin that lies at the interface between two structural domains. The residue differs between the cold-adapted Antarctic fish and temperate animals in a manner that suggests a role in microtubule stability (Detrich et al. 2000). Fungi, like the Antarctic fish, have a phenylalanine in this position (F200), while essentially all other animals have tyrosine. A remarkable architectural change occurs during microtubule depolymerization that allows rapid peeling and curling of microtubule ends (Mandelkow *et al.*, 1991; Desai and Mitchison, 1997; Tran et al., 1997). F200 is positioned at an internal interface between the nucleotide-binding and intermediate domains (Figure 4A). It has been hypothesized that movement of these domains is the principal conformational change required for depolymerization of microtubules (Amos and Löwe, 1999, Ravelli et al. 2004). Our examination of residues at this interface in various species indicates that the bulk remain constant or display only conservative substitutions (Figure 4C). Unique to this class is the residue corresponding to position 200 in mammalian  $\beta$ -tubulin (red in Figure 4A and 4B), which

displays a phyla-specific pattern of conservation (arrow in Figure 4C). The conservation of this critically positioned residue in organisms living in contrasting thermal environments further supports its role in microtubule stability.

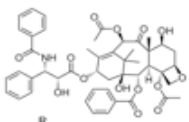
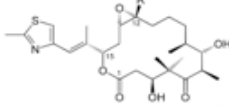
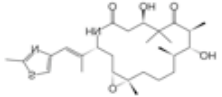
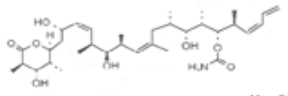
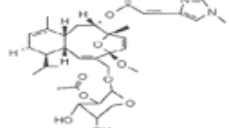
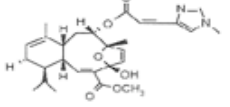
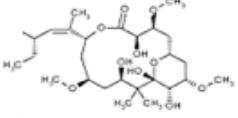
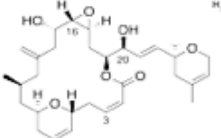


**Figure 4. Conservation of an internal residue in mammalian  $\beta$ -tubulin.** A and B. Ribbon diagram of  $\alpha/\beta$  tubulin dimer. Green: nucleotide binding domain comprising residues 1-240; red: residue 200; yellow: nucleotide; blue: remainder of protein. B. Contacts made between the nucleotide-binding (left) and intermediate (right) domains of porcine  $\beta$ -tubulin. Atoms in residues involved in contacts are shown as spheres. Backbone worm is superimposed to indicate secondary structure with selected helices and sheets labeled for orientation. Residues colored in aqua are highly conserved among all known  $\beta$ -tubulins (126 sequences from Swiss Prot); purple residues show only conservative substitutions; yellow residues show non-conservative substitutions. Residue 200 falls into this last class and is colored red for distinction. Numbered atoms are those implicated in benzimidazole binding. Alpha helices H5, H6, and H7, beta strands S6 and S7, and the M-loop (Löwe et al., 2001) are indicated. C. Primary  $\beta$ -tubulin sequences from representative eukaryotes showing the immediate region of interest: Plants (*A. thaliana*, *Z. Mays*, *O. Sativa*), Human (*H. sapiens*), mouse (*M. musculus*), chicken (*G. gallus*), pig (*S. scrofa*), Frog (*X. laevis*), Fly (*D. melanogaster*), psychrotolerant fish (*G. morhua*), worm (*C. elegans*), psychrophilic fish (*N. coriiceps*, *C. rastrorpinosus*) and fungi (*S. cerevisiae*, *A. nidulans*, *S. pombe*). Numbering is according to human  $\beta$ -tubulin. The conserved phyla-specific residue corresponds to human Y200, Antarctic fish F200 and *S. pombe* F200 and is indicated by an arrow. Residues are colored as follows: orange= G, P, S, T; red= H, K, R; blue= W, Y; aqua= F; green= I, L, M, V; and white= A, C, N, D, E, Q. The histogram at the bottom of the sequences reflects conservation of amino acids at each position.

We mutated the corresponding residue in fission yeast to tyrosine. Temperature effects were subtle, but time-lapse microscopy of microtubule dynamics revealed reduced depolymerization rates and increased stability. Mitotic exit signaled by breakdown of the mitotic spindle was delayed. In meiosis, microtubules displayed prolonged contact to the cell cortex during horsetail movement, followed by completion of meiosis I but frequent asymmetric failure of meiosis II spindle formation. Our results indicate that depolymerization dynamics modulated through interdomain motion may be important for regulating a subset of plus-end microtubule complexes in *Schizosaccharomyces pombe* (Paluh et al. 2004).

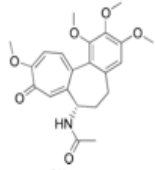
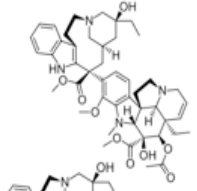
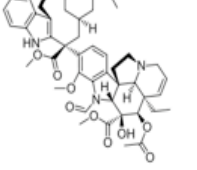
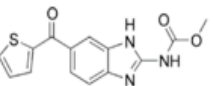
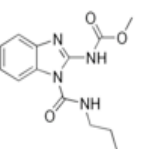
## Microtubule drugs

Because of their key role in cellular division, microtubules have been identified as excellent targets for many drug therapies directed against cancer that act by inhibiting cellular division. Microtubule-binding drugs fall into two general classes—those that stabilize microtubule dynamics (stabilizers) such as taxol and epothilone, and those that inhibit microtubule assembly (destabilizers) such as colchicine, vinblastine, vincristine (Table I and Table II). Destabilizing drugs are known to bind to two sites on  $\beta$ -tubulin, the vinca domain and the colchicine site, while with the exception of laulimalide and peloruside (Pryor et al. 2002, Huzil et al. 1998) all other known microtubule-stabilizing drugs (i.e. discodermolide, eleutherobin, sarcodictyin) bind to the taxane site (Downing 2000).

Stabilizing drugs	Structure	Source	IC <sub>50</sub>	Stage in clinical trial
Paclitaxel		Pacific Yew tree	2nM	Approved for use
Epothilone		Myxobacterium	0.1-0.6nM	Phase I-III
Ixabepilone		Semi-synthetic	3nM	Approved for limited use
Discodermolide		Marine sponge	7nM	Phase I
Eleutherobin		Marine soft coral	2nM	-
Sarcodictyin		Marine coral	200-500nM	-
Peloruside		Marine sponge	10nM	-
Laulimalide		Marine sponge	2nM	-

**Table I. Chemical structure of microtubule stabilizing drugs.** Structures for drugs, origin, IC<sub>50</sub>, and stage in clinical trial for the microtubule stabilizing drugs discussed in text.

The taxol binding site on tubulin was revealed in the 3.7 Å structure of tubulin determined by electron crystallography (Nogales et al. 1998). The electron densities along with photoaffinity labeling (Rao et al. 2001), X-ray crystallography (Mastropaolo et al. 1995), nuclear magnetic resonance (NMR) spectroscopy (Barboni et al. 2001) and molecular modeling (Snyder et al. 2001) have been used to determine the binding site and conformation of taxol (Figure 2). The diterpenoid taxol belongs to the taxane class of drugs and was the first example of a microtubule-stabilizing drug. Taxol was isolated from the bark of the pacific yew tree in 1967 after the National Cancer Institute initiated a screen of over 35,000 plants for potential anti-cancer compounds. After supply shortages (one dose requires the bark from one tree) and difficulties synthesizing such a complex structure, Nicolaou and Holton completed the full synthesis of taxol independently in 1994 (Nicolaou et al. 1994; Holton et al. 1994). Taxol was approved for clinical use to treat breast and ovarian cancer in 1995. It has been one of the best selling chemotherapeutics but has been plagued with issues such as insolubility, cytotoxicity and acquired resistance. Taxol binds to  $\beta$ -tubulin reversibly with a stoichiometry of 1:1 in a hydrophobic pocket located in the lumen of the microtubule. Binding inside the microtubule raises questions about how taxol can reach its target size so fast. The near atomic resolution map of the microtubule revealed a downward shift of the M loop that was not seen in the structure using zinc sheets. (Li et al. 2002). This shift of the M loop creates a pore in the microtubule wall of approximately 17 Å. Taxol can easily diffuse through a pore this size to bind inside the lumen of the microtubule, which explains how it can attain its fast binding rates.

Destabilizing drugs	Structure	Source	IC <sub>50</sub>	Stage in clinical trials
Colchicine		Meadon saffron	nM	Approved for gout
Vinblastine		Periwinkle plant	nM	Approved for lymphomas
Vincristine		Periwinkle plant	nM	Approved for lymphomas
Nocodazole		synthetic	nM	Research
Benomyl		synthetic	nM	Fungicide

**Table II. Chemical structure of microtubule destabilizing drugs.** Structures for drugs, origin, IC<sub>50</sub>, and stage in clinical trial for the microtubule destabilizing drugs discussed in text.

There are two current hypotheses to explain how taxol stabilizes microtubules. The first uses the near atomic structure of tubulin obtained from taxol-stabilized zinc sheets. This model supposes that binding of taxol to tubulin most likely stabilizes the M loop thereby increasing interprotofilament interactions against depolymerization (Nogales et al. 1998). The second model suggests that taxol stabilizes the movement between the intermediate and N-terminal domains seen as an 11° rotation in the crystal structures of FtsZ and the tubulin stathmin complex (Amos and Löwe 1999, Ravelli et al. 2004). It is possible that both of these models are correct to some extent in their explanation for how taxol stabilizes microtubules. This stabilization effect inhibits dynamics necessary for chromosome attachment and movement in mitosis and triggers the G2/M checkpoint that leads to eventual apoptosis. The effect of taxol on dynamics can be abrogated by overexpression of the multidrug transporter p-glycoprotein (Kavallaris 1997), modification of microtubule regulatory proteins (Larsson et al. 1999, Poruchynsky et al. 2001), mutations or changes in isotype distribution that result in more dynamic microtubules (Gonzalez-Garay et al. 1999) and mutations that interfere with drug binding (Giannakakou 1997). The new generation of microtubule-targeted drugs is overcoming these obstacles. One example is epothilone, a more water-soluble drug than taxol that is effective against many taxol-resistant cancers (Kowalski et al. 1997, Giannakakou et al. 1997). One of the most promising microtubule stabilizing drugs is ixabepilone, an analogue of epothilone with more anti-tumor activity than taxol (Lee et al. 2001). Unlike taxol, ixabepilone is not affected by overexpression of p-glycoprotein and has activity against taxol-resistant cells in vitro and in vivo that are overexpressing the  $\beta$ III isotype (Dumontet et al. 2009).

One method for overcoming the effect of microtubule drugs is upregulation of the  $\beta$ III tubulin isotype, which is thought to be more dynamic or unstable. In vitro experiments using  $\beta$ III tubulin illustrated that it was 7 times less sensitive to stabilization effects incurred by taxol on microtubule dynamics (Derry et al. 1997). Studies in several tumor cell lines including prostate, breast and ovarian, show resistance to microtubule drugs in tumors expressing increased levels of the  $\beta$ III (Rangathan et al 1998, Banerjee et al. 2002, and Kavallaris et al. 1997). Conversely, selection of human leukemia cells with the destabilizing agents vinblastine or vincristine resulted in a decrease of the  $\beta$ III isotype (Kavallaris et al. 2001). It is possible that since the  $\beta$ III isotype is a dynamic isotype, it is the increase in dynamics that overcomes taxol's stabilizing effect and enhances the destabilizing effects of vincristine and vinblastine.

Epothilone was first discovered in the soil-dwelling myxobacterium *Sorangium cellulosum* and determined to be more soluble in water and 20-50 times more potent than paclitaxel in microtubule polymerizing assays. Early experiments showed that epothilone could displace <sup>3</sup>H-labeled paclitaxel, indicating that the two drugs could share overlapping binding sites (Bollag et al. 1995). Although the two structures are distinct from each other, some groups proposed that the two drugs might share a common pharmacophore based on mutations in epothilone resistant cell lines and resulting molecular models (Giannakakou et al. 2000, He et al. 2000). The structure of epothilone has been solved by X-ray crystallography (Höfle et al. 1996), in solution bound to  $\alpha$ -,  $\beta$ -tubulin by NMR spectroscopy (Carlomango et al. 2003), and recently bound to  $\alpha$ - $\beta$ -tubulin in two-dimensional zinc sheets by electron crystallography (Nettles et al. 2004). The electron crystallographic model indicates that although paclitaxel and epothilone bind to the same pocket on  $\beta$ -tubulin, they utilize different amino acid residues and in fact share only one common contact through the C7-OH of each drug. While paclitaxel uses this hydroxyl for a long and weak polar interaction with Thr274, epothilone uses it for hydrogen bonding to Thr274

and Arg284. Thus, although the drugs share the same binding pocket, the actual binding residues differ leaving no common pharmacophore.

## **MT binding proteins**

### **MAPs**

Microtubule associated proteins (MAPs) were first identified as proteins contaminating tubulin purified from brain preparations. These initial MAPs (MAP1, MAP2, tau in neurons and the ubiquitous MAP4) have been designated as the classical MAPs (Keats and Hall 1975, Murphy and Borisy 1975, Sloboda et al. 1976, Weingarten et al. 1975). Most MAPs utilize tubulin's highly acidic C-terminal tail for binding (Serrano et al. 1984) and are regulated through phosphorylation that weakens their electrostatic interaction causing removal from the microtubule lattice (Marklund et al. 1996, Horwitz et al. 1997, Chang et al. 2001). There are many kinases involved in the regulation of MAPs some of which include MAP kinase, MAP/MT affinity regulating kinase (MARKs), casein kinase II, the stress activated protein kinases (SAP), cyclin-dependent kinase 5 (cdk5), Ca<sup>2+</sup> calmodulin-dependent protein kinase II (for review see Cassimeris and Spittle 2001).

Tau is the most abundant MAP in neurons where it likely stabilizes the microtubules in the axon bundle. Tau is also associated with the neurofibrillary tangles that characterize Alzheimer's disease. It is the most well studied MAP, including investigations by cryo EM. There are currently two very different models of tau binding microtubules. The first came from the Milligan lab and used cryo EM to identify tau binding longitudinally along the outer ridge of the microtubule (Al-Bassam et al. 2002). The second study came from the Amos lab and also used cryo EM but suggested that tau binds partially on the inside of the microtubule and has the ability to displace taxol (Kar et al. 2003). It had originally been assumed that tau binding only occurred on the outer microtubule wall but the notion of an interior binding site was strengthened when evidence was published a year after the Amos structure describing two different binding constants for tau that were dependent on whether addition of tau was before or after polymerization of microtubules (Makrides et al. 2004). Additional work to obtain structures of both tau-binding models at higher resolution is in progress in our lab and is described in chapter 3.

There are several other types of MAPs that don't bind to the microtubule lattice including cytoplasmic associated linker proteins (CLASPs) that bridge the interaction between microtubules and membranes by binding to microtubule tips (Lansbergen et al. 2006), katanin, which forms rings on the outside of the microtubule wall resulting in a microtubule severing (McNally and Vale 1993), and XMAP215, which binds to free tubulin and facilitates its addition to the microtubule lattice (Gard and Kirschner 1987). These are just a few examples of the growing field of microtubule binding proteins. One of the more recently described MAPs is parkin, a protein often found to be mutated in patients with Parkinson's disease. We are studying the novel interaction of parkin with microtubules and will discuss it further in chapter 2.

### **Microtubule motors**

Microtubule motors are proteins that hydrolyze ATP in order to move cargo along a microtubule. There are two classes of motors: kinesins, mostly plus-end directed motors, and dyneins, minus end motors. Kinesins encompass a large family of motors that usually move cargo to the plus end of the microtubule or away from the centrosome. One exception to the anterograde transport is found in the kinesin-14 family members that walk towards microtubule

minus ends (Ambrose et al. 2005). Conventional kinesins consist of a heavy chain with the motor domain connected by a flexible linker to the coiled-coil stalk that ends in the tail region formed by the light chain. The heavy chain or head is where ATP hydrolysis occurs and also binds the microtubule, and the light chain or tail region is used for binding cargo (Vale and Milligan 2000). Recent work from our lab has used cryo EM of kinesin-decorated microtubules to describe the relationship of kinesin's switch I and switch II regions to the nucleotide state (Sindelar and Downing 2007).

Dyneins are much larger, multi-subunit proteins that can be further subdivided into either axonemal or cytoplasmic dynein. Both groups of dynein have similar structures although some protein subunits differ between the two groups. In general, like kinesin, dynein has two heavy chains where hydrolysis takes place but these heavy chains do not make contact with the microtubule. The coiled-coil stalk connects the globular heavy chains to a smaller globular domain that interacts with microtubules (Holzbaur and Vallee 1994, Kardon and Vale 2009). Dynein also has several intermediate and light chains that interact with the multiprotein complex dynactin that mediates cargo binding.

### **Tubulin isotypes and posttranslational modification**

One factor that contributes to the differences in microtubule dynamics is that cells often contain several  $\alpha$ - and  $\beta$ -tubulin isotypes. Humans express 6  $\alpha$ -tubulin and 7  $\beta$ -tubulin isotypes.  $\beta$ -tubulin isotypes have the greatest sequence variation in their C-terminal tail and N-terminal region (residues 33-57) (Sullivan and Cleveland 1986). Microtubule assembly rates vary among the different isotypes and these differences are lost if the C-terminal tail is cleaved through subtilisin cleavage pointing to dynamic properties inherent to the individual isotypes (Lu and Ludueña 1994). The 8 Å microtubule structure revealed that it is more likely that the N loop plays a stronger role in interprotofilament interactions with the M loop than the previously suspected H3 (Li et al. 2002). The N loop contains a region of variability between different isotypes that might explain the difference in microtubule dynamics seen between different isotypes. Unlike  $\beta$ -tubulins,  $\alpha$ -tubulins are highly conserved, at least 94% identical, and have similar tissue distribution (Ludueña and Banjeree 2008). Like  $\beta$ -tubulins,  $\alpha$ -tubulins display the greatest sequence variation at their C-terminal tail and N-terminal region (residue 35-60) (Sullivan 1988). There are six  $\alpha$ -tubulin isotypes in humans but much less is known about the differences in their dynamic properties.

All but one type of posttranslational modification occurs at the C-terminal tails of  $\alpha$ -tubulin and  $\beta$ -tubulin, leading to distinctive dynamic properties (Panda et al. 1994, Bode et al. 2003, Westermann and Weber 2003). These include tyrosination/ detyrosination, polyglutamylation, polyglycylation, and phosphorylation. The motor protein Kinesin-1 binds preferentially to  $\alpha$ -tubulin that has been detyrosinated whereas tyrosination of  $\alpha$ -tubulin results in recruitment of +TIP proteins, proteins that localized to the plus-end of the microtubule (Liao and Gundersen 1998, Peris et al. 2006). Polyglutamylation and polyglycylation are both modifications seen in cilia and flagella where they effect formation, motility and transport (Thazhath et al. 2002, Xia et al. 2000, Ikegami et al. 2007). Work from the Detrich lab has also suggested that reduced glutamylation may explain why microtubules from Antarctic fish can assemble at low temperatures (Redeker et al. 2004). Phosphorylation is the least common of all modification but does occur on the C-terminal tail on  $\beta$ -tubulin although its function is unknown (Eipper 1974). Acetylation at lysine 40 on  $\alpha$ -tubulin is the only posttranslational modification not

to occur on the C-terminal tail. Instead, it occurs on the lumen of the microtubule that is inaccessible to most proteins. This modification is associated with microtubules that have longer lifetimes in the cell and higher resistance to destabilizing microtubule drugs (Geyp et al. 1996).

### **Zinc and microtubules**

The cytoskeleton is a known site of zinc binding in the cell, especially in microtubules. Studies have shown that zinc stabilizes microtubules against cold depolymerization and reduces the critical concentration of tubulin necessary for polymerization (Eagle et al. 1983). It has been proposed that microtubule dynamics may be disrupted when cellular zinc levels drop (Hesketh, 1982, Oteiza et al. 1990) and a report by Uzzo et al. showed that excess zinc improved the efficacy of Taxol in prostate cancer cells (PC-3 and DU145 lines) (Uzzo et al. 2002). Current drugs approved for use or in clinical trials to treat prostate cancer (taxol, docetaxel, and 2-methoxyestradiol) target the microtubule network resulting in cell death (Lapidus et al. 2004, Gilbert and Parker, 2005, Qadan et al. 2001). What is unknown is if zinc deficient individuals might have alterations in the microtubule network such that the activity of these chemotherapeutic agents is altered. Therefore, we tested the hypothesis that inadequate amounts of zinc disrupt microtubule function and decreases efficacy of microtubule-targeting chemotherapeutic agents in prostate cancer cells. As described in more detail in chapter 4, we found that taxol had reduced efficacy in causing cell cycle arrest and apoptosis when prostate cancer cells were maintained under moderately zinc deficient conditions (Killilea et al. 2007). Since zinc deficiency is common in the US, this nutritional status may be of importance when creating a treatment strategy for prostate cancer. Reduced efficacy of these drugs might exaggerate side effects and promote resistance within the cancer.



## **Chapter 2.**

### **Parkin Interactions with Microtubules**

#### **Introduction**

##### **Parkinson's Disease**

Parkinson's Disease (PD) is a disease of the central nervous system that affects 1-2% of the population over 65 years of age. PD is a degenerative disorder where the primary symptoms, muscle rigidity, tremor and bradykinesia, are a result of insufficient levels of the neurotransmitter dopamine leading to excessive muscle contraction (Forno 1996). The dopaminergic (dopamine-secreting) neurons connect the substantia nigra with the striatum in the nigrostriatal pathway. Dopamine regulates movement through a direct pathway that facilitates voluntary movement and an indirect pathway that inhibits involuntary movement thereby resulting in a smooth coordinated movement. The loss of dopaminergic neurons projecting into the striatum results in inhibition of the direct pathway and excitation of the indirect pathway (Hauber 1998). This results in inhibition of voluntary movement and disinhibition of involuntary movement. There is presently no cure for PD although current therapies available for treatment of PD symptoms include pharmacological or surgical strategies. Levodopa (L-dopa) is a metabolic precursor to dopamine that can cross the blood brain barrier and temporarily alleviate some PD symptoms (Cotzias 1968). When L-dopa treatment is no longer successful, surgical options such as a pallidotomy (ablation of the globus pallidus to relieve dyskinesias), thalamotomy (ablation of the thalamus to relieve tremors), and even stem cell therapy to create new dopamine producing cells have proven effective (Kluger et al. 2009). The cause for the loss of the dopaminergic neurons in the substantia nigra remains unknown but environmental factors, oxidative stress/mitochondrial dysfunction, and dopamine have all been suggested as possible culprits in sporadic PD.

PD is the second most frequently diagnosed neurodegenerative disorder in the elderly. Most cases of PD are sporadic (sPD) but approximately 5% of all cases have a genetic mutation and are termed familial PD (fPD). sPD has a usual age onset of over 60 years of age and is idiopathic. Current theories suggest that sPD is caused not by one insult but instead by the combination of many factors, both environmental and genetic. fPD has a usual age onset of <40 years of age and as young as 20 years of age. 50% of all cases result from a mutation in the PARK2 gene that produces parkin, an E3 ubiquitin ligase.

Environmental toxins can simulate many of the same effects of parkinsonism. These toxins include the pesticide rotenone, a complex I inhibitor and microtubule depolymerizer that causes the loss of dopaminergic neurons and the formation of Lewy bodies in mice (Betarbet et al. 2000). Trichloroethylene, another complex I inhibitor was used as an industrial solvent until it was banned in the 1970's. It has more recently been linked to Parkinson-like symptoms after it was used to clean military weapons during the Gulf War (Gash et al. 2008). 1-methyl-4-phenyl-1,2,3,6-tetrahydropyridine (MPTP) is a byproduct of opioid production that in 1982 caused rapid onset of Parkinson like symptoms in 7 Santa Cruz residents by selectively killing dopaminergic neurons (Chiueh et al. 1994, Fahn 2002). It was only after this incident that researchers had a way to induce Parkinson like symptoms in mice using MPTP.

Initial studies focused on oxidative stress as the cause of PD after autopsy tissues from patients with PD revealed a reduction in the activity of complex I and increased oxidative

damage to its components in the substantia nigra (Mizuno et al. 1989). Such damage has not been seen in other neurodegenerative diseases and cannot be linked to levodopa treatment. Several proteins involved in oxidative stress are mutated in the genetic form of PD. Five of the nine known genes that affect PD are associated with the mitochondria ( $\alpha$ -synuclein, parkin, DJ-1, PINK1, LRRK1 and HtrA2).

The neurotransmitter dopamine is unique to dopaminergic neurons and may be one cause of their susceptibility to oxidative stress. Metabolism of dopamine results in production of the reactive oxygen species peroxide, superoxide and hydroxyl radicals (Lotharius and Brundin 2002, Stokes et al. 1999). Dopamine can also easily oxidize into the dangerous protein modifier dopamine quinone. LaVoie et al. observed that upon oxidation to dopamine quinone, a covalent interaction occurs with parkin, an E3 ubiquitin ligase, eventually disabling its ubiquitin ligase activity (LaVoie et al. 2005). Under the same conditions, similar E3 ubiquitin ligases (HHARI and c-cbl) were shown to be insensitive to such oxidation. Wong et al. demonstrated that parkin is sensitive to dopamine oxidation because of two cysteines (C268, C323) that are unique to parkin among similar E3 ubiquitin ligases (Wong et al. 2007).

While the cause of sporadic PD remains unknown, the presence of genetic mutations in the familial form, Autosomal Recessive Juvenile Parkinsonism (ARJP), provides insights into the mechanism of neuronal loss associated with PD. ARJP has an onset at <40 years of age and over 50% of cases are associated with mutations that occur throughout the PARK2 gene while only 18% of sporadic PD occurs with mutations in the PARK2 gene (Lucking et al. 2000). Kitada et al. first identified the PARK2 gene in 4 Japanese ARJP patients with chromosomal deletions using positional cloning (Kitada et al. 1998). Their initial analysis identified that PARK2 contained 12 exons and that deletions in exons 3-7 were the cause of ARJP in sequenced patients. PARK2 is highly conserved across species of vertebrates and invertebrates (Kahle et al. 2000) and with 1.5 Mbp it is the second largest gene in the human genome. The introns in the PARK2 gene are unusually large (over 180 kb) and that, along with the presence of over twice as many transposable elements in the beginning of intron 2, could explain the high frequency of recombinant events observed in PARK2 that result in deletions and duplications seen in exons 2,3 and 4 (Hedrich et al. 2004, Periquet et al. 2001). Furthermore, the PARK2 gene is located in a particularly active fragile site in the genome (FRA6E, chromosome 6q25-q27) that is associated with genomic instability such as exon deletions, alterations and rearrangements (Hedrich 2004).

## **Overall structure and function of parkin**

### **Domain structure**

Parkin belongs to a class of proteins described as RING E3s. Typical RING (Really Interesting New Gene) fingers are identified by the cysteine-rich consensus sequence CX<sub>2</sub>CX<sub>(9-39)</sub>CX<sub>(1-3)</sub>HX<sub>(2-3)</sub>C/HX<sub>2</sub>CX<sub>(4-48)</sub>CX<sub>2</sub>C. RING fingers are a type of zinc finger that mediate protein-protein interactions similar to zinc fingers that mediate protein-DNA interactions. Classical RING finger motifs coordinate 2 zinc atoms in a cross brace system by utilizing 4 cysteines for the first zinc ion and 3 cysteines and 1 histidine to ligate the second zinc atom (Figure 5). Borden and colleagues demonstrated that these domains require zinc ligation for proper folding and function by expressing a RING finger in the presence and absence of zinc and using NMR spectroscopy to evaluate whether the RING finger was properly folded (Borden et al. 1995, Capilli et al. 2004).

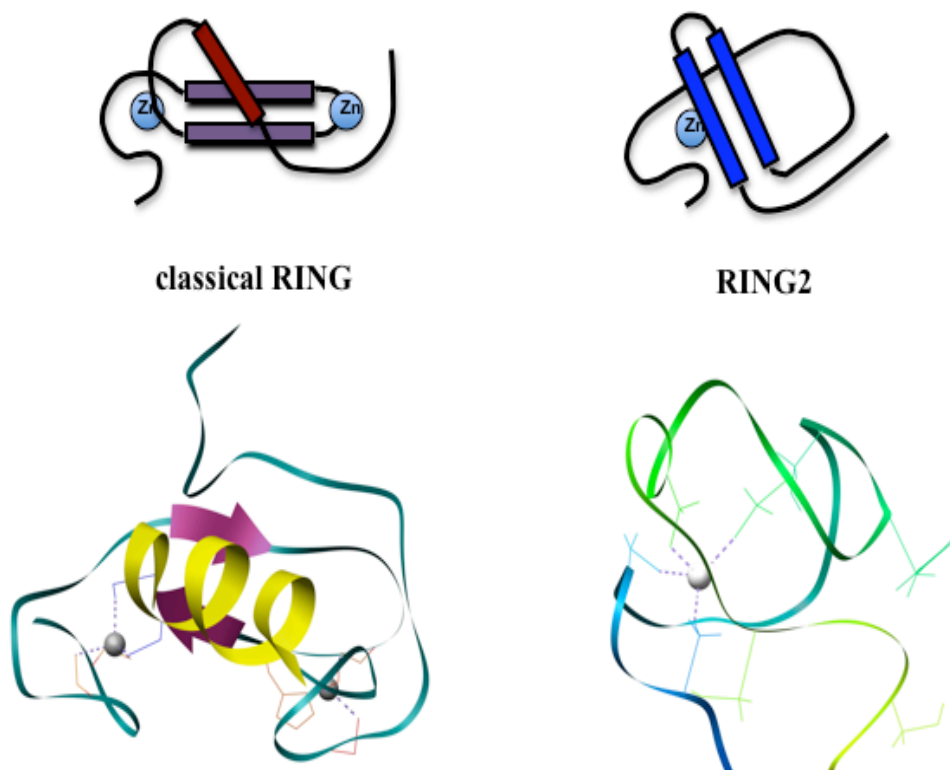


**Figure 5. Schematic of classical and non-classical RING finger domains with representative structures.** RING1 of c-cbl, a classical RING finger that binds 2 zinc ions in a cross brace manner (left structure). RING2 (the C-terminal RING from the human homologue of *Drosophila* Ariadne) is shown as an example of a non-classical RING finger that binds one zinc ion (blue circle) in a linear fashion (right structure). C-cbl and HHARI ribbon diagrams made in Chimera using the coordinates from the Protein Database files 1FBV and 1WD2, respectively.

RING domains seem to be important for the formation of multi protein complexes and have been found in proteins that are involved in very diverse processes such as transcriptional repression in the case of the RING-containing KAP-1 (Peng et al. 2000), translational repression by inhibition of the eukaryotic translation initiation factor 4E (eIF4E) by the RING finger protein promyelocytic leukemic (PML) proto-oncoprotein (Cohen et al. 2001), and finally in the ubiquitin-proteasome pathway by E3 ubiquitin ligases (Joazeiro and Weissman 2000). The cysteines that form the RING finger domains in parkin are highly conserved throughout species emphasizing the importance of each domain in parkin (Figure 6).

Parkin has five domains, which include the Ubl (ubiquitin-like), linker, RING1, IBR (in between RING), and RING2 domains (Figure 7). Parkin has RING finger motifs in its RING1, IBR and RING2 domains. These domains make up the RIR (RING-IBR-RING) superdomain. Proteins containing the RIR superdomain have only been found in eukaryotes and thus far all have E3 ligase activity (Joazeiro and Weissman 2000). Recently, a new RING, RING0, has been proposed in the linker domain (Hristova et al. 2009). This final RING finger was likely not identified before due to the unusual gap of 26 residues between the two zinc sites. This arrangements points to the possibility that the two zinc ions will not be coordinated in the classical crossbrace manner but instead linearly as in the IBR domain of parkin.

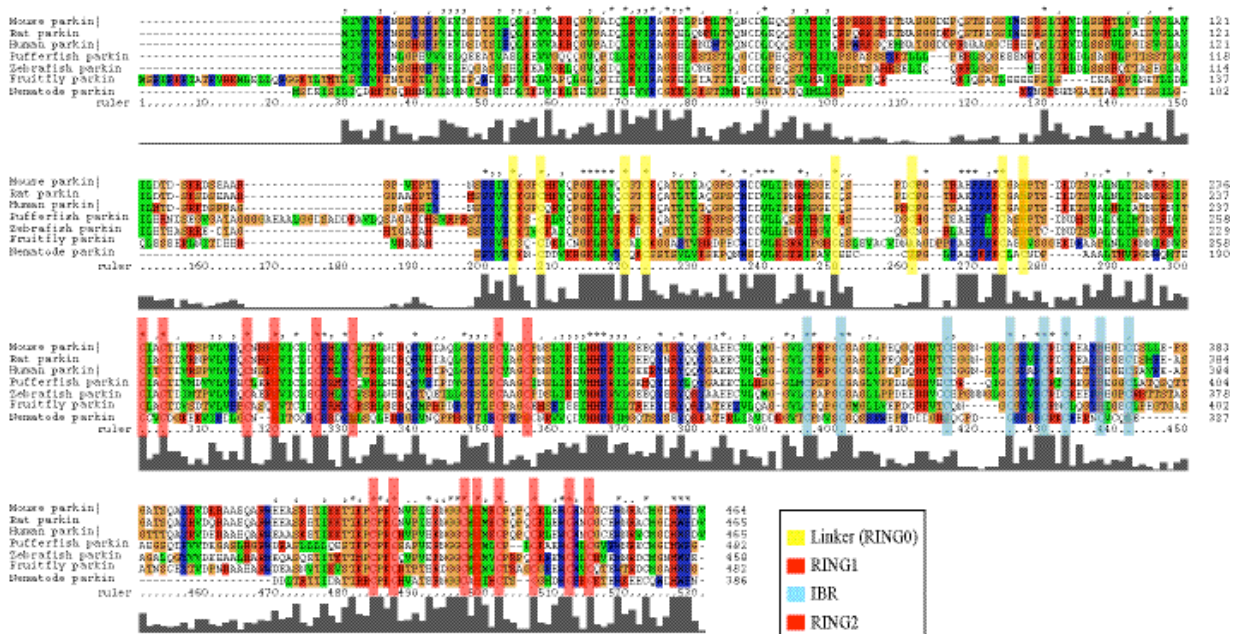


**Figure 6. Alignment of parkin protein sequences from representative eukaryotes reveal conservation of cysteines in RING fingers.** Parkin sequences were retrieved from the National Center for Biotechnology Information (NCBI) for *Mus musculus* (mouse), *Rattus norvegicus* (rat), *Homo sapiens* (human), *Takifugu rubripes* (pufferfish), *Danio rerio* (zebrafish), *Drosophila melanogaster* (fruitfly), and *Caenorhabditis elegans* (nematode). Sequences were aligned using ClustalX. Conserved cysteines are highlighted in colors used to distinguish domains in legend at bottom of figure. Residues are colored as follows: orange= G, P, S, T; red= H, K, R; blue= W, Y; aqua= F; green= I, L, M, V; and white= A, C, N, D, E, Q. The histogram at the bottom of the sequences reflects conservation of amino acids at each position.

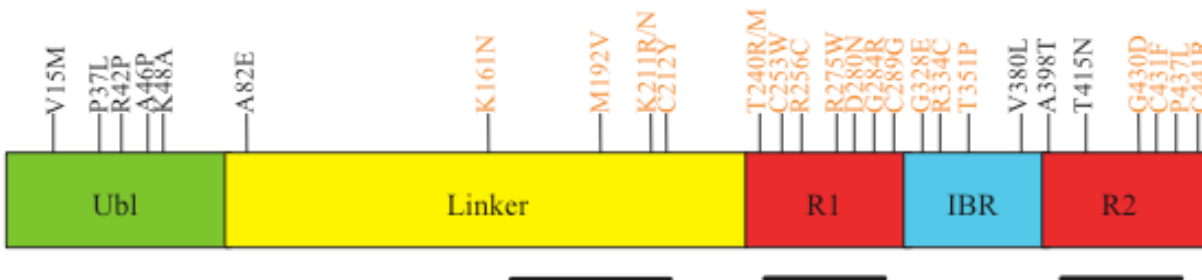


**Figure 7. Domain structure of the mammalian PARK2 gene with mutations associated with Parkinson's Disease.** The parkin gene (PARK2) has five highly-conserved domains identified as the ubiquitin-like domain (Ubl), linker domain (Linker), RING1 domain (R1), in between RING domain (IBR), and RING2 domain (R2). Bars below domain structure indicate known microtubule-binding regions. Mutations found in Parkinson's Disease not associated with RING finger domains are indicated in black text. Mutations found in Parkinson's Disease associated with RING finger domains are indicated in orange text.

Parkin's N-terminal ubl domain consists of 76 amino acids and shares 32% sequence identity with ubiquitin (Kitada et al. 1998). The solution structure obtained by NMR reveals a similar fold between parkin and ubiquitin (Figure 8), two  $\alpha$ -helices and five  $\beta$ -sheets arranged similarly (Sakata et al. 2003). Two mutations in the N-terminal ubl domain in parkin resulted in the inability of target protein ubiquitination even though the E2 could be recruited (Shimura et al. 2000). This could indicate that the ubl domain is responsible for recognizing the target protein. Additional ARJP mutations in this domain cause unfolding, inability of the ubl to recognize the proteasome and protein instability (Safadi and Shaw 2007). The ubl domain also binds to the Rpn10 subunit of the 26S proteasome and may act to facilitate proteasome recognition and processing (Sakata et al. 2003).

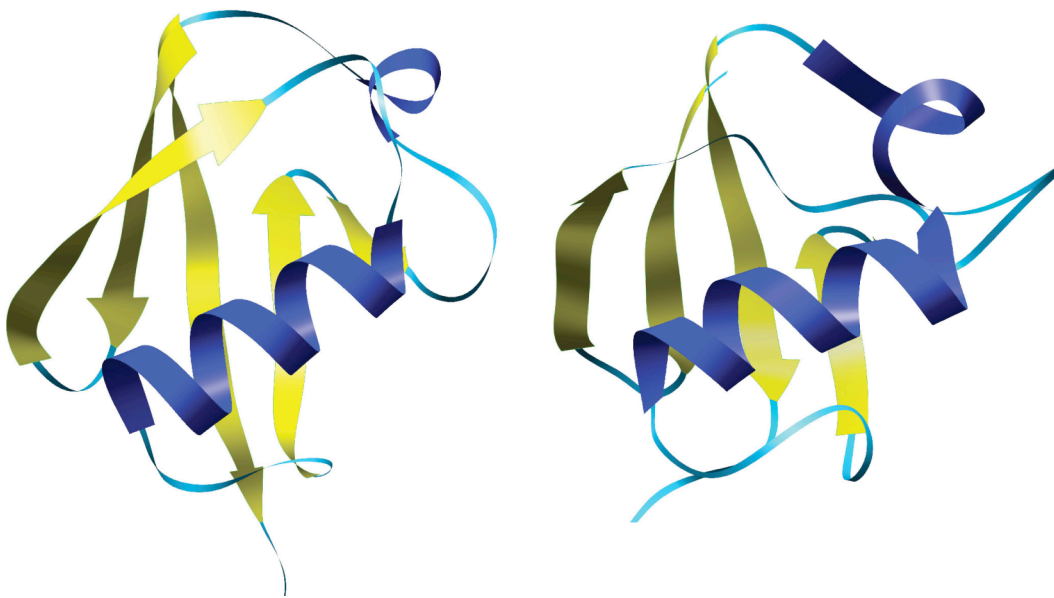


**Figure 8. Ubiquitin and the parkin ubiquitin like domain share a similar fold.** Ubiquitin (left) has a similar fold to the ubiquitin like domain from parkin (right). The proteins share 20% sequence identity. Figures made in Chimera using the coordinates from the Protein Database files for ubiquitin (1D3Z) and the ubl for parkin (1IYF).

The linker region of parkin was thought to be mostly unstructured until recent work by Hristova et al. used limited trypsin digestion, circular dichroism and inductively coupled plasma atomic emission spectroscopy to identify a new RING finger domain, RING0 (Hristova et al. 2009). The positions of the cysteines that coordinate the zinc ions in this new RING finger are similar to those of the RING1 and RING2 domains but a 26-residue linker that is atypical of other RING fingers separates each pair of cysteines. Five of the 6 ARJP mutations that map to the linker domain reside within the new RING finger. Recently, Kitami et al. have suggested that two mutations in the linker domain result in loss of substrate binding and hypothesize that this domain might also be responsible for recognizing the target protein (Tanaka et al. 2001).

Of the five RING finger domains in parkin, RING1 is the only classical RING finger that is predicted to coordinate zinc ions in a crossbrace fashion. Although no structure exists for RING1 in parkin, similar RING finger domains that ligate zinc in a crossbrace fashion have been

determined using NMR for the PML structure and crystallographic methods for c-Cbl (Casitas B-lineage Lymphoma), also an E3 ubiquitin ligase (Borden et al. 1995, Zheng et al. 2000 respectively). These RING fingers are both very spherical and ligate two zinc ions (Figure 5). The PML RING finger comprises four  $\beta$ -strands, a  $3_{10}$  helix and many loops and turns while the c-Cbl RING domain has three  $\beta$ -strands, an  $\alpha$ -helix and two large loops.

The RIR superdomain consists of two RING finger domains (RING1 and RING2) flanking another RING finger domain, the IBR domain. Parkin's IBR domain was solved using NMR spectroscopy and was shown to lack both  $\alpha$ -helical or  $\beta$ -sheet secondary structure (Beasley et al. 2007). It displays a unique hydrophobic core and binds two zinc ions linearly unlike a classical RING domain. These domains were described by Beasley et al. as forming a dual scissor-like and GAG knuckle-like structure (Figure 9) when binding the 2 zinc ions (Beasley et al. 2007). The IBR domain aids in recognition of the E2 conjugating enzyme.

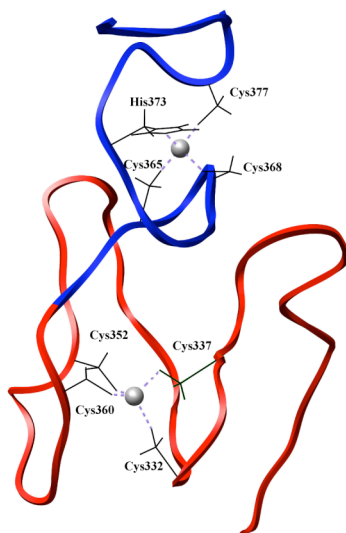


**Figure 9. Ribbon diagram of the IBR RING finger in parkin forms a scissor-like GAG knuckle.** The IBR forms a bilobal fold over two zinc ions with no notable secondary structure. The scissor-like domain is colored red (zinc binding site I cysteines are labeled). Site I resembles a zinc ribbon with extended loops resulting in ‘scissor-like’ term. The GAG knuckle domain is colored blue (zinc binding site II cysteines are labeled). A typical GAG knuckle is very short and made from two short  $\beta$ -strands, a turn and a short helix. The figure was made in Chimera using the coordinates from the Protein Database file 2JMO (Beasley et al. 2007).

The C-terminal RING finger of the human homologue of *Drosophila* Ariadne (HHARI), another RIR with E3 ligase activity, has also been solved using NMR spectroscopy (Capilli et al. 2004). The C-terminal RING finger of HHARI is predicted to be similar to the RING2 domain in parkin and surprisingly binds only one zinc atom in a zinc ribbon motif (Figure 5). It is possible that parkin may adopt a similar fold and bind one zinc ion since like HHARI it is missing 2 of the hydrophobic residues thought to be necessary for folding into a typical cross brace structure that binds two zinc atoms. Recent experiments done by the Beasley group contradict this and use electrospray ionization-MS and inductively coupled plasma atomic emission spectroscopy (ICP-AES) to confirm the presence of eight zinc ions in parkin, two in each RING finger domain.

## Function

The ubiquitin-proteasome system is responsible for protein quality control, cell cycle progression, and signaling cascades. The system is composed of a ubiquitin molecule, a series of three enzymes, E1, E2, and E3 and the proteasome. Ubiquitin, a highly conserved protein consisting of 76 amino acid residues, is most frequently added covalently to a single lysine in the target protein. A minimal chain of four ubiquitin molecules (polyubiquitination) is required as a signal for degradation by the proteasome (Hershko and Ciechanover 1998). Monoubiquitination is a non-proteolytic signal used in many processes including receptor internalization, DNA repair and endosomal sorting (Mukhopadhyay and Riezman 2007). Multiubiquitination, addition of ubiquitin to multiple lysines on one substrate, can also play a role in receptor internalization and endocytosis (Haglund et al. 2003). These processes are regulated by the deubiquitinating enzymes termed DUBs. There are over 100 of these DUBs in humans and their role in the cell is to reverse the ubiquitination of target proteins (Reyes-Turcu et al. 2009). DUBs also regenerate monoubiquitin from polyubiquitin chains and are believed to negatively regulate ubiquitin conjugation by associating with E3 ligases (Ventii and Wilkinson 2008).

The ubiquitin activating enzyme (E1) initially forms a thioester bond with the ubiquitin molecule through an ATP dependent process. A similar thioester bond is formed with the ubiquitin conjugating enzyme (E2) when the ubiquitin is transferred from the E1. At this point, the ligating enzyme (E3), parkin in this case, recognizes the E2 with the activated ubiquitin and also recognizes the substrate protein and facilitates the transfer of the ubiquitin molecule to the substrate. E3 ubiquitin ligases are divided into two main categories: HECT E3s and RING E3s. HECT (homologous to E6AP carboxy terminus) E3's form an intermediate with the ubiquitin molecule whereas RING E3s only provide a scaffold for E2s and substrate proteins to interact and never form an intermediate with ubiquitin (Rankin et al. 2001).

Eukaryotic cells have one E1, a few dozen E2s and over a hundred E3s. The two E2s that interact with parkin are Ubc7 and Ubc8 (Zhang et al. 2000). A crystal structure of UbcH7 bound to c-Cbl, another E3, was solved by the Pavletich group (Zheng et al. 2000). c-Cbl shares some similarity to parkin in that they both have a linker domain and a classical RING finger domain but c-Cbl lacks any other RING finger domains. It is possible that the E2 UbcH7 will bind to parkin in a very similar manner as c-cbl. The structure from the Pavletich group revealed that both the linker and the RING finger are involved in binding of UbcH7. They showed that UbcH7 loops L1 and L2 insert into the shallow groove provided by the RING domain.

## Substrates

In the last ten years parkin's known substrates have slowly been revealed. It is still unclear what method parkin uses to recognize its substrates. In yeast, some E3s bind to exposed hydrophobic areas of the substrate protein, (Johnson et al. 1998) while the E3 CHIP (carboxyl terminus of the Hsc70-interacting protein) binds to chaperones that then identify substrate proteins (Cyr et al. 2002), and other E3s recognize substrates that have been phosphorylated; these motifs are called phosphodegrons (Rogers et al. 1986). The first of these substrates to be identified was the synaptic vesicle-associated protein CDCrel-1, (cell division control-related protein 1) a member of the septin family (Zhang et al. 2000). CDCrel-1 is expressed primarily in the nervous system and its association with synaptic vesicles could signify some involvement in dopamine secretion but its role in vesicles is still unclear. Overexpression of CDCrel-1 in substantia nigral neurons results in dopamine-dependent neurodegeneration (Dong et al. 2003) and it is not surprising that CDCrel-1 accumulates in the brains of ARJP patients (Choi et al

2003). In addition, it has been shown to interact with the C-terminal RING domain of parkin and mutations in ARJP inhibit its degradation by parkin (Zhang et al. 2000).

Another parkin substrate is Pael-R, (Parkin associated endothelin-receptor like receptor) a G-protein coupled transmembrane protein (Imai et al 2001). Pael-R is expressed in brain tissue and can induce the unfolded protein response (UPR) when it is unfolded or insoluble and then becomes a substrate for parkin ubiquitination. Expression of UPR is a stress response to accumulation of misfolded or unfolded proteins in the endoplasmic reticulum (Mori 2000). Upregulation of parkin mRNA results in protection of cells from UPR. Additional experiments using transfected cells resulted in an increased resistance to UPR whereas a mutant parkin protein lacking the ability to recruit E2s resulted in no protection from UPR (Imai et al. 2000). Parkin, like other RING E3s (e. g. Mdm-murine double minute oncogene) is also its own substrate and self-ubiquitinates to promote its own degradation (Zhang et al. 2000, Yamamoto et al. 2005). Many of the mutations associated with ARJP in the RING finger domains within the RIR either impair or inhibit parkin's self-ubiquitination.

One of the most well studied parkin substrates is  $\alpha$ -synuclein.  $\alpha$ -synuclein is found mainly in the presynaptic termini of neurons but as of yet has no known function although it does interact with several proteins that regulate dopamine release (Murphy et al. 2000). Ubiquitinated  $\alpha$ -synuclein is the major component of the Lewy bodies (inclusion bodies for protein aggregates specific to neurons) seen in sporadic PD, which are not present in ARJP. This is a distinct difference between the familial and genetic form of PD and could be explained if parkin's ability to ubiquitinate proteins is required for Lewy body formation. As of yet, only a rare form of O-glycosylated  $\alpha$ -synuclein has been identified as a substrate for parkin and this same rare form has been shown to accumulate in the brains of ARJP patients (Shimura et al. 2001). While searching for parkin substrates using a yeast two-hybrid screen, the Feng group identified MAP1A as a positive clone. They observed that the binding was very weak but significantly stronger at 37°C versus 4°C indicating that parkin might be binding to MAP1A indirectly (Ren et al. 2003). This led them to identify  $\alpha$ - tubulin and  $\beta$ -tubulin as substrates for parkin. They showed that parkin enhances both the ubiquitination and the degradation of  $\alpha$ - tubulin and  $\beta$ -tubulin. They also demonstrated that parkin mutants associated with ARJP patients were not able to ubiquitinate or degrade  $\alpha$ - tubulin and  $\beta$ -tubulin.

### **Parkin-microtubule associations**

Alpha- and beta-tubulin are not only substrates for parkin's E3 ligase activity but may also act as unique binding partners. In addition to their work showing  $\alpha$ - tubulin and  $\beta$ -tubulin as ubiquitination substrates for parkin, the Feng group also used confocal microscopy to demonstrate that parkin colocalizes with tubulin in rat neuron and glial cells (Ren et al. 2003). They also used coassembly assays to demonstrate that parkin binds to assembled microtubules in vitro even in the presence of 2M salt (Ren et al. 2003) and more surprisingly suggested that parkin remains bound to the heterodimer in the presence of the microtubule depolymerizer colchicine. To date, no other microtubule binding protein has demonstrated the ability to remain bound to the heterodimer after microtubule depolymerization. Yang et al. used coassembly assays to define the microtubule binding domains in parkin as the linker, RING1 and RING2 domains (Yang et al. 2005). These are large domains so specific amino acid interactions are still not known.



Parkin has recently been shown to enhance taxol's ability to stabilize microtubules in vitro and in MCF7 breast cancer cells in a dose dependent manner (Wang et al. 2009). Binding experiments using parkin and preformed microtubules with or without subtilisin treatment to remove the C-terminus were preformed and followed by cosedimentation. Parkin remained in the pellet of the microtubules without subtilisin but was found in the supernatant in subtilisin-treated microtubules indicating that not only is the C-terminal tail required for parkin binding but that parkin binds along the outside of the microtubule (Wang et al. 2009).

To further investigate the role of parkin with microtubules, Wang et al. evaluated parkin expression in breast cancer tissues taken from patients who had received preoperative taxol treatment. They observed that patients with the highest parkin expression had the best response to the taxol treatment and those with no or low parkin expression had the poorest response to taxol treatment; no relationship was observed between parkin expression and drugs that did not target microtubules. In addition, Wang et al. investigated taxol sensitivity in primary cultures of breast cancer cells taken from patients who did not elect for preoperative chemotherapy. He found similar results in those primary cells treated with taxol. Samples taken from patients who had the highest parkin expression levels responded the best to taxol treatment whereas those samples with no or low parkin expression had little if any response to taxol treatment. Interestingly, the effect of parkin on taxol sensitivity was abrogated by deletion of the microtubule binding domain indicating that a physical interaction between parkin and the microtubule must occur. It is unfortunate that in Wang's publication they are unclear as to which microtubule-binding domain was deleted and thus these experiments should be repeated if possible.

It is clear that parkin plays a critical role as an E3 ubiquitin ligase and that alteration of this activity is most likely related to ARJP. What hasn't been addressed is the role of microtubule binding in parkin's function. Our goal was to define the interaction interfaces between parkin and the microtubule by using a combination of cryo EM and image processing. Our lab has previously used methods that resulted in an 8 Å resolution map of the microtubule (Li et al. 2002) and 8-9 Å maps of kinesin bound to a microtubule (Sindelar and Downing 2007, Sindelar and Downing, in preparation). Similar methods will be used to determine the orientation of parkin bound to microtubules including docking of the solution structures for the ubl and IBR domains. At the expected resolution of 9 Å, we would be able to dock the known structures of the ubl and IBR domains precisely into the parkin structure. This would provide insights on how the domains of parkin, a new microtubule associated protein, interact with each other and with tubulin, and also show where the mutations associated with ARJP are within in the structure. In order to test whether we would be able to distinguish the RING domains from each other in an experimental density map, we calculated 3-D maps of candidate RING domains at the resolution that was achieved in earlier work with kinesin in our lab. We used known structures of RING finger domains, (c-cbl to represent parkin's RING1 domain and HHARI to represent parkin's RING2 domain) obtained from both crystallographic and NMR methods, along with the "copy from pdb" function in SPIDER, to produce maps at about 8 Å resolution. At this resolution the differences in the domain structures are sufficiently clear that we expect that we could identify the individual domains in a map of parkin bound to microtubules at this resolution. Understanding the relationships among these various elements should improve our understanding of how parkin function is lost, and could even eventually lead to therapies to recover its function.

## Experimental Procedures

### Cloning

We have investigated expression and purification of full length human parkin, a version truncated by removal of the ubl, and full length rat parkin. All reagents were purchased from Sigma unless otherwise noted. PARK2 cDNA (human) was a generous gift from Jian Feng (State University of Buffalo). Full length PARK2 cDNA and a truncated PARK2 cDNA (minus the N-terminal 76 amino acids) were originally cloned into the pMAL p2X expression vector with the malE gene encoding the maltose binding protein (MBP; 42,000 Daltons) fused to the lacZ $\alpha$  gene, disruption of which causes a color change in colonies when spread on Xgal plates (New England Biolabs) (Figure 10A). The recognition site for Factor Xa (IEGR) is located between the malE gene and the multiple cloning site. Resistance is conferred by the ampicillin gene. This vector was chosen because the MBP tag would not interfere with the ligase activity located at the C-terminal end of parkin and previous reports that parkin with a His tag was insoluble. The pMAL p2X vector also has a short signal peptide to direct the fusion protein to the periplasm to assist with proper protein folding. PARK2 cDNA was amplified by PCR using oligos with incorporated EcoRI and BamHI restriction sites FullPARK 5'=CGTCTAGGATCCATGATAGTGTGGTTCAGGTTTC, TruncPARK 5'= CGTCTAGGATCCGGTCAAGAAATGAATGCAACTG; PARK 3'=GTGTACGAATTCCTACACGTCGAACCAGTGG. Utilizing the EcoRI and BamHI sites for cloning of PARK2 cDNA leaves an isoleucine and a serine after removal of the MBP tag by Factor Xa. Both constructs were transformed into RIPL BL21 codon specific E. coli competent cells to avoid mistranslation of lysine for arginine. RIPL BL21 competent cells contain extra copies of the tRNA genes for arginine, isoleucine, proline and leucine. The plasmid containing the tRNAs confers chloramphenicol resistance.

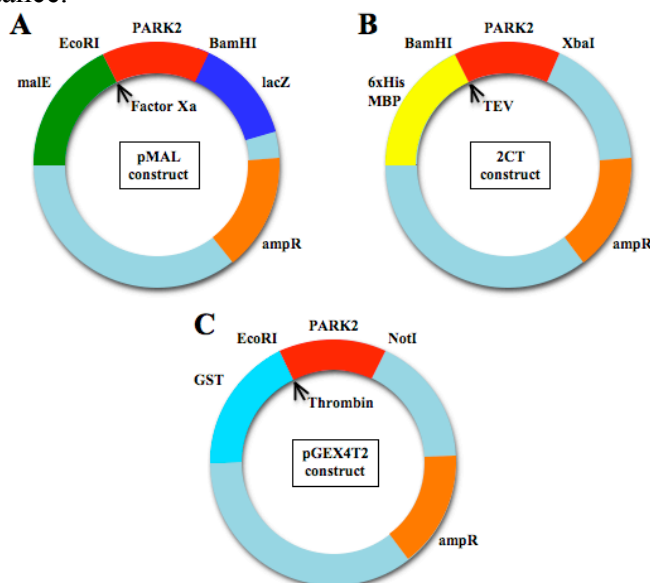


**Figure 10. Schematic of expression vectors.** A. pMAL construct with N-terminal MBP tag and Factor Xa cleavage site. B. 2CT construct with 6xHisMBP tag and TEV cleavage site. C. pGEX4T2 construct with GST tag and thrombin cleavage site.

Additionally, full length and truncated PARK2 cDNA were cloned into the 2CT vector (Figure 10B) using BamHI and XbaI restriction sites (Macro Lab, University of California, Berkeley). The 2CT vector has an N-terminal 6His and MBP tag followed by a Tobacco Etch Virus (TEV) cleavage site (ENLYFQG). The ampicillin gene confers resistance.

Rat PARK2 cDNA was a generous gift from Edward Fon (McGill University). Full length rat PARK2 cDNA was amplified by PCR using oligos with incorporated EcoRI and NotI restriction sites pGEX 5' = GGGCTGGCAAGCCACGTTTGGTG and pGEX 3' = CCGGGAGCTGCATGTGTCAGAGG. Cloning into the pGEX4T1 expression vector utilized the EcoRI and NotI sites (Figure 10C). The pGEX4T1 vector has an N-terminal glutathione S-transferase (GST) tag (26,000 Daltons) followed by a thrombin cleavage site (LVPRGS). The ampicillin gene conferred resistance. The pGEX4T1 parkin was transformed into RIPL BL21 codon plus E. coli competent cells (Stratagene).

All transformants (full length and truncated PARK2 in pMAL, full length and truncated PARK2 in 2CT and full length PARK2 in pGEX4T2 vectors) were grown in LB supplemented with 50 µg/ml ampicillin and 50 µg/ml chloramphenicol.

## Purification

For all constructs, cells were grown at 37°C to an OD<sub>600</sub> of 0.6. Cells were then moved to 15°C and protein expression was induced with 50µM IPTG for 16 hours in the presence of 500µM ZnSO<sub>4</sub>. Harvested cells were resuspended in lysis buffer (20mM Tris HCl pH 7.4, 120 mM NaCl, 1mM DTT) with EDTA-free protease inhibitor (Roche) and stored at -20°C. All remaining purification steps took place at 4°C.

For pMAL and CT2 parkin purification, cells were lysed using three passes through an EmulsiFlex-C5 (Avestin) followed by centrifugation at 9,000 x g for 20 minutes. Supernatant from the spin was applied to an amylose column on a Pharmacia FPLC using 10mM maltose for elution. Collected fractions were assayed for protein content prior to cleavage. The MBP tag was cleaved from the pMAL parkin constructs using 1mg Factor Xa for every 100mg of parkin fusion protein.

The 6xHisMBP tag was cleaved from the 2CT parkin constructs with 1mg TEV protease/20 mg parkin for 16 hours. Parkin was separated from the 6HisMBP tag using a HisTrap FF (GE Life Sciences) column after addition of an additional 300 mM NaCl. The flow through was desalted and concentrated using an Amicon Ultra (Millipore) with a 10 KDa cutoff and separated on a Superdex 200 gel filtration column (GE Life Sciences).

For pGEX4T1 parkin, cells were lysed using three passes through an EmulsiFlex-C5 (Avestin). The cell lysate was supplemented with Triton X-100 to a final concentration of 1% and rotated end-on-end at 10 seconds/rotation for 30 minutes prior to centrifugation at 20,000 x g for 20 minutes. Supernatant from the spin was applied to a GSTrap FF column (GE Life Sciences) on a Pharmacia FPLC using 20 mM reduced glutathione for elution. Collected fractions were assayed for protein content prior to combined dialysis and cleavage with 10 units thrombin/mg of pGEX4T1 parkin for 16 hours. Parkin was dialyzed 300 fold against 20mM Tris HCl pH 7.4, 120 mM NaCl, 1mM DTT using a Slide-a-lyzer cassette (Pierce) for removal of glutathione. The GST tag was removed using a GSTrap FF column. Protease inhibitor was added to the flow through to inactivate the thrombin and parkin was concentrated using an Amicon Ultra (Millipore) with a 10 KDa cutoff and then separated on a Superdex 200 gel filtration column (GE Life Sciences).

## **Binding assay**

Collected samples were used in microtubule pelleting assays to verify binding to microtubules. Tubulin (Cytoskeleton Inc.) was centrifuged for at 4°C for 10 minutes at 100,000 x g to remove aggregates. Microtubules were polymerized by adding GTP to a final concentration of 1mM with incubation at 37°C for 30 minutes and then stabilized with 50µM Taxol. Parkin was added in equimolar and two molar excess to preformed microtubules and incubated for 10 minutes at 37°C before centrifugation at 50,000 x g for 20 minutes. Samples from the supernatants and pellets were separated using a denaturing 4-20% polyacrylamide gradient gel (Pierce) and stained for protein using GelCode (Pierce) or transferred to PVDF (Millipore) and probed with mouse anti-tubulin or mouse anti-parkin antibodies (Sigma) and a goat anti-mouse HRP secondary antibody (Santa Cruz Biotechnology).

## **Computational alignment**

Protein sequences obtained from the UniProt database were used for multiple sequence alignments using ClustalW (Jain et al. 2009).

## **Cryo electron microscopy**

Parkin was added to taxol-stabilized microtubules in two- to four- molar excess. Parkin decorated microtubules were prepared for EM by applying 3 µl of solution to Quantafoil 300 mesh copper grids at room temperature with 80% humidity. All grids were glow discharged for 15-20 seconds. The grid was blotted for 3.5-4 seconds using #1 Whatman filter paper and then plunge frozen in liquid ethane using a Vitrobot (FEI). Negatively stained samples were prepared by applying 3 µl of sample to a carbon coated 300 mesh grid, washing with water, blotting with #1 Whatman filter paper, floating the grid over a 15 µl drop of 2% uranyl acetate and blotting with #1 Whatman filter paper. Frozen-hydrated samples were examined using a JEOL 4000 electron microscope at 400 kV with the specimen held at approximately -170°C. Images were taken 1-2 µm underfocus on film (Kodak) at a magnification of 60,000.

## **Image processing and analysis**

Film was scanned on a Nikon scanner robot with a 6.35 µm step size, resulting in a pixel size of 1.14 Å. Microtubules were boxed into short segments with 90% overlap according to the criterion of Egelman (Egelman 2007). The segments were binned 4 fold to speed computation, and masked such that 2 helical turns were present in each image using programs from the EMAN (Ludtke et al. 1999) and SPIDER (Frank et al. 1996) processing packages. The segments were then subjected to cycles of reference-free classification using a topology-representing network algorithm (van Heel et al. 1996) to generate node images alternating with multi-reference alignment using the IMAGIC software package (Ogura et al. 2003), implemented as described by Ramey et al. (Ramey et al. 2009). This procedure sorts segments based on microtubule protofilament number, the presence of bound protein, and helical order. Power spectra and 1-D projections were generated using a procedure implemented in the SPIDER processing package (Frank et al. 1996).

## Results

### Purification

All constructs of parkin were expressed cytoplasmically in RIPL BL21 cells at reasonable levels, 3-4 mg/liter of culture. Proper expression requires supplementing the media with zinc, since parkin coordinates 5-8 Zn<sup>++</sup> ions chelated by interactions with cysteines and will not fold properly without the zinc ions resulting in aggregation (Capilli et al. 2004). pMAL parkin expressed in the absence of zinc had increased aggregation and unsuccessful cleavage of the MBP tag. Cleavage of full length parkin and truncated parkin should result in parkin fragments with a size of 52,000 and 42,000 Daltons, respectively. Cleavage using Factor Xa resulted in parkin fragments that didn't match expected molecular weight sizes. Western blots of cleavage reactions using an antibody to parkin detected a fragment with a molecular weight of 34,000 Daltons. Western blots using an MBP antibody detected an MBP fragment at 60,000 Daltons for the full length construct and at 49,000 Daltons for the truncated construct. This cleavage pattern indicated the presence of a possible secondary cleavage site. Secondary cleavage sites become more accessible to Factor Xa if the protein is unstable or unfolded. A glycine/arginine site is present in the linker region of parkin (residue 139-140) and cleavage at this site results in a parkin fragment of 34,000 Daltons as seen above.

Full length and truncated parkin were cloned into the 2CT vector due to the higher specificity of the thrombin site. Prior to these experiments, DTT was not used in the interest of the cysteines used to coordinate zinc ions. Further inspection of the parkin sequence revealed 2 cysteines out of 36 that were not involved in RING fingers. Because of these additional cysteines and the previous problems with aggregation, 1mM DTT was added to all purification buffers. Even with protection against cysteine crosslinking, protein aggregation increased after cleavage of the N-terminal tag from the truncated CT2 vector accounting for approximately 90% of total protein (Figure 11). Full length constructs in the CT2 vector reproducibly had immense protein aggregation and an unexplained cleavage in the linker domain leaving a 35 KDa truncated protein. Truncated parkin in the CT2 vector also suffered from protein aggregation and the same 35 KDa truncation. Increasing the DTT concentration was not possible based on experiments performed using increasing amounts (0.1, 1 and 10mM) of DTT on taxol stabilized microtubules that showed 10mM DTT unraveled microtubules (data not shown). Aggregation increased after removal of the MBP tag and resulted in final protein yields of < 50 µg.

In hopes of avoiding both the truncation and aggregation problems, rat parkin in pGEX4T2 was expressed in BL21 codon specific competent cells. Hristova et al. demonstrated that the rat parkin sequence differed enough from human at the highly susceptible linker region to be stable during purification (Hristova et al 2009). After removal of the GST tag the parkin concentration was ~ 6mg/ml. Gel filtration of rat parkin designated half of the total protein as aggregated (Figure 11). The total soluble parkin content was still considerably higher than previous constructs using human parkin and rat parkin could be concentrated to higher levels than human parkin for unknown reasons.

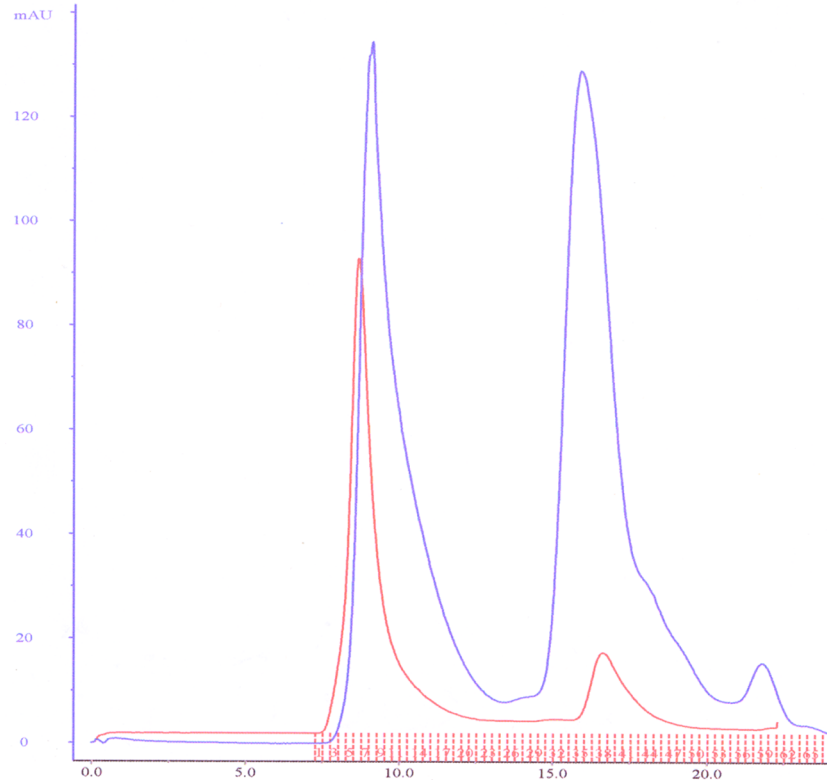


**Figure 11. Aggregation levels differ between rat and human parkin.** Representative chromatogram from gel filtration of human (red line) and rat (blue line) parkin protein using a Superdex 200 column. The left peaks are in the high molecular range (>500,000 Daltons) of elution while the peaks on the right are approximately 50,000 Daltons as determined by sizing calibration beads. The additional peak seen in the rat parkin profile is approximately 35,000 Daltons and corresponds to thrombin. Human parkin has a higher tendency to form protein aggregates as seen by the larger distribution of parkin in the left, high molecular weight peak. Rat parkin has an equal distribution of aggregated (left peak-blue) to non-aggregated parkin (right peak-blue) distribution.

### **Binding assay**

Parkin was added to taxol-stabilized microtubules in two-fold excess for binding assays. To confirm parkin was bound to microtubules, the complex was centrifuged and samples from the supernatant and pellet were analyzed by Western blot. Parkin bound to microtubules remains in the pellet fraction while unbound parkin is found in the supernatant fraction. As seen in the tubulin blot in the 1:1 and 2:1 pellet lanes (Figure 12) parkin cosediments with microtubules. A positive control, parkin without microtubules, is shown in the parkin blot in the 1:0 and 2:0 pellet lanes (Figure 11) to confirm that parkin alone does not pellet.

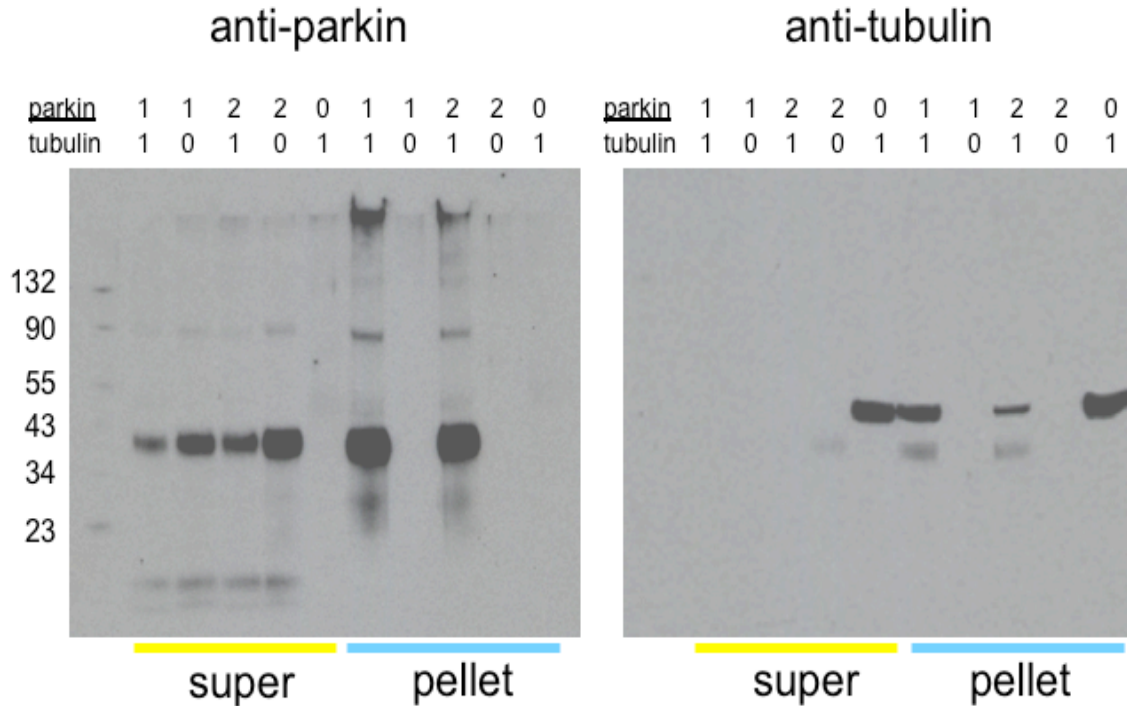


**Figure 12. Parkin binds to microtubules in pelleting assays.** Western blots show hybridization of parkin protein (left) and tubulin protein (right) in pelleting fractions at different molar ratios. Parkin was added to taxol-stabilized microtubules in one- and two-fold excess for binding assays. To confirm parkin was bound to microtubules, the complex was centrifuged and samples from the supernatant and pellet were analyzed by Western blot. Parkin bound to microtubules or highly aggregated parkin remains in the pellet fraction while unbound parkin is found in the supernatant fraction. Parkin without microtubules is shown in the 1:0 and 2:0 lanes on the parkin blot to confirm that parkin alone does not pellet. Blots were probed with mouse anti-tubulin or mouse anti-parkin antibodies and a goat anti-mouse HRP secondary antibody. Western blots are not quantitative.

### Electron microscopy

Initial preparations of parkin bound to microtubules prepared for cryo EM resulted in microtubules with partial parkin decoration (Fig 13). The monomeric repeat of tubulin produces a 40 Å layer line in the Fourier transform of an image. The 80 Å dimer spacing is very weak due to the similarity of  $\alpha$ -tubulin and  $\beta$ -tubulin and therefore indistinguishable at low resolution. An object bound to the dimer will produce an 80 Å spacing. The presence of an 80 Å layer line in the power spectrum suggests parkin bound specifically to the dimer (Figure 14). The low intensity of the 80 Å layer line denotes incomplete occupancy of parkin on the microtubule. Full decoration of the microtubule by parkin would result in a much stronger 80 Å layer line.

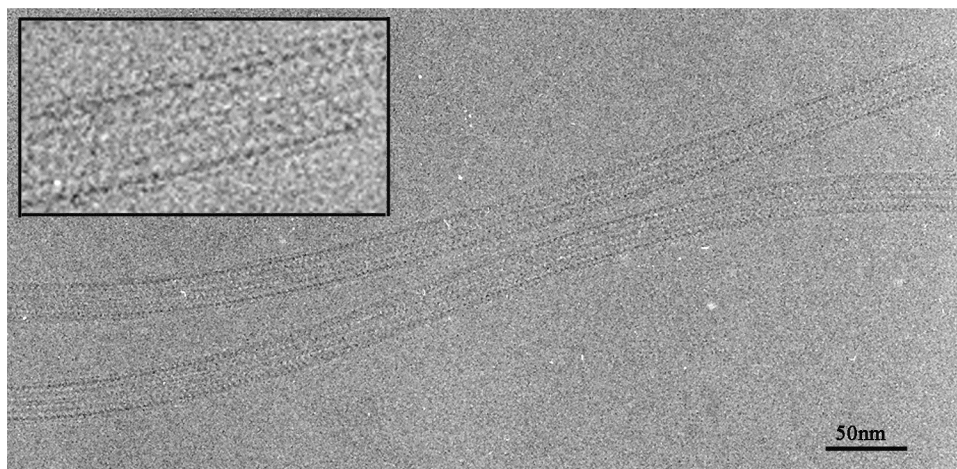


**Figure 13. Electron micrograph of parkin-decorated microtubules.** Parkin decorated microtubules were imaged on the JEOL 4000 electron microscope at a magnification of 60,000 in cryo conditions. The protofilaments number of pictured microtubules were identified as 14 based on the profile of intensity across the microtubule and the variation of contrast along the microtubule. Scale bar=50nM.

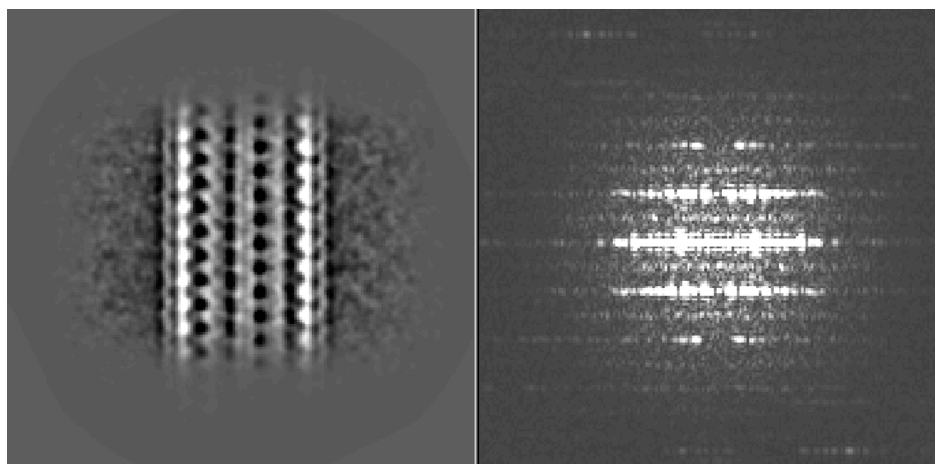


Figure 14. Class average and associated power spectrum of parkin-decorated microtubules. Small segments from micrographs of parkin decorated microtubules were assigned different classes based on similarity and averaged. The left image is one of many class averages with an increased signal to noise ratio. The power spectrum shows the 40 Å layer line that correlates to the monomeric spacing of tubulin. An 80 Å layer line represents parkin binding to the dimer and not individual monomers. The weak intensity in the 80 Å layer line (in comparison to the 40 Å layer line) indicates incomplete decoration of the microtubule by parkin.



## Discussion

This work reports the first attempt to visualize the E3 ubiquitin ligase parkin bound to microtubules. Previous groups reported a strong binding affinity between parkin and not only the microtubule but also the heterodimers (Ren et al. 2003). Their work lacked evidence to confirm that parkin was binding to intact microtubules and not aggregated tubulin. They also did not attempt to describe how parkin was binding along the microtubule.

Initial attempts at parkin purifications were plagued by complications arising from improper folding of the RING fingers, due to the requirement for 8 zinc atoms per parkin molecule, truncation of the protein caused by cleavage in the linker domain by an unspecified source, and aggregation presumably from free cysteines forming disulfide bonds. To ensure proper folding of RING fingers initial cultures were expressed in 500  $\mu\text{M}$   $\text{ZnSO}_4$  and all buffers used during purification procedures were supplemented with 100  $\mu\text{M}$   $\text{ZnSO}_4$ . In addition to the  $\text{ZnSO}_4$ , 1 mM DTT or 1 mM TCEP was used to keep the remaining cysteines reduced. Work done in the 1970's by Cornell and Crivaro revealed that metal ions can form stable complexes with low molecular weight thiols (Cornell and Crivaro, 1972) which would explain why our initial attempts to use 1mM DTT with 100  $\mu\text{M}$   $\text{ZnSO}_4$  were unsuccessful. This study showed that 20  $\mu\text{M}$   $\text{Zn}^{+2}$  was sufficient to completely reverse the inhibitory action that 1.7 mM DTT would have on rat liver histadase. While TCEP is tolerant of nickel, making it useful for histidine tagged protein purification, metals like copper, silver and zinc completely inactivate TCEP (Thermo Scientific 2009). Using  $\text{ZnSO}_4$  in the growth media during protein expression and leaving zinc out of the buffers used in the purification strategy circumvented these problems. This allowed for the use of 1 mM DTT during the purification.

Hristova et al. have been the only group to successfully purify parkin free of a tag by using rat parkin in a pGEX4T1 expression vector. We along with several other groups observed a 12 KDa cleavage product when purifying human parkin (Rankin et al. 2001, Hrsitova et al. 2009). The cleavage occurs in the linker domain resulting in a protein missing the ubl domain and the first 28 residues of the linker domain (Figure 7). This region contains the most variability between human and rat parkin and use of the rat gene may account for the successful purification of several milligrams of full length parkin by Hristova et al. Therefore, we switched to the rat parkin cloned in a pGEX4T1 vector, which reduced aggregation, and obtained a full length form of parkin. The improvement in aggregated to non-aggregated parkin is clear in the elution profile from gel filtration (Figure 11).

Alignment of rat and human parkin protein using ClustalW confirmed that the linker domain was the area with the most variation. (Figure 15) Analysis of the cysteine content revealed that the rat parkin has one less cysteine in the linker region than human parkin. Thirty-two of the thirty-six cysteines in parkin are located in the RING finger domains. Of the remaining four cysteines, three are found in structured domains. The remaining cysteine is in an area of the linker believed to be unstructured. This cysteine is not present in rat parkin, and its absence could be responsible for the improved solubility of rat parkin. In the future, mutating this cysteine could prove to be useful.

To confirm earlier experiments by Feng et al. that showed parkin binding to microtubules, full length rat parkin was added to taxol-stabilized microtubules and used in a binding experiment. The results from the Western blot show that parkin pellets with microtubules in a binding experiment but that parkin alone does not pellet (Figure 12). One interesting observation on the tubulin blot is seen in the tubulin control (0:1 lanes in the super

and the pellet). During the pelleting assay, some tubulin that does not assemble into microtubules remains in the supernatant fraction. This unassembled tubulin is not seen in the lanes where parkin has been added, consistent with the observation that parkin enhances tubulin polymerization (Wang et al. 2009). This effect has been observed in several Western blots and has also been observed by the Zhou group (Wang et al. 2009). In their experiments using parkin with an MBP tag they showed that increasing amounts of parkin resulted in increased taxol binding, increased G2/M arrest and increased ability to promote microtubule assembly.

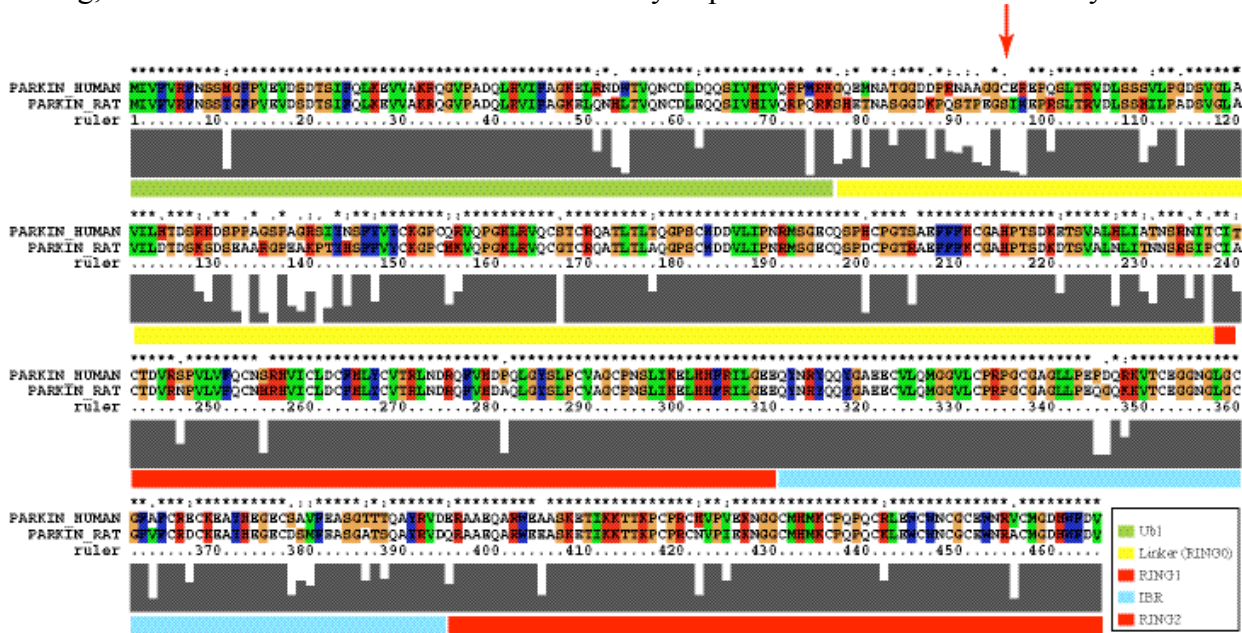


**Figure 15. Alignment of parkin protein sequences from human and rat.** Parkin sequences were retrieved from the National Center for Biotechnology Information (NCBI) for *Rattus norvegicus* (rat) and *Homo sapiens* (human). Sequences were aligned using ClustalX. Variability among sequences seen in the linker region. Arrow identifies cysteine 95 in human parkin and the corresponding serine in rat. Residues are colored as follows: orange= G, P, S, T; red= H, K, R; blue= W, Y; aqua= F; green= I, L, M, V; and white= A, C, N, D, E, Q. The histogram at the bottom of the sequences reflects conservation of amino acids at each position.

Promising results have been obtained in our early attempts to visualize the parkin-microtubule complex. Initial attempts to view parkin bound to taxol-stabilized microtubules using 2% uranyl acetate were unsuccessful. The expected 80 Å layer line was not visible in the Fourier transform of the images. On the other hand, cryo EM samples had an obvious 80 Å layer line visible in transforms of the raw images indicating that parkin is binding to the dimer repeat (Figure 14). It was observed that the 80 Å layer line was weaker than the 40 Å layer line, indicating that microtubules were not fully decorated or occupied. Addition of more parkin to taxol-stabilized microtubules prior to sample preparation for EM should solve this problem. If there is an unforeseen issue with how parkin binds additional constructs can be prepared that solely contain the RIR supradomain (R1, IBR, and R2). It is also still unclear in which part of the linker the microtubule-binding domain resides. Peptides representing different segments of the linker region could be synthesized and used in binding assays to map this region. Currently,

more EM data is needed at a better occupancy for a reconstruction with sufficient detail to provide insights on the nature of the parkin-tubulin interaction.

## **Chapter 3.**

# **Tau-Microtubule Interactions**

## **Introduction**

### **Structure and function of tau**

Tau was first identified as a microtubule binding protein by the Kirschner group and accounts for greater than 80% of total MAPs in neural tissue (Weingarten et al. 1975, Cleveland et al. 1977). MAPT, the gene that encodes the tau protein, is located on the long arm of chromosome 17 and has 16 exons. Alternative splicing of exons 2, 3, and 10 produces the 6 major isoforms of tau found in adult brains ranging in size from 352-441 amino acids (Andreadis et al. 1992). Splice variants differ in the presence of two inserts at the N-terminal region and three (3R) or four (4R) imperfect repeats in the C-terminal region (Figure 16). Fetal brains have only one isoform, 3R, and is more highly phosphorylated than tau in adult brain (Goedert et al. 1995). All tau isoforms promote tubulin polymerization and stabilize microtubules. 3R tau induces slower microtubule assembly than 4R tau and has a weaker stabilizing effect. Since the developing brain needs to have a more dynamic cytoskeleton, the 3R isoform would allow for such dynamics. An imperfect repeat domain in tau makes up the microtubule-binding domain (Gustke et al. 1994, Goode and Feinstein 1994). This distinction separates tau into 2 domains: the projection domain that encompasses the N-terminal two-thirds of the protein and the microtubule domain, which consists of the C-terminal third of protein. The role of the projection domain is still unclear although it is postulated to participate in determining the spacing between microtubules in neurons (Chen et al. 1992). The microtubule binding domains are positively charged allowing them to bind to the highly negatively charged C-terminal tail of tubulin and promote microtubule assembly and stabilize microtubules once formed in the axons. The 3R and 4R repeats in the microtubule binding domains are composed of repetitive sequences of 31 or 32 residues (Figure 17). Each repeat contains a proline-glycine-glycine-glycine (PGGG) repeat that binds tightly to microtubules but does not promote assembly and has been suggested by Mandelkow to form a  $\beta$ -turn (von Bergen et al. 2001).

Tau shares similar characteristics with the other neuronal MAP, MAP2. MAP2 has three to four microtubule binding domains at its C-terminal and like tau and has a highly negatively charged projection domain, although the MAP2 projection domain is much larger accounting for its molecular weight (280,000 Da versus 45,000-60,000 Da for tau). Splicing of the MAP2 gene results in 4 isoforms; MAP2a and MAP2b, which have the largest projection domains and MAP2c and MAP2d with sizes closer to those of tau. MAP2c is only expressed during early phases of neuronal development and is then downregulated (Garner et al. 1988). MAP2b is expressed constitutively while MAP2a expression rises as MAP2c levels drop (Dehmelt and Halpain 2005). In rats, MAP2d expression is detected at day five postnatal but mRNA is detected throughout all stages of development (Fehrat et al. 1994). Unlike tau, MAP2c and MAP2d have been shown to interact with f-actin through their microtubule-binding domains and this interaction is essential for neurite initiation (Griffith and Pollard 1982, Roger et al. 2004, Ferhat et al. 1996).

Phosphorylation is important for tau's physiological function and also key to understanding its pathological activity. Human tau has an unusually high cysteine and threonine content that is susceptible to phosphorylation (45 serines and 35 threonines). Tau can be

phosphorylated by several kinases including cAMP-dependent protein kinase, Ca<sup>2+</sup>-calmodulin-dependent protein kinase, casein kinases, cdc2 kinase, protein kinase C, and MAPK (for review see Cassimeris and Spittle 2001). Phosphorylation of tau can result in weakening of the electrostatic interactions between tau and the microtubule and removal from the microtubule lattice (Marklund et al. 1996, Horwitz et al. 1997, Chang et al. 2001).

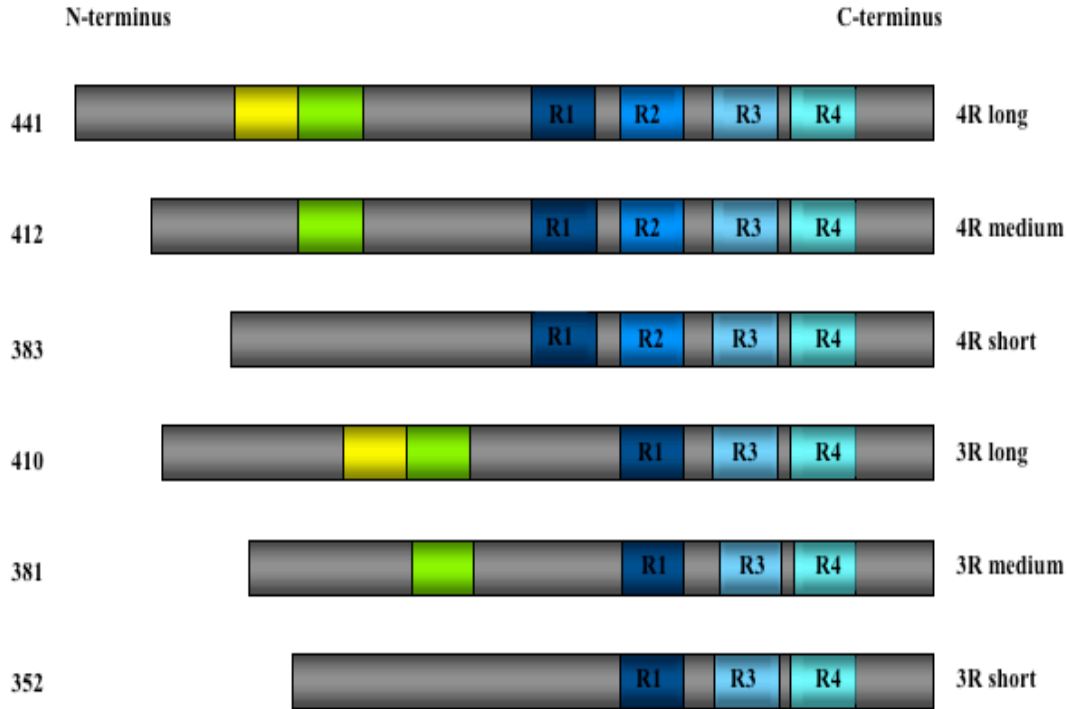


**Figure 16. Schematic of the six isoforms of tau.** Alternative splicing of tau yields six isoforms that differ in their combination of two domains in the N-terminal projection domain and the four C-terminal microtubule binding repeats. Molecular weights are listed on the N-terminal region.

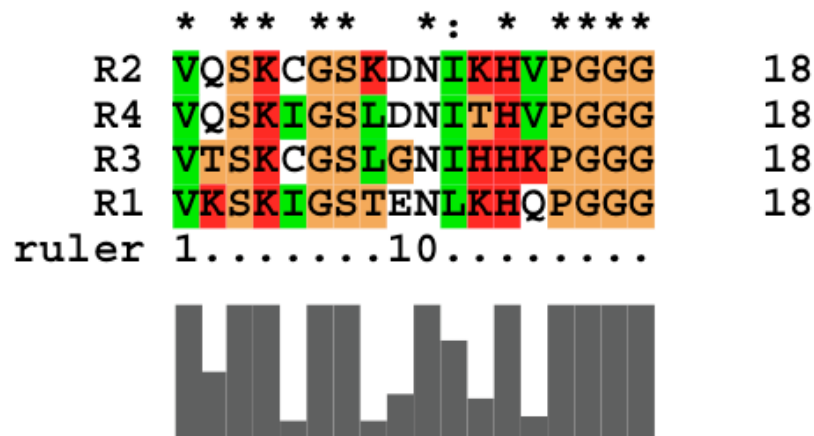


**Figure 17. Alignment of tau microtubule binding repeats from human protein sequence.** Microtubule binding repeats R1, R2, R3, R4 were aligned using ClustalX. PGGG region is completely conserved in all domains. Residues are colored as follows: orange=G, P, S, T; red=H, K, R; blue=W, Y; aqua=F; green=I, L, M, V; and white=A, C, N, D, E, Q. The histogram at the bottom of the sequences reflects conservation of amino acids at each position.

## **Alzheimer's disease**

Tau is highly expressed in neurons where it can form paired helical filaments (PHF) found in brain tissue of patients suffering from Alzheimer's disease (Goedert et al. 1988, Kondo et al. 1988). Alzheimer's disease is the most common form of dementia and is estimated to affect 35 million people worldwide. In the AD brain, tau is hyperphosphorylated at physiological sites but additionally at sites considered to be pathological. Hyperphosphorylated tau assembles into paired helical filaments that form the neurofibrillary tangles (NFT) found in the plaques of AD brains (Grundke-Iqbal et al. 1986, Lee et al. 1991). Abnormal phosphorylation of tau seen in AD is a result of upregulation of tau specific kinases or downregulation of tau phosphatases and not mutation of the tau sequence. Tau mutations are seen in a familial form of dementia, frontotemporal dementia, where most mutations cluster in the microtubule-binding domain emphasizing the importance of these domains in a functional tau (Hong et al. 1998, Bunker et al. 2006). Over 30 sites of phosphorylation in tau found in AD patient brains have been identified though only a few have been characterized. Phosphorylation of sites Thr231 and Thr181 seem to be an early event in the process that leads to AD (Arai et al. 2000, Hansson et al. 2006). Phosphorylation of Ser262 in the microtubule-binding domain results in the inability of tau to bind microtubules resulting in highly unstable microtubules (Drewes et al. 1995).

## **Microtubule-tau interaction**

Under normal conditions tau is associated with microtubules in neurons. Overexpression of tau inhibits the motor protein kinesin from binding to microtubules and thus interferes with plus-end directed trafficking of vesicles, mitochondria and other cargo (Ebner et al. 1998). Kinesin binds along the crest of the microtubule protofilaments and results indicating competition between kinesin and tau have been interpreted to indicate that tau is also binding along the crest of the protofilament (Trinczek et al. 1999). Secondary protein prediction, rotary shadowing and circular dichroism experiments have led people to believe that tau proteins are highly linear polypeptides with no detectable secondary structure (Voter and Erickson 1982, Schweers et al. 1994) but others suggest that the microtubule binding domain of tau could adopt a helical structure upon binding to the microtubule (Eliezer et al. 2005, Gamblin 2004)

Three models have been proposed for how tau binds to the microtubule. The first two models come from the Itoh lab's work on MAP2 (Ichihara et al. 2001). In their first model they suggest that MAP2 or tau could form a 'hoop' by bridging between dimers between adjacent protofilaments on the outside of the microtubule (Figure 18; model I). This stabilizing hoop surrounding the microtubule would decrease the curvature of protofilaments and restrict them from peeling away from the microtubule as seen in depolymerization. Their other model suggests that MAP2 or tau could bind along single protofilaments stabilizing the interdimer contacts (Figure 18; model II). In this model tau serves as a splint restricting curvature in the protofilament. They fail to clarify in the model whether tau would bind along the crest of the protofilaments or in the groove between the two protofilaments. A case can be made for both since binding along the crest of the protofilament supports data suggesting competition between kinesin and tau (Trinczek et al. 1999) while binding in the groove between protofilaments could stabilize the interprotofilament interaction. A third model was inspired by the observation that the PGGG motif in tau matches a part of the  $\alpha$ -tubulin sequence that fills a site analogous to the taxol binding site (Nogales et al. 1999), along with subsequent experiments which showed competition between tau and taxol (Figure 18; model III) (Kar et al. 2003, Makrides et al. 2004).

This model is very similar to the ‘hoop’ model in directionality and stabilization method but on the inside of the microtubule lumen versus the outside. These observations suggested a binding site for tau on the inside of the microtubule.

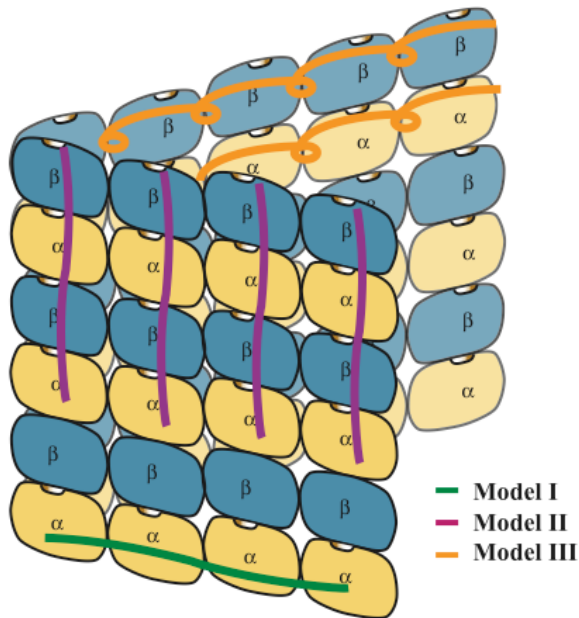


**Figure 18. Three models for tau binding to microtubules.** Schematic of microtubule showing tau binding models in green, forming a ‘hoop’ by bridging between dimers between adjacent protofilaments on the outside of the microtubule, purple, binding along single protofilaments stabilizing the interdimer contacts restricting curvature in the protofilament, and orange, bridging between dimers between adjacent protofilaments on the inside of the microtubule.

The first attempt to determine tau’s orientation on microtubules came from the Milligan lab and resulted in a structure with the resolution of around 20 Å (Al-Bassam et al. 2002). Their data showed that tau runs longitudinally along the outside ridge of the protofilaments and interacts with helices H11 and H12. Their labeling of MAP2c with undecagold demonstrated that it binds specifically to sites on the dimer, rather than indiscriminately to alpha and beta monomers. Their data on MAP2c can be translated to tau since both proteins appear to bind in the same manner.

A second cryo-EM study by the Amos lab suggested an opposing model for tau binding where tau binds partially on the inside of the microtubule and can be displaced by Taxol (Kar et al. 2003). Again, a gold label attached to one of the microtubule-binding repeats of tau localized to beta tubulin in the microtubule lumen, with minimal density on the microtubule exterior. Both models indicate that one tau molecule binds to two heterodimers or one tau for every four monomers of tubulin. The report from the Amos lab was not initially supported until meticulous kinetic analysis showed that binding constants for tau could dramatically change if tau is added before or after microtubule polymerization (Makrides et al. 2004). Adding tau before microtubule polymerization allows for incorporation inside of the microtubule lumen resulting in a tau molecule that is irreversibly bound. Addition of tau to taxol-stabilized microtubules results in tau decoration along the outside of the preformed microtubule. By obtaining our own models of tau binding under the two polymerization conditions at higher resolution we hope to clarify the discrepancy between the two models at limited resolution.

## Experimental Procedures

### Binding assays

4R-Tau was a generous gift from Christopher Berger (University of Vermont). As described in previous work tau in BRB80 buffer (80 mM PIPES, 1 mM MgSO<sub>4</sub>, 1 mM EGTA) was added at a 1:4 molar ratio to tubulin samples for both polymerization conditions binding to microtubules. We performed binding experiments using the 1:4 molar ratio followed by centrifugation at 50,000 x g to pellet microtubules and bound tau. Samples of supernatant and pellet fractions were collected and applied to a denaturing 4-20% polyacrylamide gradient gel (Pierce) and stained for protein using GelCode (Pierce) (Figure 19). For tau added after tubulin polymerization, microtubules were stabilized with 50 μM taxol prior to tau addition and then centrifuged through a 20% glycerol cushion to remove excess tau and tubulin (unbound and unpolymerized, respectively). For polymerization in the presence of tau, tau was mixed with tubulin on ice in a buffer containing 0.1 M TMAO and 5% DMSO. GTP was added to 1 mM and the sample was warmed to 37°C to polymerize microtubules. Both samples were resuspended in a low salt buffer. Microtubules polymerized in the presence of tau lack taxol and were kept at 37°C to ensure stabilization in the absence of taxol.

Additional samples of tau decorated taxol-stabilized microtubules were prepared using a molar ration of tau to tubulin of 1:2 and 1:10.

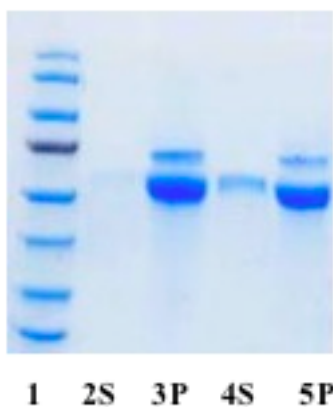


**Figure 19. Co-sedimentation of tau and tubulin.** 4-20% gradient polyacrylamide denaturing gel. S - supernatant; P - pellet. Lanes 2,3 - tau added to Taxol-stabilized microtubules; lanes 4,5, tau added before microtubule polymerization. Tau added with dimeric tubulin strongly enhances polymerization, although apparently not as much as Taxol. In all cases, essentially all tau pellets with the microtubules.

### Computational alignment

Protein sequences obtained from the UniProt database were used for multiple sequence alignments using ClustalW (Jain et al. 2009).

### Cryo electron microscopy

Tau-decorated microtubules were prepared for EM by applying 3 μl of solution to Quantafoil 300 mesh copper grids at room temperature or at 37°C with 80% humidity. All grids were glow discharged for 15-20 seconds. The grid was blotted for 3.5-4 seconds using #1



Whatman filter paper and then plunge frozen in liquid ethane using a Vitrobot (FEI). Frozen-hydrated samples were examined using a JEOL 4000 electron microscope at 400 kV with the specimen held at approximately  $-170^{\circ}\text{C}$ . Images for high resolution structure work were taken 1-2  $\mu\text{m}$  underfocus on film (Kodak) at a magnification of 60,000. To more clearly visualize protofilaments images were recorded at 4  $\mu\text{m}$ .

### **Image processing and analysis**

Film was scanned on a Nikon scanner robot with a 6.35  $\mu\text{m}$  step size, resulting in a pixel size of 1.14  $\text{\AA}$ . The image processing approach was basically similar to that described in chapter 2 for images of parkin-decorated microtubules.

#### **Image analysis:**

Images of microtubules were boxed into short segments that were then treated as single particles for alignment and averaging. Unlike the parkin case, where it was necessary to identify the tubulin dimer as well as the seam in the microtubule lattice, for this stage of the work the microtubule could be considered as a true helix with no difference between alpha and beta tubulins. This allowed easier averaging within each box and refinement of helical parameters in order to improve the alignments. The boxed images were first aligned parallel to the box edge using the strategy described by (Li et al. 2002) and then subjected to supervised classification to ensure that they were sorted into classes of the correct microtubule type. The iterative helical real space reconstruction strategy (IHRSR; Egelman, 2007) was applied to refine the symmetry parameters and reconstruct density maps.

#### **Image extraction and in-plane rotation alignment:**

The coordinate of the head and tail of each microtubule were marked out manually and used to calculate the approximate orientations of the microtubules, along with the centers of each box along the microtubule. To align the microtubule segment within each box, following the methodology described by (Li et al. 2002), the power spectrum of each box was subjected to a Radon transform. The peak position in the resultant sinogram provided the in-plane rotational angle to precisely align the microtubules parallel to the box edge.

#### **Supervised classification based on multiple model volumes:**

Classification of images by the type of microtubule (i.e., the number of protofilaments) was carried out using a supervised classification strategy. Models for several microtubule types were generated using the tubulin structure (PDB ID 1JFF, (Lowe et al., 2001)) and the theoretically predicted symmetry parameters (Chretien and Wade, 1991). The model maps for supervised classification were filtered to resolution of 36 $\text{\AA}$  in order to avoid biasing the results. Projections of the models were calculated and used as the reference set for correlation with the images to determine PF number, polarity, and start number of the microtubule, as well as the orientation. All of the images from a given microtubule were processed as a group, and only when the majority of the images (70%) fell into a certain class, the class of that group was confirmed.

#### **Refinement of symmetry parameters:**

In order to ensure that addition of tau did not alter the symmetry parameters for the microtubules, the iterative helical real space reconstruction (IHRSR) strategy was applied to the images of each microtubule type separately. The final 3D volume was obtained by weighted back projection following (Sindelar and Downing, 2007, Yonekura and Toyoshima, 2000). The symmetry was then imposed followed by compensation for the falloff in structure factor amplitudes at high resolution.

## Results and Discussion

Previous reports on visualization of tau and MAP2c bound to microtubules had all used helical reconstruction methods based on selection of microtubules with 15-protofilaments. Our lab has developed procedures that take advantage of the parallel protofilaments in 13- protofilament microtubules, which are more amenable to averaging within short microtubule segments, and led to a series of 3D reconstructions at much higher resolution. Our original approach of selecting the 13- protofilament microtubule images for data processing was not giving a signal for tau when a report appeared indicating that the presence of tau induces formation of 14- protofilament microtubules based on X-ray scattering (Choi et al. 2009). We confirmed this observation by taking cryo-EM images of microtubules without tau, with 1:10 and 1:2 (tau:tubulin monomer) at sufficiently high defocus to easily visualize protofilaments. These images were analyzed for the presence of a moiré pattern and characteristic longitudinal fringe patterns generated by projection of the protofilaments from the front and back of the microtubule wall that are characteristic of each type of microtubule (Figure 20). Our results confirmed that increasing concentrations of tau resulted in a shift from 13- to 14- protofilament microtubules. 30% fewer 13- protofilament microtubules were observed in the 1:10 samples and 40% fewer 13- protofilament microtubules were observed in the 1:2 samples (Figure 21).

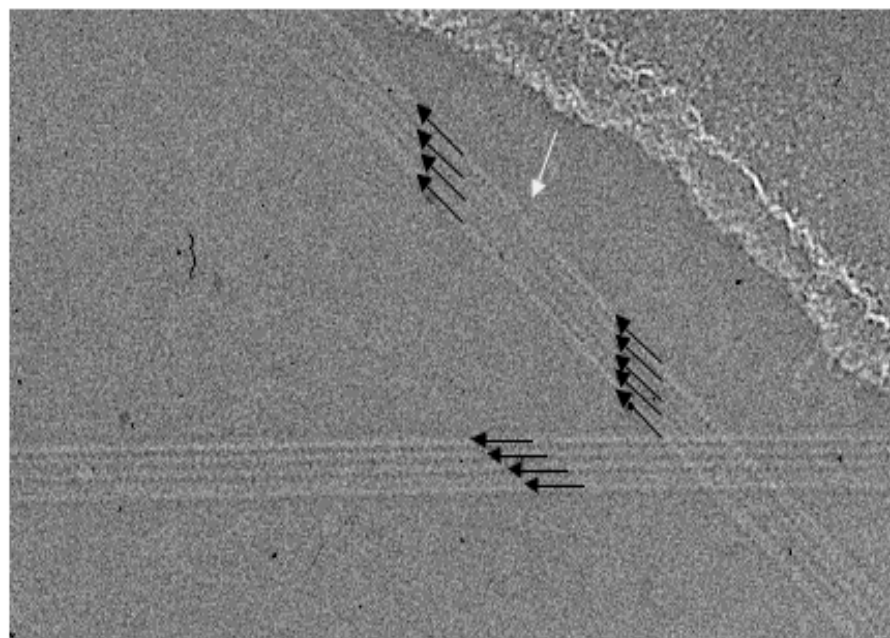


**Figure 20. Increasing concentrations of tau result in a shift from 13- to 14- proto-filament microtubules.** Cryo-EM images of microtubules with 1:10 tau (tau:tubulin monomer) at sufficiently high defocus to visualize protofilaments. Images were analyzed for the presence of a moiré pattern and characteristic longitudinal fringe patterns to determine protofilament number. Black arrows indicate protofilaments. White arrow identifies moiré pattern.

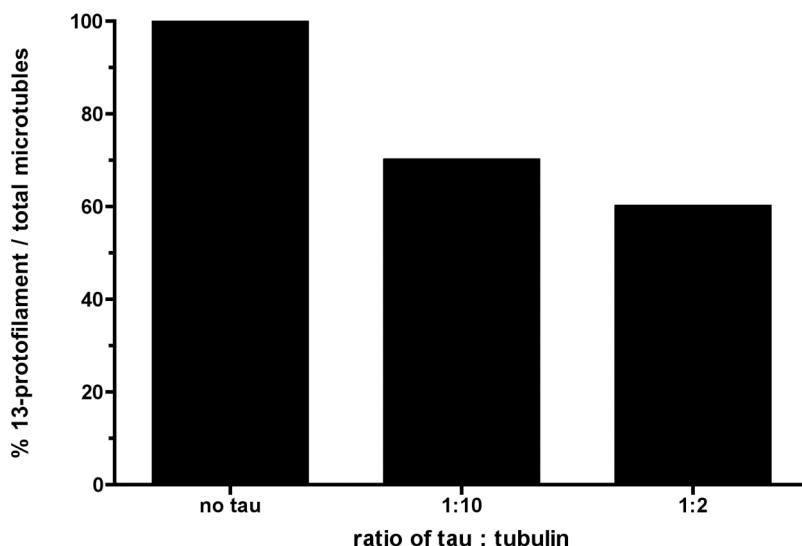


**Figure 21. Addition of tau to taxol-stabilized microtubules decreases fraction of 13-protofilaments.** Cryo-EM images of microtubules without tau, with 1:10 and 1:2 (tau:tubulin monomer) at high defocus were used to categorize the distribution of proto-filament number in microtubules. Of the 13- and 14-protofilament microtubules counted 30% fewer 13-protofilament microtubules were observed in the 1:10 samples and 40% fewer 13-protofilament microtubules were observed in the 1:2 samples.

Therefore, we altered our processing strategy to select the images of 14-protofilament microtubules. Initial experiments have focused on tau bound to Taxol-stabilized microtubules. A reference-based approach, previously used in the lab for the reconstruction of bare microtubules with different protofilament numbers, as well as the iterative helical real space reconstruction approach (IHRSR) were used since we did not expect to be able to distinguish the difference between the monomers of tubulin when tau is bound along the outside. These two methods gave indistinguishable results. For reasons that could be related to specimen preparation, the resolution in the reconstructions is limited to around 16-20 Å (Figure 22). Comparing the tau structure to a reconstruction of a bare 14-protofilament microtubule there is clearly extra density along the crest of the protofilament after tau decoration, comparable to the report by Al-Bassam and Milligan but somewhat more distributed across the tubulin monomer. Adding more data to this reconstruction will improve the resolution, since only 30 microtubules were used for this figure, compared to the typical 100 for our usual 8 Å reconstructions. Being more selective in which images are used and perhaps more careful in proper CTF correction with these images will help us approach our target resolution. We have collected but not yet processed additional images of microtubules that were polymerized in the presence of tau.

In addition to the 4R construct the Berger lab will also provide us with a mutated 4R tau in which only one cysteine remains. This will allow for the use of Monomaleimido-NANOGOLD (Nanoprobes, Inc) for gold labeling. Nanaogold uses a discrete gold compound of either 0.8 or 1.4 nM in size versus colloidal gold. Each nanogold particle has a single maleimide group incorporated into the ligand on the surface of the gold particle that reacts specifically with sulfhydryl groups. Nanogold is well suited for electron microscopy and has been used by both

the Amos and Milligan labs. The gold labeled tau should distinguish specific binding to the dimer and be especially useful for the inside model where tau is proposed to bind to  $\beta$ -tubulin.

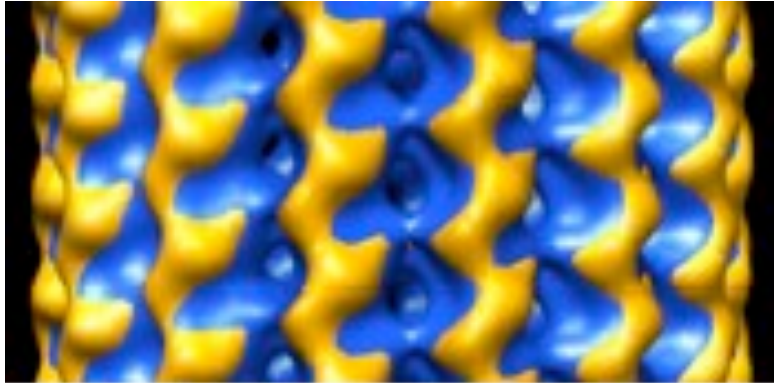


**Figure 22. Reconstruction of a tau decorated microtubule.** Superposition of maps of bare 14-pf microtubule (blue) and tau-decorated microtubules (yellow). Resolution in both is cut off at 15-20 Å, and isosurface levels were chosen to produce the same surface on the inside of the microtubule.

## **Chapter 4.**

# **Zinc Deficiency Reduces Taxol Efficacy in Human Prostate Cancer Cells**

### **Introduction**

According to 2006 statistics from the American Cancer Society, 1 out of every 6 men will be diagnosed with prostate cancer during his lifetime; consequentially, prostate cancer will result in nearly 10% of all cancer deaths in men (ACS 2007). This makes prostate cancer the second most common cancer (after skin cancer) and second leading cause of cancer death (after lung cancer) in men from the United States. If the prostate cancer is detected at an early stage, treatments including surgery, radiation, and hormone therapy are preferred. However, advanced stages of prostate cancer often become too complex for surgical removal and refractory to hormone therapy, so chemotherapy is then a recommended therapeutic approach. One of the most common drug classes for chemotherapy used in the treatment of prostate cancer are the taxanes, such as the first generation drug taxol. Taxol and related taxanes suppress normal microtubule dynamics, resulting in mitotic block and eventual apoptosis (Schiff et al. 1979, Downing 2000, Xiao et al. 2006). Taxol has been used to successfully treat a variety of cancers from ovarian, breast, and lung (Jordan and Wilson 2004). More recently, taxol and other taxanes have been shown to improve survival in prostate cancer patients, especially in combination with estramustine (Vaughn et al. 2004, Athanasiadis et al. 2003). However, the taxanes have a narrow therapeutic window and often cause significant negative side-effects. Therefore, any approach that enhances the efficacy of the taxanes would be valuable to reduce the amount of drug necessary for clinical effect.

In 2002, Kolenko and colleagues reported that taxol activity was enhanced by increased levels of the micronutrient zinc in cultured prostate cancer cell lines (Uzzo et al. 2002). Increased intracellular zinc was achieved by addition of zinc to the culture media along with a selective ionophore. This treatment resulted in increased cellular sensitivity to taxol compared to sham-treated cells. This finding will have clinical importance if elevated zinc availability similarly increases taxol efficacy *in vivo*. However, zinc deficiency - not zinc excess - is a major public health problem; in the United States, approximately 50% of men over the age of 50 are getting less than the recommended daily allowance (RDA) and over 10% are getting less than the estimated average requirement (EAR), two standard deviations below the RDA (Moshfegh et al. 2005). In fact, there is epidemiological evidence that inadequate zinc can promote cancer development, including in prostatic tissue (for reviews, see Kristal et al. 1999, Ames and Wakimoto 2002, Prasad and Kucuk 2002, Ho 2004). This observation prompted us to investigate whether reduced zinc availability could cause decreased sensitivity to taxol in prostate cancer cells.

We found that the ability of taxol to arrest the cell cycle and to cause apoptosis in a prostate cancer cell line was significantly reduced when cells were maintained under zinc-deficient conditions. Reduced zinc alone had no apparent effect on cellular growth, viability, cell cycle distribution, or apoptosis levels, indicating that the cell lines adapted well to zinc-deficient conditions. However, zinc deficiency did appear to alter the physiologic context of cellular response to taxol, resulting in reduced sensitivity. It is too early to speculate whether this observation is relevant to the success rate of taxanes in treating prostate cancer patients, but if so, then zinc supplementation may be an inexpensive and safe co-therapy. It should be noted

that excessively high zinc supplementation has actually been associated with increased risk of prostate cancer (Leitzmann et al. 2003). Thus we suggest that correcting zinc deficiency (rather than supraphysiological zinc dosing) along with taxane chemotherapy may be worth investigation.

## **Experimental Procedures**

### **Reagents**

LNCaP and PC3 prostate-derived cell lines were purchased from American Type Culture Collection (Rockville, MD). Fetal bovine serum (FBS) was purchased from Hyclone (Logan, UT). RPMI-1640 growth media, 4',6-diamidino-2-phenylindole (DAPI), trypsin-EDTA, and all other cell culture reagents were purchased from InVitrogen (Carlsbad, CA). AG MP-50 (100-200 mesh), BioRex MSZ 501D (25-35 mesh), and Chelex-100 (50-100 mesh) resins were purchased from BioRad (Hercules, CA). Sample 1577b bovine liver reference material was purchased from National Institute of Standards and Technology (NIST; Gaithersburg, MD). OmniTrace 70% HNO<sub>3</sub> and OmniTrace water were purchased from VWR International (West Chester, PA). Tris(2-aminoethyl)amine-agarose (TAEA; A-1579), Duolite C467 (16-50 mesh) resin, diethylenetriamine pentaacetic acid (DTPA), and all other chemicals were purchased from Sigma-Aldrich (St. Louis, MO), unless otherwise indicated.

### **Cell culture**

LNCaP and PC3 cell lines were cultured in 90% RPMI-1640 media supplemented with 10% FBS in an incubator maintaining 100% humidity and 5% CO<sub>2</sub>. Cultures were passaged weekly with trypsin-EDTA and counted using a Z2 Coulter Counter (Beckman Coulter, Fullerton, CA). Cell lines were adapted to standard or zinc-deficient media for 3 months. Afterwards, a subset of zinc-deficient cultures was transferred to media in which zinc levels were returned to control levels. Cells were continuously cultured under these conditions during drug sensitivity testing.

### **Zinc-deficient media**

FBS was depleted of zinc by incubation with immobilized TAEA (10% w/v) for 10 min at 4°C and then elemental content of calcium, iron, magnesium, potassium, rubidium, sodium, sulfur, and zinc was measured as described below. Non-zinc metal levels in all TAEA-stripped FBS were adjusted to levels in control FBS with appropriate metal salts as needed. Additionally, the zinc levels in the zinc-repleted condition were adjusted to control FBS levels with zinc sulfate. All metal salts were cell culture-certified. Then TAEA-stripped FBS was sterilized using 0.22µm Millex-GV filters (Millipore, Billerica, MA) and periodically checked for endotoxin (Endosafe Endochrome-K assay; Charles River Laboratories, Charleston, SC). FBS used for control media was prepared in an identical fashion but without TAEA resin (sham). FBS protein content was measured by a commercial bicinchoninic acid (BCA) assay (Pierce Biotechnology Inc, Rockford, IL) using bovine serum albumin as the standard according to manufacturer's instructions.

### **Cell viability assays**

Cell viability was assessed for early toxicity using an MTT (3-(4,5-Dimethylthiazol-2-yl)-2,5-diphenyltetrazolium bromide) assay. Reduction of MTT by reductases in the cell result in

a purple precipitate and is an indicator of cell viability. Vital dye exclusion (trypan blue) was used to measure end-stage toxicity. Trypan blue is a bulky, charged dye that only enters cells if there are large holes present, as in late stage apoptosis. For early toxicity, cells cultured in multi-well plates were incubated with CellTiter-Blue Cell Viability Assay (Promega Corporation; Madison, WI) for 2 hours according to manufacturer's instructions. Fluorescence yield was monitored using a microplate fluorescence reader at an excitation of 560nm and emission at 590nm. For end-stage toxicity, cells cultured in multi-well plates were incubated with 0.2% trypan blue in PBS for 5 min and then scored for exclusion of trypan blue dye.

## **Elemental analysis**

The elemental content of media and cells was determined by inductively-coupled plasma atomic emission spectrometry (ICP) (Killilea et al. 2003). Media or cell pellets were dissolved in OmniTrace 70% HNO<sub>3</sub> for 12-16 hours at 60°C with orbital shaking. Lysates were then diluted with OmniTrace water to 5% HNO<sub>3</sub> and introduced via a pneumatic concentric nebulizer using argon as the carrier gas into a Vista Pro ICP (Varian Inc., Palo Alto, CA). Elemental values were calibrated using NIST-traceable elemental standards and validated using NIST-traceable 1577b bovine liver reference material. The coefficient of variation (CV) of intraassay precision for zinc was 4.8% (n=10 in 1 run) and interassay precision for zinc was 7.0% (12 independent runs) for the NIST reference material. Total intraassay precision for all elements measured in the NIST reference material had CVs ranging from 1.1-7.8% (n=10 in 1 run). Cesium (50 ppm) was used for ionization suppression and yttrium (5 ppm) was used as an internal standard. All reagents and plasticware were certified or routinely tested for trace metal work. Data were collected and summarized using native software (ICP Expert; Varian Inc.).

## **Immunocytochemistry**

Cells were cultured on glass chamber slides precoated with polylysine. Slides were washed with TBS, fixed in 100% methanol for 5 min at -20°C, rehydrated in TBS, permeabilized with TBS and 0.1% Triton X-100 (TBST), and then incubated in blocking solution (TBST and 2% bovine serum albumin). Cells were incubated with 500µg/ml monoclonal mouse anti-human β tubulin antibody (Sigma-Aldrich) for 1 hour, washed with TBST, incubated with 10µg/ml donkey-anti-mouse IgG secondary antibody labeled with Alexa Fluor 488 (Invitrogen), and co-stained with 300nM DAPI. Slides were mounted and imaged by fluorescence microscopy. Apoptotic cells were defined as having pinocytotic nuclei, membrane blebbing, and non-filamentous microtubule staining. The identity of the culture conditions was randomly coded prior to scoring for apoptosis by a trained observer.

## **Cell cycle analysis**

Randomly cycling cell populations were analyzed for cell cycle distribution by propidium iodide staining. Cells were harvested by trypsin-EDTA treatment and washed in PBS. Pellets were resuspended in staining solution (50µg/ml propidium iodide, 0.1mg/ml sodium citrate, 2µg/ml ribonuclease A, and 0.03% Triton X-100) and vortexed for cell lysis (Krishan 1975). DNA content was analyzed using a FACSCalibur flow cytometer (BD, Franklin Lakes, NJ). Data were collected using 500,000 events per sample and mean fluorescence was summarized using native software (CellQuest Pro, BD).

## Statistical analysis

Graphing, regression, and statistical analysis were performed using Prism 4.0 (GraphPad, San Diego, CA) software. Significance was accepted at  $p < 0.05$ .

## Results

The predominant source of the zinc in culture media for LNCaP and PC3 cell lines is FBS, so chelation was used to deplete zinc levels. Previous approaches have removed zinc from FBS using dialysis and/or non-selective metal chelators, but many metals other than zinc are depleted with these methods. A search for a commercially available chelator with high selectivity for zinc revealed TAEA as a good option (Table III). TAEA at 10% w/v depleted the level of zinc in FBS from  $32.6 \pm 4.0 \mu\text{M}$  ( $n=15$ ) to  $11.4 \pm 2.7 \mu\text{M}$  ( $n=15$ ), a significant reduction of 65% of zinc compared to control media. However, all other metals analyzed were depleted by  $< 15\%$ , except for copper which was depleted by 30-40%. All TAEA-stripped FBS was repleted with copper and other metals as needed, while zinc-repleted media was also supplemented with zinc to levels of control media. TAEA-stripped FBS were routinely measured for endotoxin, which was never detectable above sham treated FBS levels (data not shown). Additionally, resins with bound metal ions can trap proteins, so TAEA-stripped FBS protein levels were routinely measured. Total protein recovery was  $95.7 \pm 3.9\%$  ( $n=5$ ).

	sham	AG MP-50	BioRex MSZ	Chelex-100	Duolite C467	TAEA
Ca	$99.6 \pm 2.5$	$3.12 \pm 2.2$	$4.5 \pm 0.3$	$2.9 \pm 2.1$	$4.3 \pm 0.2$	$89.1 \pm 1.1$
Cu	$109.3 \pm 27.0$	$45.8 \pm 10.3$	$62.5 \pm 6.1$	$60.8 \pm 12.6$	$84.4 \pm 27.0$	$57.5 \pm 0.1$
Fe	$103.5 \pm 12.2$	$6.9 \pm 11.9$	$73.9 \pm 8.2$	$66.8 \pm 2.6$	$0.7 \pm 12.1$	$87.7 \pm 0.1$
K	$98.7 \pm 2.2$	$9.7 \pm 0.1$	$19.3 \pm 0.1$	$77.4 \pm 1.2$	$76.2 \pm 1.6$	$89.8 \pm 0.4$
Mg	$99.2 \pm 2.1$	$2.6 \pm 0.1$	$2.6 \pm 0.1$	$0.52 \pm 0.1$	$0.3 \pm 0.1$	$87.6 \pm 0.1$
Na	$99.2 \pm 2.2$	$25.4 \pm 0.1$	$33.7 \pm 0.6$	$102.8 \pm 0.7$	$148.2 \pm 2.4$	$99.3 \pm 0.6$
Rb	$98.1 \pm 1.9$	$4.0 \pm 1.9$	$13.6 \pm 0.5$	$72.2 \pm 1.1$	$72.2 \pm 0.8$	$88.9 \pm 0.4$
S	$99.4 \pm 2.8$	$69.4 \pm 0.6$	$62.3 \pm 1.1$	$92.3 \pm 1.1$	$92.7 \pm 1.1$	$88.0 \pm 0.2$
Zn	$89.1 \pm 4.7$	$16.9 \pm 1.0$	$75.6 \pm 2.3$	$38.4 \pm 1.2$	$42.2 \pm 1.7$	$30.6 \pm 0.7$

**Table III: Extraction profile of commercial immobilized chelators in FBS.** Chelators were incubated with FBS at 10% w/v for 10 min at  $4^\circ\text{C}$  with constant rotation. Remaining elemental content was determined by ICP. Representative data shows mean  $\pm$  SD for  $n=2-3$  replicate measurements. For TAEA extractions, only copper (Cu) and zinc (Zn) were decreased by more than 15% of sham treatment.

Freshly thawed LNCaP and PC3 cell lines were passaged directly into control or zinc-deficient media and cultured for 3 months for adequate adaptation. After this time, a subpopulation of zinc-deficient cells was transferred to zinc-deficient media supplemented with zinc to the level of control media (zinc-replete media). The cells were then tested for changes in cell physiology and drug sensitivity. During this time, no change in cell population growth rates was observed (Figure 23A-B). These data were fit to a linear regression model, yielding a high goodness of fit ( $r^2 > 0.99$ ) for all cells and conditions. Average native doubling times were calculated as 1.8-1.9 days for LNCaP cells and 1.6-1.7 days for PC3 cells. Additionally, no change in relative viability between culture conditions was observed for either cell type when tested for resazurin dye reduction (Figure 23C-D). Cells were plated at varying densities to detect changes in viability over a range of culture confluency. There was no significant loss of cell viability in zinc-deficient compared to zinc-replete conditions for either cell type. These



findings were corroborated with experiments showing no difference in trypan blue dye exclusion as an end-stage cell viability marker (data not shown).

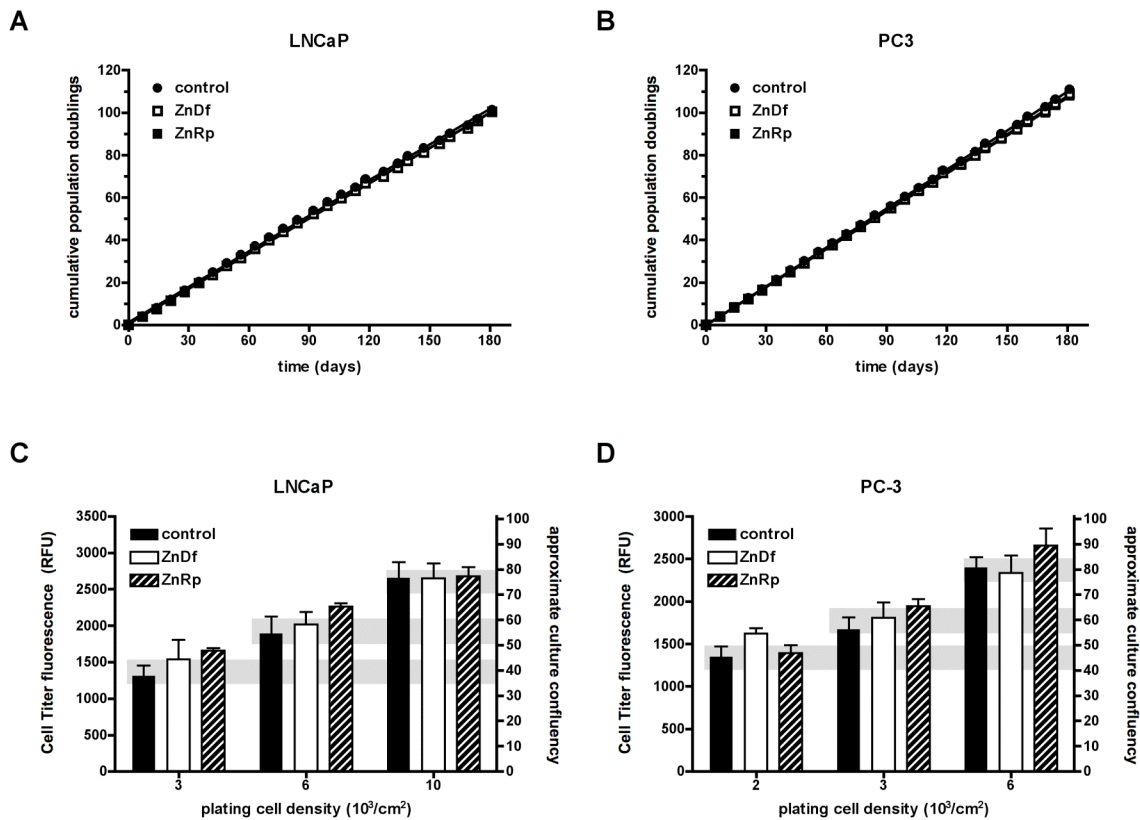


**Figure 23: Zinc deficiency did not reduce cellular growth rates or viability in prostate cell lines.** Mean population doublings were plotted as a function of time in culture for LNCaP (A) and PC3 (B) cells under control (circle), zinc-deficient (ZnDf; open square), or zinc-replete (ZnRp; solid square) conditions, and then fit with linear regression model ( $r^2 > 0.99$ , all conditions). The slopes for ZnDf and ZnRp conditions were less than 3% lower compared to control for each cell type. Cell viability was determined by resazurin dye reduction in LNCaP (C) and PC3 (D) cells under control (solid), zinc-deficient (ZnDf; open), or zinc-replete (ZnRp; hatched) conditions. Cells were plated at indicated concentrations as allowed to grow for 3 days before application of CellTiter-Blue reagent for an additional 2 hours. Fluorescence was measured at 560nm/590nm and plotted in conjunction with culture confluency. PC3 cells in ZnDf media at the 2000 cells/cm<sup>2</sup> density were significantly different from control conditions using two-tailed ANOVA with Tukey post test; however, this trend was not consistent with other plating densities.

LNCaP and PC3 cell lines were also tested for changes in cell physiology following the 3 months adaptation period. There were no changes in cell cycle distribution from cultures maintained in zinc-deficient conditions in either cell type (Figure 24A-B). There were also no detectable differences in apoptosis rates between culture conditions for each cell type (Figure 26A-B - no drug treatment). Additionally, the severity of zinc deficiency was assessed by analyzing intracellular zinc content. Even after months of exposure to reduced extracellular zinc, the levels of total intracellular zinc from cells maintained in zinc-deficient media showed no consistent variation from control cells in either cell type (Figure 24C-D). Linear regression analysis indicated that the slopes of the fit data were not significantly different from each other and not significantly different from zero, indicating no change in intracellular zinc over time. Thus, zinc-deficient culture conditions appeared to be mild and well-tolerated by LNCaP and PC3 cells and could be used to test the influence of zinc status on chemotherapeutic activity.

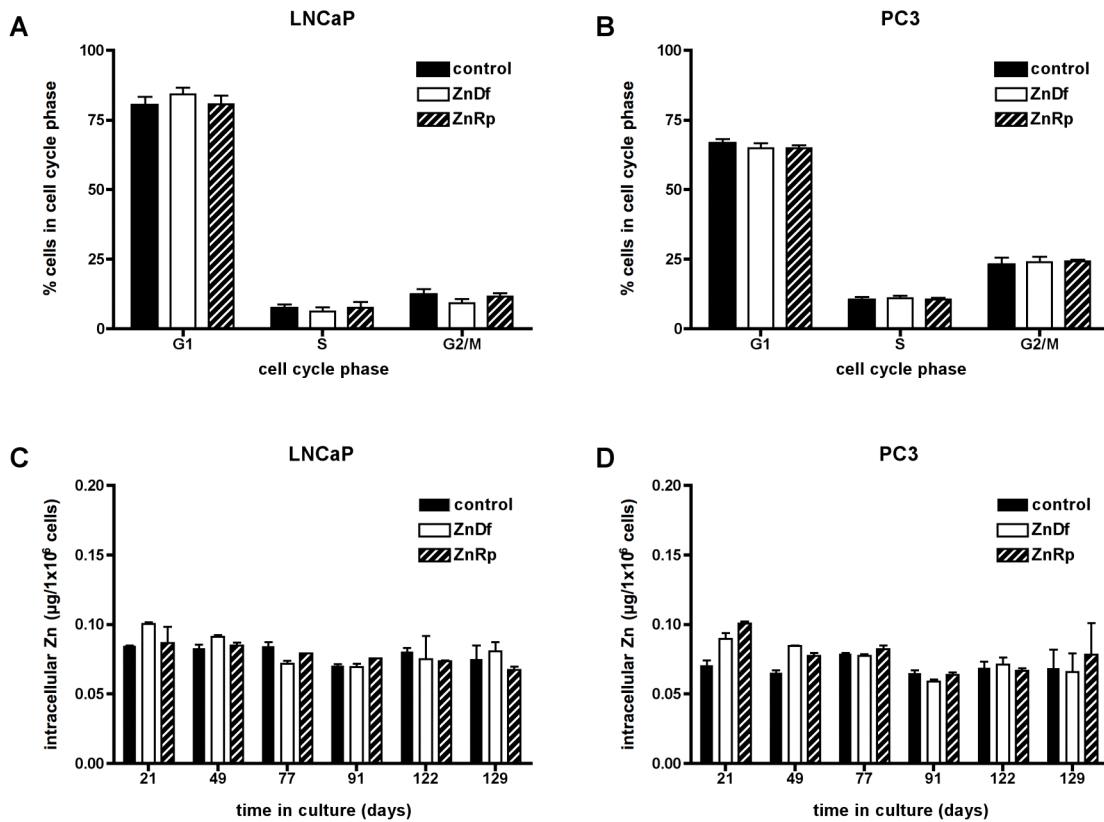


**Figure 24: Zinc deficiency did not alter cell cycle distribution or intracellular iron levels in LNCaP and PC3 cells.** Representative data show mean  $\pm$  SD of cells in randomly-cycling populations within each phase of the cycle after 3 months acclimation to control (solid), zinc-deficient (ZnDf; open), or zinc-replete (ZnRp; hatched) conditions (A). No significant differences were observed in either cell type from zinc-deficient or replete conditions compared to control using one-way ANOVA with Tukey post test. Cells from same conditions were also sampled for total intracellular zinc levels as determined by ICP. Representative data show mean  $\pm$  SD of zinc content normalized to  $1 \times 10^6$  cells (B). No consistent trend was detectable in either cell type or media conditions. Linear regression analysis of data indicated that slopes were not significantly different from each other and were not significantly non-zero.

The effect of taxol on LNCaP and PC3 cell cycle distribution was then investigated as a function of zinc status. Taxol disrupts normal microtubule function during mitosis and thereby stalls the cell cycle in G2/M phase. Randomly-cycling cells were plated and cultured until approximately 60-70% confluent before being exposed to a range of taxol concentrations for 24 hours. Cells were then analyzed for cell cycle distribution by propidium iodide staining of DNA content quantitated by flow cytometry. In PC3 cells, taxol demonstrated similar efficacy in all groups (Figure 25B). However in LNCaP cells, taxol demonstrated decreased efficacy in zinc-deficient conditions, resulting in a significant increase in IC<sub>50</sub> by a factor of 5 compared to control and zinc-repleted cells (Figure 25A). The calculated IC<sub>50</sub> values of cells under standard media conditions were similar to literature reported values (Perez-Stable 2006). In 4 independent experiments, the average IC<sub>50</sub> for taxol-induced G2/M arrest in zinc-deficient conditions in LNCaP cells was 2.4-fold greater than matched controls. In 4 independent experiments, the average IC<sub>50</sub> for taxol-induced G2/M arrest in zinc-deficient conditions in PC3 cells was 0.9-fold greater than matched control.

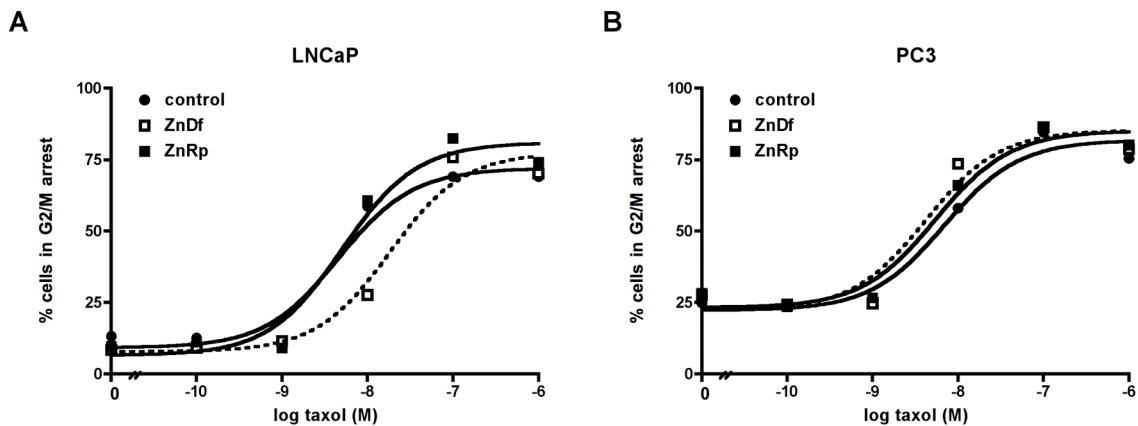


**Figure 25: Zinc deficiency was associated with reduced paclitaxel-induced cell cycle arrest in LNCaP cells.** Subconfluent cultures were exposed to increasing paclitaxel concentrations for 16 hours and then analyzed for G2/M arrest by flow cytometry. Representative data show summarized mean data fit to sigmoidal dose-response curves for cells from control (circle/solid line), zinc-deficient (ZnDf; open square/dotted line), or zinc-replete (ZnRp; solid square/solid line) conditions. In LNCaP cells, the dose-response curve of paclitaxel in zinc-deficient conditions was significantly right-shifted relative to control conditions, whereas zinc-replete conditions were similar to control (A). The mean  $\pm$  SEM IC<sub>50</sub> were determined to be  $4.6 \pm 1.8$  nM,  $18.3 \pm 1.7$  nM, and  $5.1 \pm 1.7$  nM for control, ZnDf, or ZnRp conditions respectively. In PC3 cells, the dose-response curve of paclitaxel in all conditions was similar (B). The mean  $\pm$  SEM IC<sub>50</sub> were determined to be  $6.9 \pm 1.6$  nM,  $4.2 \pm 2.0$  nM, and  $5.5 \pm 1.6$  nM for control, ZnDf, or ZnRp conditions respectively.

The eventual consequence of stalled mitosis is apoptosis. To see if taxol-stimulated apoptosis was determined in LNCaP and PC3 cell lines as a function of zinc status. Randomly-cycling cells were plated and cultured until approximately 60-70% confluent before being exposed to 25 nM taxol for 24 hours. Cells were then fixed and visually scored for apoptotic cells with pinocytotic nuclei, membrane blebbing, and disrupted microtubule networks using fluorescence microscopy. In LNCaP cells, taxol treatment resulted in a reduced number of cells with pinocytotic nuclei in zinc-deficient compared to zinc-replete conditions; the number of cells positive for apoptosis was reduced by approximately 50% in zinc-deficient conditions (Figure 26). In PC3 cells, taxol treatment under the same conditions resulted in similar efficacy in all groups (Figure 26). This pattern was also seen when analyzing cell cycle distribution described above for increases in cells containing sub-G1 DNA content, indicative of late apoptosis (data not shown). In LNCaP cells, taxol treatment resulted in fewer cells with sub-G1 DNA content as compared to control and zinc-repleted cells. In PC3 cells, taxol demonstrated similar efficacy in all groups. These data paralleled the findings from taxol-induced changes in cell cycle distribution.

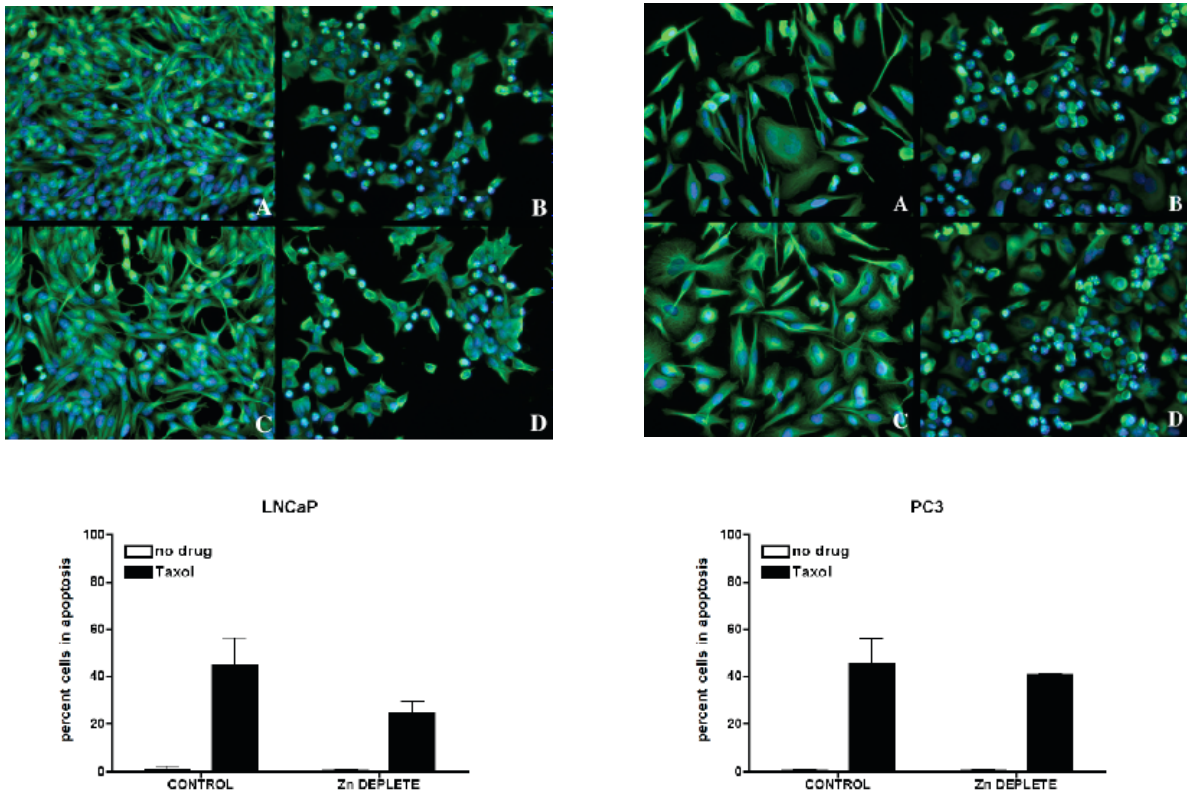


**Figure 26: Zinc deficiency reduced Taxol's efficacy in LNCaP, but not PC3, to initiate apoptosis.** Cultures were acclimated for 4 months under zinc deplete or replete conditions. Cells were exposed to increasing Taxol concentrations for 16 hours and then scored for apoptosis. Representative data shows cells in control media with (B) or without Taxol (A) or zinc deficient media with (D) or without Taxol (C) for each cell type, with quantitation in subsequent graphs. In LNCaPs, Taxol-mediated apoptosis was reduced.

## Discussion

A report showing that excess zinc improved the efficacy of taxol in prostate cancer cells (Uzzo et al. 2002) stimulated our interest in whether taxol would be less efficacious when zinc was limited. This question has important public health implications because zinc deficiency is surprisingly common (Moshfegh et al. 2005, DRI 2001). Zinc deficiency is especially pronounced in the elderly and underprivileged groups due in part to excessive consumption of calorie-rich, micronutrient poor diets (Wakimoto and Block 2001, Ames 2006). Zinc is an essential micronutrient that is required for a vast number of physiological functions, including reproductive health (DRI 2001). In men, the prostate may be particularly sensitive to zinc deficiency due to the high levels of zinc required for proper function (Boyle et al. 2003). In fact, zinc uptake in prostate epithelial cells can be up to 10 times higher than other cells types in the body; interestingly, zinc levels in prostate epithelial cells rapidly decline upon transformation to a cancerous phenotype (Costello and Franklin 1998, Huang et al. 2006). Zinc homeostasis may play important regulatory roles in both normal growth and carcinogenesis within the prostate, though the exact details remain obscured.

To study the effects of zinc deficiency on prostate cancer cells, culture media with reduced zinc content was prepared. Previous approaches to deplete zinc in culture media have employed dialysis against chelators such as EDTA and DTPA (Pilz et al. 1982, Mackenzie et al. 2002). However, these chelators are not selective for zinc and cause severe depletion of many divalent metals. In some cases, the investigators repleted at least some of the lost non-zinc metals, but it is difficult to assess whether exogenously added metals return to correct functional pools. Our laboratory and others have previously extracted zinc from FBS with EDTA-analogs immobilized on beads (e.g. Chelex-100) that had somewhat better specificity for zinc than other methods (Tate et al., 1999, Ho and Ames 2002). We continued to evaluate other immobilized chelators and found TAEA extracted a sizable fraction of zinc with only a modest depletion of other metals. To our knowledge, the selectivity of TAEA for zinc has not been previously reported. Additionally, TAEA did not substantially trap protein or add detectable amounts of endotoxin. The main drawback is that zinc extraction capacity for TAEA (60-70%) is somewhat lower than EDTA-analogs (often >90%) in FBS, but this level was sufficient for this study. Therefore, TAEA was used to prepare the zinc-deficient culture media.

Both LNCaP and PC3 prostate cell lines appeared to adapt well to moderately zinc-deficient conditions. No losses in cellular growth, viability, cell cycle distribution, or apoptosis rates were detected under zinc-deficient conditions alone. Moreover, the total intracellular zinc content was not significantly altered despite months of culturing in zinc-deficient conditions. We previously found that several other cell types did respond with reduced intracellular zinc levels when cultured in culture media containing zinc-depleted FBS prepared using Chelex-100 (Ho and Ames 2002, Ho et al. 2003). This is likely due to cell type differences and a more severe zinc deficiency. In the current study, we calculated that the number of moles of zinc in the zinc-deficient media was still 100-fold greater than the moles of zinc in the combined intracellular volume of plated cells. Thus cells cultured in zinc-deficient media would still be able to meet intracellular zinc requirements by increasing zinc intake and/or reducing zinc export. Moreover, other reports have shown that some cell types are efficient in maintaining their intracellular zinc levels (Walsh et al. 1994, Uzzo et al. 2006). The lack of severe phenotypic alteration due to zinc-deficient conditions was beneficial for this study because it provided a cell model that was

uncomplicated by additional toxicities for evaluating the chemotherapeutic drug taxol. The major phenotypic difference we detected in zinc-deficient media was a loss of sensitivity to the taxol-induced cell cycle arrest and apoptosis. This effect was not seen with zinc deficiency alone, but zinc deficiency was necessary for the effect since cells cultured in zinc-deficient media repleted with zinc responded to taxol similarly to control cells.

Zinc-dependent loss of taxol activity was observed in LNCaP, but not PC3, cell lines. The means by which zinc deficiency confers taxol sensitivity to LNCaP cells are unclear, though earlier studies have also shown differential responses of LNCaP and PC3 cells to alterations in zinc homeostasis. For example, Feng and colleagues reported a greater inhibition of cell growth, delayed cell cycle kinetics, and increased apoptosis for LNCaP compared to PC3 cells when exogenous zinc was added to culture media (Liang et al. 1999). Other groups have shown increased LNCaP cell sensitivity to apoptosis sensitizing agents such as camptothecin, nutraceuticals such as lycopene, and anti-proliferative hormones such as vitamin D3 (Wang et al. 1999, Ivanov et al. 2007, Zhuanh and Burnstein 1998). Two known differences in these cell lines may explain these findings. LNCaP cells are p53<sup>+/+</sup> whereas PC3 cells are p53<sup>-/-</sup>. P53 is a known zinc-dependent enzyme and severe zinc deficiency has been shown to inactivate p53 (Ho and Ames 2002), which may make LNCaP cells more sensitive to zinc-deficient conditions. Also, LNCaP cells are androgen-sensitive whereas PC3 cells are androgen-insensitive. Androgens are known to regulate prostate cell zinc homeostasis in vitro and in vivo (Liu et al. 1997), thus androgen-sensitivity may cause LNCaP cell physiology to be more affected by zinc-deficient conditions. However, other cell lines differences to be revealed in future studies may also play a role.

The molecular mechanisms through which zinc deficiency diminishes taxol efficacy in the LNCaP cell line are not yet known, though several possibilities can be proposed. Zinc levels modulate key apoptosis-related proteins such as bax, bcl-2, and caspases (Feng et al. 2000, Untergasser et al. 2000, Ganju and Eastman 2003, Kondoh et al. 2005, Zago et al. 2005), so reduced zinc could alter apoptotic cascades. However, these perturbations would occur downstream to the effects on cell cycle kinetics and thus not explain the changes seen in cells cultured in zinc-deficient media. It has been proposed that microtubule dynamics themselves may be disrupted by altered intracellular zinc levels, perhaps due to reduced tubulin polymerization rates (Hesketh 1982, Oteiza et al. 1990). However, intracellular zinc levels were not decreased in our study; moreover, zinc deficiency alone had no effect on cell cycling. Yet we cannot rule out that zinc deficiency might have caused a decrease in the labile zinc pool, which represents a small fraction of the total zinc in the cell, that was sufficient to affect taxol action on the microtubule network. Another reported consequence of zinc deficiency was increased oxidative stress and depressed oxidative damage repair systems (Ho and Ames 2002, Ho et al. 2003, Zago et al. 2005, Oteiza et al. 2000, Clegg et al. 2005). Taxol targeting of microtubule networks may be influenced by redox imbalances, although this has not been previously reported. Moreover, the zinc-deficient conditions in our study were more moderate than in most previous studies, so oxidative stress levels were probably not pronounced. In fact, preliminary experiments in LNCaP and PC3 cells did not show any increase in protein carbonyl levels in zinc-deficient conditions (data not shown). Yet the involvement of subtle or regional bursts of oxidants cannot be ruled out.

An alternative mechanism for zinc-dependent loss of taxol efficacy could involve changes in signal transduction caused by decreased extracellular zinc levels. Hershinkel, Moran, and colleagues have reported that at least some cell types contain membrane-bound

receptors that sense extracellular zinc levels and couple with intracellular signal transduction pathways without necessitating a concomitant rise or fall in intracellular zinc levels (Hershinkel et al. 2001). In their studies, zinc deficiency conditions triggered an extracellular zinc receptor resulting in activation of the mitogen-activated protein kinase (MAPK) pathway; these findings support previous work showing increased MAPK signaling with exposure to reduced zinc levels (Zago et al. 2005). MAPKs phosphorylate a variety of target proteins in the cell, including a family of proteins called microtubule-associated proteins (MAPs). MAPs are normally present along the microtubule network and serve to both stabilize microtubules and regulate microtubule dynamics (Mandelkow and Mandelkow 1995). Phosphorylation of MAPs typically causes dissociation from the microtubule network and thereby results in increased microtubule dynamics (Illenberger et al. 1996). Increased dynamics in the microtubule network can reduce the ability for taxol to bind and stabilize the microtubules (Derry et al. 1997). A microtubule-stabilizing drug like taxol would therefore be less efficacious when microtubules do not contain MAPs. Currently, no studies have reported the presence of the extracellular zinc receptor or difference in MAP content between LNCaP and PC3 cells, so the plausibility of this mechanism is unclear at this time.

This study shows that some prostate cancer cells cultured in zinc-deficient conditions demonstrate reduced sensitivity to the chemotherapeutic taxol. There are no data as to whether zinc status has any consequence on the efficacy of taxol or other taxane compounds in individuals being treated for prostate cancer. If zinc availability does attenuate taxol activity in vivo, this would have important clinical implications since zinc is a common micronutrient deficiency in the United States. Adjusting zinc intake by dietary means or modest zinc supplementation might prove to be a safe and inexpensive approach to improving success with taxol. This would also highlight the importance of the nutritional context for evaluation of therapeutic efficacy, an issue that in our assessment is greatly underappreciated.

## Chapter 5. Summary

Tubulin interacts with an astounding number of proteins that play such diverse roles as maintaining cellular shape, transporting cargo along microtubules and proper segregation of chromosomes during cellular division. The goal of this work is to advance our understanding of the structural interactions between tubulin and its molecular partners in order to reveal the complex interplay that takes place in the cell.

Parkin plays the role of a multi-faceted neuroprotective agent in the cell. Through its ubiquitin ligase activity it protects cells from the unfolded protein response (Imai et al. 2000). Phosphorylation of parkin by PTEN-induced kinase 1 (PINK1) results in translocation to the mitochondria where it acts as a signal for autophagy, protecting dopaminergic neurons from accumulation of defective mitochondria (Narendra et al. 2008). Recently it has been suggested that the absence of parkin in many tumor biopsies, its presence in a fragile site of the chromosome and its high frequency of loss of heterozygosity (LOH) could implicate it as a tumor suppressor (Cesari et al. 2003). Another recent role for parkin as a transcriptional repressor of p53 has been suggested (da Costa et al. 2009). This seems feasible since parkin is a member of the RIR family of proteins that has several members that participate in transcriptional repression. One such member is MDM2, another transcriptional repressor and E3 ubiquitin ligase for p53 (Geyer et al. 2000).

Our work with parkin has revealed that it is highly sensitive to aggregation and the substitution of human parkin for rat parkin is sufficient to improve solubility. It is possible that loss of a cysteine (C95) located in the linker domain of human but not rat parkin could be the reason for improved solubility (Figure 15). Parkin-decorated microtubules were used for cryo EM studies to identify the interaction interfaces involved in binding. The class averages and associated power spectra indicate that parkin is binding to the dimer and not the monomer of tubulin. Due to insufficient decoration we were unable to obtain a final reconstruction of parkin binding to microtubules. The incomplete decoration of microtubules is easily solved and additional samples can be prepared for cryo EM using higher parkin to microtubule ratio. These samples should solve the problem of low occupancy seen during processing. If there is an unforeseen issue with how parkin binds, additional constructs can be prepared that solely contain the RIR supradomain (R1, IBR, and R2).

In the future, it would be interesting to make a complex of parkin decorated microtubules with UbcH7 (the E2 for parkin) and a possible substrate bound to parkin. Since crystallization of parkin with its partners has so far been unsuccessful, this complex would further help us understand the geometry that occurs during ubiquitination. Several labs have demonstrated through coimmunoprecipitation (Shimura et al. 2001), NMR analysis (Sakata et al. 2003), and x-ray crystallography and molecular modeling (Tomoo et al. 2008) that parkin binds to the lid of the 26S proteasome through the ubiquitin like and linker domains. Cryo EM would be an ideal method to investigate this interaction.

In work with tau-decorated microtubules, we were perplexed when our standard processing approach to select 13-protofilament microtubule images was not giving a clear signal for tau. The results from tau pelleting assays were clearly indicating that tau was fully decorating microtubules. It wasn't until a report appeared indicating that tau induces formation of 14-pf microtubules that we could explain the lack of tau in micrographs with 13-protofilament microtubules (Choi et al, 2009). We were initially skeptical but performed experiments using



increasing amounts of tau bound to microtubules, recording images by cryo EM at high defocus. These images confirmed that protofilament number shifted distribution from 13 to 14 upon increasing concentration of tau. We set about processing the 14-protofilament images of tau bound to Taxol-stabilized microtubules and have a reconstruction at 16-20 Å but so far have only processed 30 microtubules. Many more micrographs await processing and we are confident that the addition of more microtubules to the data set will greatly improve the resolution. We also anticipate receiving a mutated version of the 4R tau that will make addition of a gold label possible. A gold labeled tau would distinguish specific binding to the dimer and be especially useful for the inside model where tau is proposed to bind to  $\beta$ -tubulin.

With regards to our research investigating the role that zinc plays in microtubule drug binding we were able to establish a novel cell culture model for zinc deficiency using a more zinc selective chelator than had been used in previous work. Zinc deficiency was more moderate, and thus more physiological, than previously described studies; moreover, cells were exposed for many months to these new zinc levels to allow them to fully acclimate. Our characterization studies showed that the prostate cancer cell lines LNCaPs and PC3s tolerated these culture conditions well with no obvious lack of viability. Because there are few studies reported on the role of zinc in microtubule structure/function relationships, we characterized the effects of zinc on purified microtubules in addition to the microtubules from the cell lines. We found that zinc levels did affect dynamics in isolated microtubules. The dynamic nature is critical for normal cellular division and thus a major target of anti-cancer therapeutics. These findings now need to be assessed in cells, as different cell types can have radically different microtubule assemblies due to differential expression of tubulin isoforms and/or microtubule-associating proteins. These studies are underway, but preliminary evidence suggests that microtubule dynamics may be altered by zinc status in (prostate) cells as well. Additionally, chromatin processing, an immediate downstream target of microtubule activity, may also be altered during zinc deficient conditions. The most translational part of the study is the interaction between zinc status and chemotherapeutic efficacy. We found that a drug used to treat prostate cancer (taxol) had reduced efficacy in causing cell cycle arrest and apoptosis when prostate cancer cells were maintained under moderately zinc deficient conditions. These findings should now be tested to animal models to see if the effect translates to whole animals, and molecular studies should determine the mechanisms. Since zinc deficiency is common in the US, this nutritional status may be of importance when creating a treatment strategy for prostate cancer. Reduced efficacy of these drugs might exaggerate side effects and promote resistance within the cancer.

## Cited Literature

Al-Bassam, J., Ozer, R. S., Safer, D., Halpain, S., Milligan, R. A. (2002). "MAP2 and tau bind longitudinally along the outer ridges of microtubule protofilaments." J Cell Biol **157**: 1187-96.

Ambrose, J. C., Li, W., Marcus, A., Ma, H., Cyr, R. (2005). "A minus-end-directed kinesin with plus-end tracking protein activity is involved in spindle morphogenesis." Mol Biol Cell **16**: 1584-92.

American Cancer Society. Cancer facts & figures 2007. (2007) Atlanta (GA): American Cancer Society.

Ames, B. N., Wakimoto, P. (2002). "Are vitamin and mineral deficiencies a major cancer risk?" Nat Rev Cancer **2**: 694-704.

Ames, B. N. (2006). "Low micronutrient intake may accelerate the degenerative diseases of aging through allocation of scarce micronutrients by triage." Proc Natl Acad Sci USA **103**: 17589-94.

Amos, L. A., Löwe, J. (1999). "How taxol stabilizes microtubule structure." Chem Biol **6**: R65-69.

Andreadis, A., Brown, W. M., Kosik, K. S. (1992). "Structure and novel exons of the human tau gene." Biochem **31**: 10626-33.

Arai, H., Ishiguro, K., Ohno, H., Moriyama, M., Itoh, N., Okamura, N., Matsui, T. Morikawa, Y., Horikawa, E., Kohno, H., Sasaki, H., Imahori, K. (2000). "CSF phosphorylated tau protein and mild cognitive impairment: a prospective study." Exp Neurol **166**: 201-3.

Athanasiadis, A., Tsavdaridis, D., Rigatos, S. K., Athanasiadis, I., Pergantas, N., Stathopoulos, G. P. (2003). "Hormone refractory advanced prostate cancer treated with estramustine and paclitaxel combination." Anticancer Res **23**: 3085-8.

Banerjee, A. (2002). "Increased levels of tyrosinated  $\alpha$ -,  $\beta$  III-, and  $\beta$ IV-tubulin isotypes in paclitaxel-resistant MCF-7 breast cancer cells." Biochem Biophys Res Commun **293**: 598-601.

Barboni, L., Lambertucci, C., Appendino, G., Vander Velde, D. G., Himes, R. H., Bombardelli, E., Wang, M., Snyder, J. P. (2001). "Synthesis and NMR-driven conformational analysis of taxol analogues conformationally constrained on the C13 side chain." J Med Chem **44**: 1576-87.

Beasley, S. A., Hristova, V. A., Shaw, G. S. (2007). "Structure of the Parkin in-between-ring domain provides insights for E3-ligase dysfunction in autosomal recessive Parkinson's disease." Proc Natl Acad Sci U S A **104**: 3095-100.

Betarbet, R., Sherer, T. B., MacKenzie, G., Garcia-Osuna, M., Panov, A. V., Greenamyre, J. T. (2000). "Chronic systemic pesticide exposure reproduces features of Parkinson's disease." Nat Neurosci **3**: 1301–6.

Bode, C. J., Gupta, M. L., Jr., Suprenant, K. A., and Himes, R. H. (2003). "The two  $\alpha$ -tubulin isotypes in budding yeast have opposing effects on microtubule dynamics in vitro." EMBO Rep **4**: 94-9.

Bollag, D. M., McQuene, P. A., Zhu, J., Hensens, O., Koupal, L., Liesch, J., Goetz, M., Lazarides, E., Woods, C. M. (1995). "Epothilones, a new class of microtubule-stabilizing agents with a Taxol-like mechanism of action." Can Res **55**: 2325-33.

Borden, K. L. (1998). "RING fingers and B-boxes: zinc-binding protein-protein interaction domains." Biochem Cell Biol **76**: 351-8.

Boyle, P., Severi, G., Giles, G. G. (2003). "The epidemiology of prostate cancer." Urol Clin N Am **30**: 209-17.

Bunker, J. M., Kamath, K., Wilson, L., Jordan, M. A., Feinstein, S. C. (2006). "FTPD-17 mutations compromise the ability of tau to regulate microtubule dynamics in cells." J Biol Chem **281**: 11856-63.

Capili, A. D., Edghill, E. L., Wu, K., Borden, K. L. (2004). "Structure of the C-terminal RING finger from a RING-IBR-RING/TRIAD motif reveals a novel zinc-binding domain distinct from a RING." J Mol Biol **340**: 1117-29.

Caplow, M., Shanks, J. (1996). "Evidence that a single monolayer tubulin-GTP cap is both necessary and sufficient to stabilize microtubules." Mol Biol Cell **7**: 663-75.

Carlomango, T., Blommers, M. J. J., Meiler, J., Jahnke, W., Schupp, T., Petersen, F., Schinzer, D., Altmann, K. H., Griesinger, C. (2003). "The high-resolution solution structure of epothilone A bound to tubulin: An understanding of the structure-activity relationships for a powerful class of antitumor agents." Angew Chem Int Ed **42**: 2511-5.

Cassimeris, L., Spittle, C. (2001). "Regulation of microtubule-associated proteins." Int Rev Cytol **210**: 163-226.

Cesari, R., Martin, E. S., Calin, G. A., Pentimalli, F., Bichi, R., McAdams, H., Trapasso, F., Drusco, A., Shimizu, M., Masciullo, V., D'Andrilli, G., Scambia, G., Picchio, M. C., Alder, H., Godwin, A. K., Croce, C. M. (2003). "Parkin, a gene implicated in autosomal recessive juvenile parkinsonism, is a candidate tumor suppressor gene on chromosome 6q25-q27." Proc Natl Acad Sci U S A **100**: 5956-61.

Chang, W., Gruber, D., Chari, S., Kitazawa, H., Hamazumi, Y., Hisanaga, S., Bulinski, J. C. (2001). "Phosphorylation of MAP4 affects microtubule properties and cell cycle progression." J Cell Sci **114**: 2879-87.

- Chen, J., Kanai, Y., Cowan, N. J., Hirokawa, N. (1992). "Projection domains of MAP2 and tau determine spacings between microtubules in dendrites and axons." Nature **360**: 674-7.
- Chiueh, C., Wu, R., Mohanakumar, K., Sternberger, L., Krishna, G., Obata, T., Murphy, D. (1994). "In vivo generation of hydroxyl radicals and MPTP-induced dopaminergic toxicity in the basal ganglia". Ann N Y Acad Sci **738**: 25–36.
- Choi, M. C., Raviv, U., Miller, H. P., Gaylord, M. R., Kiris, E., Ventimiglia, D., Needleman, D. J., Kim, M. W., Wilson, L., Feinstein, S. C., Safinya, C. R. (2009). "Human microtubule-associated-protein tau regulates the number of protofilaments in microtubules: a synchrotron x-ray scattering study." Biophys J **97**: 519-27.
- Choi, P., Snyder, H., Petrucelli, L., Theisler, C., Chong, M., Zhang, Y., Lim, K., Chung, K. K., Kehoe, K., Adamio, L., Lee, J. M., Cochran, E., Bowser, R., Dawson, T.M., Wolozin, B. (2003). "SEPT5\_v2 is a parkin-binding protein." Brain Res Mol Brain Res **117**: 179–89.
- Chrétien, D., Wade, R. H. (1991). "New data on the microtubule surface lattice." Biol Cell **71**: 161-74.
- Clegg, M. S., Hanna, L. A., Niles, B. J., Momma, T. Y., Keen, C. L. (2005). "Zinc Deficiency-Induced Cell Death." IUBMB Life **57**: 661-9.
- Cleveland, D. W., Hwo, S. Y., Kirschner, M. W. (1977). "Physical and chemical properties of purified tau factor and the role of tau in microtubule assembly." J Mol Biol **116**: 227-47.
- Cohen, N., Sharma, M., Kentsis, A., Perez, J. M., Strudwick, S., Borden, K. L. (2001). "PML RING suppresses oncogenic transformation by reducing the affinity of eIF4E for mRNA." EMBO J **20**: 4547-59.
- Cornell, N. W., Crivaro, K. E. (1972). "Stability constant for the zinc-dithiothreitol complex." Anal Biochem **47**: 203-8.
- Costello, L. C., Franklin, R. B. (1998). "Novel role of zinc in the regulation of prostate citrate metabolism and its implications in prostate cancer." Prostate **35**: 285-96.
- Cotzias, G.C. (1968). "L-Dopa for Parkinsonism." N Engl J Med **278**: 630.
- Cyr, D. M., Höhfeld, J., Patterson, C. (2002). "Protein quality control: U-box-containing E3 ubiquitin ligases join the fold." Trends Biochem Sci **27**: 368-75.
- da Costa, C. A., Sunyach, C., Giaime, E., West, A., Corti, O., Brice, A., Safe, S., Abou-Sleiman, P. M., Wood, N. W., Takahashi, H., Goldberg, M. S., Shen, J., Checler, F. (2009). "Transcriptional repression of p53 by parkin and impairment by mutations associated with autosomal recessive juvenile Parkinson's disease. Nat Cell Biol **11**: 1370-5.

Dehmelt, L., Halpain, S. (2005). "The MAP2/Tau family of microtubule-associated proteins." Genome Biol **6**: 204.1-204.9.

Derry, W. B., Wilson, L., Khan, I. A., Ludueña, R. F., Jordan, M. A. (1997). "Taxol differentially modulates the dynamics of microtubules assembled from unfractionated and purified beta-tubulin isotypes." Biochem **36**: 3554-62.

Desai, A., Mitchison, T.J. (1997). "Microtubule polymerization dynamics." Annu Rev Cell Dev Biol **13**: 83-117.

Detrich, H. W., III, Parker, S. K., Williams, R. C., Jr., Nogales, E., Downing, K. H. (2000). "Cold adaptation of microtubule assembly and dynamics: structural interpretation of primary sequence changes present in the  $\alpha$  and  $\beta$  tubulins of Antarctic fishes." J Biol Chem **275** 37038-47.

"Dietary Reference Intakes for Vitamin A, Vitamin K, Arsenic, Boron, Chromium, Copper, Iodine, Iron, Manganese, Molybdenum, Nickel, Silicon, Vanadium, and Zinc." Standing Committee on the Scientific Evaluation of Dietary Reference Intakes, Food and Nutrition Board, Institute of medicine, National Academy Press, Washington, D.C., pp 442-501, 2001.

Dong, Z., Ferger, B., Paterna, J. C., Vogel, D., Furler, S., Osinde, M., Feldon, J., Bueler, H. (2003). "Dopamine-dependent neurodegeneration in rats induced by viral vector-mediated overexpression of the parkin target protein, CDCrel-1." Proc Natl Acad Sci USA **100**: 12438-43.

Downing, K. H. (2000). "Structural basis for the action of drugs that affect microtubule dynamics." Emerg Ther Targ **4**: 219-37.

Drewes, G., Trinczek, B., Illenberger, S., Biernat, J., Schmitt-Ulms, G., Meyer, H. E., Mandelkow, E. M., Mandelkow, E. (1995). "Microtubule-associated protein/microtubule affinity-regulating kinase (p110mark). A novel protein kinase that regulates tau-microtubule interactions and dynamic instability by phosphorylation at the Alzheimer-specific site serine 262." J Biol Chem **270**: 7679-88.

Dumontet, C., Jordan, M. A., Lee, F. F. (2009). "Ixabepilone: targeting betaIII-tubulin expression in taxane-resistant malignancies." Mol Cancer Ther **8**: 17-25.

Eagle, G. R., Zombola, R. R., and Himes, R. H. (1983). "Tubulin-zinc interactions: Binding and polymerization studies." Biochem **22**: 221-8.

Ebnet, A., Godemann, R., Stamer, K., Illenberger, S., Trinczek, B., Mandelkow, E. (1998). "Overexpression of tau protein inhibits kinesin-dependent trafficking of vesicles, mitochondria, and endoplasmic reticulum: implications for Alzheimer's disease." J Cell Biol **143**: 777-94.

Egelman, E. H. (2007). "The iterative helical real space reconstruction method: surmounting the problems posed by real polymers." J Struct Biol **157**: 83-94.

- Eipper, B. A. (1974). "Properties of rat brain tubulin." J Biol Chem **249**: 1407-16.
- Eliezer, D., Barré, P., Kobaslija, M., Chan, D., Li, X., Heend, L. (2005). "Residual structure in the repeat domain of tau: echoes of microtubule binding and paired helical filament formation." Biochem **44**: 1026-36.
- Fahn, S. (1996). "The Case of the Frozen Addicts: How the Solution of an Extraordinary Medical Mystery Spawned a Revolution in the Understanding and Treatment of Parkinson's Disease." New Engl J Med **335**: 99.
- Feng, P., Liang, J. Y., Li, T. L., Guan, Z. X., Zou, J., Franklin, R., Costello, L. C. (2000). "Zinc induces mitochondria apoptosis in prostate cells." Mol Urol **4**: 31-6.
- Ferhat, L., Bernard, A., Ribas, d. P. L., Ben, A. Y., Khrestchatisky, M. (1994). "Structure, regional and developmental expression of rat MAP2d, a MAP2 splice variant encoding four microtubule-binding domains." Neurochem Int **25**: 327-38.
- Forno, L.S. (1996). "Neuropathology of Parkinson's disease." J Neuropathol Exp Neurol **55**: 259-72.
- Frank, J. Radermacher, M., Penczek, P., Zhu, J., Li, Y., Ladjadj, M., Leith, A. (1996). "SPIDER and WEB: processing and visualization of images in 3D electron microscopy and related fields." J Struct Biol **119**: 190-9.
- Gaitanos, T. N., Buey, R. M., Díaz, J. F., Northcote, P. T., Teesdale-Spittle, P., Andreu, J. M., Miller, J. H. (2004). "Peloruside A does not bind to the taxoid site on beta-tubulin and retains its activity in multidrug-resistant cell lines." Cancer Res **64**: 5063-7.
- Ganju, N., Eastman, A. (2003). "Zinc inhibits Bax and Bak activation and cytochrome c release induced by chemical inducers of apoptosis but not by death-receptor-initiated pathways." Cell Death Differ **10**: 652-61.
- Gard, D. L. and Kirschner, M. W. (1987). "A microtubule-associated protein from *Xenopus* eggs that specifically promotes assembly at the plus-end." J Cell Biol **105**: 2203-15.
- Garner, C. C., Brugg, B., Matus, A. (1988). "A 70-kilodalton microtubule-associated protein (MAP2c), related to MAP2." J Neurochem **50**: 609-15.
- Gash, D. M., Rutland, K., Hudson, N. L., Sullivan, P. G., Bing, G., Cass, W. A., Pandya, J. D., Liu, M., Choi, D. Y., Hunter, R. L., Gerhardt, G. A., Smith, C. D., Slevin, J. T., Prince, T. S. (2008). "Trichloroethylene: Parkinsonism and complex 1 mitochondrial neurotoxicity." Ann Neurol **63**: 184-92.
- Geyer, R. K., Yu, Z. K., Maki, C. G. (2000). "The MDM2 RING-finger domain is required to promote p53 nuclear export." Nat Cell Biol **2**: 569-73.

- Geyp, M., Ireland, C. M., Pittman, S. M. (1996). "Increased tubulin acetylation accompanies reversion to stable ploidy in vincristine-resistant CCRF-CEM cells." Cancer Genet Cytogenet **87**: 117-22.
- Giannakakou, P., Sackett, D. L., Kang, Y. K., Zhan, Z., Buters, J. T., Fojo, T., Poruchynsky, M. S. (1997). "Paclitaxel-resistant human ovarian cancer cells have mutant beta-tubulins that exhibit impaired paclitaxel-driven polymerization." J Biol Chem **272**: 17118–25.
- Giannakakou, P., Gussio, R., Nogales, E., Downing, K. H., Zaharevitz, D., Bollbuck, B., Poy, G., Sackett, D., Nicolaou, K. C., Fojo, T. (2000). "A common pharmacophore for epothilone and taxanes: Molecular basis for drug resistance conferred by tubulin mutations in human cancer cells." Proc Natl Acad Sci USA **97**: 2904-9.
- Gilbert, D. C., Parker, C. (2005). "Docetaxel for the treatment of prostate cancer." Future Oncol **1**: 307-14.
- Goedert, M., Wischik, C. M., Crowther, R. A., Walker, J. E., Klug, A. (1998). "Cloning and sequencing of the cDNA encoding core of the paired helical filament of Alzheimer's disease." Proc Natl Acad Sci USA **85**: 4051-5.
- Goedert, M., Spillantini, M. G., Jakes, R., Crowther, R. A., Vanmechelen, E., Probst, A., Götze, J., Bürki, K., Cohen, P. (1995). "Molecular dissection of the paired helical filament." Neurobiol Aging **16**: 325-34.
- Gonzalez-Garay, M. L., Chang, L., Blade, K., Menick, D. R., Cabral, F. (1999). "A beta-tubulin leucine cluster involved in microtubule assembly and paclitaxel resistance." J Biol Chem **274**: 23875–23882.
- Goode, B. L., Feinstein, S. C. (1994). "Identification of a novel microtubule binding and assembly domain in the developmentally regulated inter-repeat region of tau." J Cell Biol **124**: 769-82.
- Griffith, L. M., Pollard, T. D. (1982). "The interaction of actin filaments with microtubules and microtubule-associated proteins." J Biol Chem **257**: 9143–51.
- Grundke-Iqbal, I., Iqbal, K., Tung, Y. C., Quinlan, M., Wisniewski, H. M., Binder, L. I. (1986). "Abnormal phosphorylation of the microtubule-associated protein tau (tau) in Alzheimer cytoskeletal pathology." Proc Natl Acad Sci U S A **83**: 4913-7.
- Gustke, N., Trinczek, B., Biernat, J., Mandelkow, E. M., Mandelkow, E. (1994). "Domains of tau protein and interactions with microtubules." Biochem **33**: 9511-22.
- Haglund, K., Sigismund, S., Polo, S., Szymkiewicz, I., Di Fiore, P. P., Dikic, I. (2003). "Multiple monoubiquitination of RTKs is sufficient for their endocytosis and degradation." Nat Cell Biol **5**: 461-6.

Hansson, O., Zetterberg, H., Buchhave, P., Londos, E., Blennow, K., Minthon, L. (2006). "Association between CSF biomarkers and incipient Alzheimer's disease in patients with mild cognitive impairment: a follow-up study." Lancet Neurol **5**: 228-34. Erratum in: Lancet Neurol (2006) **5**: 293.

Hauber, W. (1998). "Involvement of basal ganglia transmitter systems in movement initiation." Prog Neurobiol **45**: 507-40.

He, L., Jagtap, P. G., Kingston, D. G., Shen, H. J., Orr, G. A., Horwitz, S. B. (2000). "A: A common pharmacophore for Taxol and the epothilones based on the biological activity of a taxane molecule lacking a C-13 side chain." Biochem **39**: 3972-8.

Hershko, A., Ciechanover, A. (1998). "The ubiquitin system." Ann Rev Biochem **67**: 425-79.

Hershinkel, M., Moran, A., Grossman, N., Sekler, I. (2001). "A zinc-sensing receptor triggers the release of intracellular Ca<sup>2+</sup> and regulates ion transport." Proc Natl Acad Sci USA **98**: 11749-54.

Hesketh, J. E. (1982). "Zinc-stimulated microtubule assembly and evidence for zinc binding to tubulin." Int J Biochem **14**: 983-90.

Ho, E. (2004). "Zinc deficiency, DNA damage and cancer risk." J Nutr Biochem **15**: 572-8

Ho, E., Ames, B. N. (2002). "Low intracellular zinc induces oxidative DNA damage, disrupts p53, NFkappa B, and AP1 DNA binding, and affects DNA repair in a rat glioma cell line." Proc Natl Acad Sci U S A **99**: 16770-5.

Ho, E., Courtemanche, C., Ames, B. N. (2003). "Zinc deficiency induces oxidative DNA damage and increases p53 expression in human lung fibroblasts." J Nutr **133**: 2543-8.

Höfle, G., Bedorf, N., Steinmetz, H., Schomburg, D., Gerth, K., Reichenbach, H. (1996). "Epothilone A and B-Novel 16-membered macrolides with cytotoxic activity: Isolation, crystal structure, and conformation in solution." Angew Chem Int Ed Engl **35**: 1567-9.

Holton, R. A., Somoza, C., Baik, H., Liang, F., Biediger, R. J., Boatman, P. D., Shindo, M., Smith, C. C., Kim, S., Nadizadeh, H., et al. (1994). "First total synthesis of taxol. 1. Functionalization of the B ring". J Am Chem Soc **116**: 1597-8.

Holzbaur, E. L., Vallee, R. B. (1994). "DYNEINS: molecular structure and cellular function." Annu Rev Cell Biol **10**: 339-72.

Hong, M., Zhukareva, V., Vogelsberg-Ragaglia, V., Wszolek, Z., Reed, L., Miller, B. I., Geschwind, D. H., Bird, T. D., McKeel, D., Goate, A., Morris, J. C., Wilhelmsen, K. C., Schellenberg, G. D., Trojanowski, J. Q., Lee, V. M. (1998). "Mutation-specific functional impairments in distinct tau isoforms of hereditary FTDP-17." Science **282**: 1914-7.



- Horwitz, S. B., Shen, H. J., He, L., Dittmar, P., Neef, R., Chen, J., Schubart, U. K. (1997). "The microtubule-destabilizing activity of metablastin (p19) is controlled by phosphorylation." J Biol Chem **272**: 8129-32.
- Hristova, V. A., Beasley, S. A., Rylett, R. J., Shaw, G. S. (2009). "Identification of a novel Zn<sup>2+</sup>-binding domain in the autosomal recessive juvenile parkinson's related E3 ligase parkin." J Biol Chem **284**:14978-86.
- Huang, L., Kirschke, C. P., Zhang, Y. (2006). "Decreased intracellular zinc in human tumorigenic prostate epithelial cells: a possible role in prostate cancer progression." Cancer Cell Int **6**:10.
- Huzil, J. T., Chik, J. K., Slysz, G. W., Freedman, H., Tuszyński, J., Taylor, R. E., Sackett, D. L., Schriemer, D. C. (2008). "A unique mode of microtubule stabilization induced by peloruside A." J Mol Biol **378**: 1016-30.
- Hyams, J. S., Lloyd, C. W. eds. (1994). "Microtubules." New York: Wiley-Liss.
- Ichihara, K., Kitazawa, H., Iguchi, Y., Hotani, H., Itoh, T. J. (2001). "Visualization of the stop of microtubule depolymerization that occurs at the high-density region of microtubule-associated protein 2 (MAP2)." J Mol Biol **312**: 107-18.
- Ikegami, K., Heier, R. L., Taruishi, M., Takagi, H., Mukai, M., Shimma, S., Taira, S., Hatanaka, K., Morone, N., Yao, I., Campbell, P. K., Yuasa, S., Janke, C., Macgregor, G. R., Setou, M. (2007). "Loss of alpha-tubulin polyglutamylation in ROSA22 mice is associated with abnormal targeting of KIF1A and modulated synaptic function." Proc Natl Acad Sci U S A **104**: 3213-8.
- Illenberger, S., Drewes, G., Trinczek, B., Biernat, J., Meyer, H. E., Olmsted, J. B., Mandelkow, E. M., Mandelkow, E. (1996). "Phosphorylation of microtubule-associated proteins MAP2 and MAP4 by the protein kinase p110mark. Phosphorylation sites and regulation of microtubule dynamics." J Biol Chem **271**: 10834-43.
- Imai, Y., Soda, M., Takahashi, R. (2000). "Parkin suppresses unfolded protein stress-induced cell death through its E3 ubiquitin-protein ligase activity." J Biol Chem **275**: 35661-4.
- Imai, Y., Soda, M., Inoue, H., Hattori, N., Mizuno, Y., Takahashi, R. (2001). "An unfolded putative transmembrane polypeptide, which can lead to endoplasmic reticulum stress, is a substrate of parkin." Cell **105**: 891-902.
- Ivanov, N. I., Cowell, S. P., Brown, P., Rennie, P. S., Guns, E. S., Cox, M. E. (2007). "Lycopene differentially induces quiescence and apoptosis in androgen-responsive and -independent prostate cancer cell lines." Clin Nutr **26**: 252-63.
- Jain, E., Bairoch, A., Duvaud, S., Phan, I., Redaschi, N., Suzek, B. E., Martin, M. J., McGarvey, P., Gasteiger, E. (2009). "Infrastructure for the life sciences: design and implementation of the UniProt website." BMC Bioinformatics **10**: 136.

- Jánosi, I. M., Chrétien, D., Flyvbjerg, H. (1998). "Modeling elastic properties of microtubule tips and walls." Eur Biophys J **27**: 501-13.
- Joazeiro, C. A., Weissman, A. M. (2000). "RING finger proteins: Mediators of ubiquitin ligase activity." Cell **102**: 549-52.
- Johnson, P. R., Swanson, R., Rakhilina, L., Hochstrasser, M. (1998). "Degradation signal masking by heterodimerization of MATA $\alpha$ 2 and MATA1 blocks their mutual destruction by the ubiquitin-proteasome pathway." Cell **94**: 217-27.
- Jordan, M. A., Wilson, L. (2004). "Microtubules as a target for anticancer drugs." Nat Rev **4**: 253-65.
- Kahle, P. J., Leimer, U., Haass, C. (2000). "Does failure of parkin-mediated ubiquitination cause juvenile parkinsonism?" Trends Biochem Sci **25**: 524-7.
- Kar, S., Fan, J., Smith, M. J., Goedert, M., Amos, L. A. (2003). "Repeat motifs of tau bind to the insides of microtubules in the absence of taxol." EMBO J **22**: 70-7.
- Kardon JR, Vale RD. (2009). "Regulators of the cytoplasmic dynein motor." Nat Rev Mol Cell Biol **10**: 854-65.
- Kavallaris, M. (1997). "The role of multidrug resistance-associated protein (MRP) expression in multidrug resistance." Anticancer Drugs **8**: 17-25.
- Kavallaris, M., Kuo, D. Y. S., Burkhart, C. A., et al. (1997). "Taxol-resistant epithelial ovarian tumors are associated with altered expression of specific  $\beta$ -tubulin isotypes." J Clin Invest **100**: 1282-93.
- Kavallaris, M., Tait, A. S., Walsh, B. J., He, L., Horwitz, S. B., Norris, M. D., Haber, M. (2001). "Multiple microtubule alterations are associated with Vinca alkaloid resistance in human leukemia cells." Cancer Res **61**: 5803-9.
- Keats, R. A. and Hall, R. H. (1975). "Tubulin requires an accessory protein for self-assembly into microtubules." Nature Lond **257**: 418-20.
- Killilea, A. N., Downing, K. H., Killilea, D. W. (2007). "Zinc deficiency reduces paclitaxel efficacy in LNCaP prostate cancer cells." Cancer Lett **258**: 70-9.
- Killilea, D. W., Atamna, H., Liao, C., Ames, B. N. (2003). "Iron accumulation during cellular senescence in human fibroblasts in vitro." Antioxid Redox Signal **5**: 507-16.
- Kitada, T., Asakawa, S., Hattori, N., Matsumine, H., Yamamura, Y., Minoshima, S., Yokochi, M., Mizuno, Y., Shimizu, N. (1998). "Mutations in the parkin gene cause autosomal recessive juvenile parkinsonism." Nature **392**: 605-8.

- Kluger, B. M., Klepitskaya, O., Okun, M. S. (2009). "Surgical treatment of movement disorders." Neurol Clin **27**: 633-77.
- Kondo, J., Honda, T., Mori, H., Hamada, Y., Miura, R., Ogawara, H., Ihara, Y. (1988). "The carboxyl third of tau is tightly bound to paired helical filaments." Neuron **1**: 827-34.
- Kondoh, M., Tasaki, E., Takiguchi, M., Higashimoto, M., Watanabe, Y., Sato, M. (2005). "Activation of caspase-3 in HL-60 cells treated with pyrithione and zinc." Biol Pharm Bull **28**: 757-9.
- Kowalski, R. J., Giannakakou, P., Hamel, E. (1997). "Activities of the microtubule-stabilizing agents epothilones A and B with purified tubulin and in cells resistant to paclitaxel (Taxol(R))." J Biol Chem **272**: 2534-41
- Krishan, A. (1975). "Rapid flow cytofluorometric analysis of cell cycle by propidium iodide staining." J Cell Biol **66**: 188-93.
- Kristal, A. R., Stanford, J. L., Cohen, J. H., Wicklund, K., Patterson, R. E. (1999). "Vitamin and mineral supplement use is associated with reduced risk of prostate cancer." Cancer Epidemiol Biomarkers Prev **8**: 887-92.
- Lansbergen, G., Grigoriev, I., Mimori-Kiyosue, Y., Ohtsuka, T., Higa, S., Kitajima, I., Demmers, J., Galjart, N., Houtsmuller, A. B., Grosveld, F., Akhmanova, A. (2006). "CLASPs attach microtubule plus ends to the cell cortex through a complex with LL5beta." Devel Cell **11**: 21-32
- Lapidus, R. G., Dang, W., Rosen, D. M., Gady, A. M., Zabelinka, Y., O'Meally, R., DeWeese, T. L., and Denmeade, S. R. (2004). "Anti-tumor effect of combination therapy with intratumoral controlled-release paclitaxel (PACLIMER Microspheres) and radiation." Prostate **58**: 291-8.
- Larsson, N., Segerman, B., Gradin, H. M., Wandzioch, E., Cassimeris, L., Gullberg, M. (1999). "Mutations of oncoprotein 18/stathmin identify tubulin-directed regulatory activities distinct from tubulin association." Mol Cell Biol **19**: 2242-50.
- LaVoie, M. J., Ostaszewski, B. L., Weihofen, A., Schlossmacher, M. G., Selkoe, D. J. (2005). "Dopamine covalently modifies and functionally inactivates parkin." Nat Med **11**: 1214-21.
- Lee, F. Y., Borzilleri, R., Fairchild, C. R., Kim, S. H., Long, B. H., Reventos-Suarez, C., Vite, G. D., Rose, W. C., Kramer, R. A. (2001). "BMS-247550: a novel epothilone analog with a mode of action similar to paclitaxel but possessing superior antitumor efficacy." Clin Cancer Res **7**: 1429-37.
- Lee, V. M., Balin, B. J., Otvos, L. Jr, Trojanowski, J. Q. (1991). "A68: a major subunit of paired helical filaments and derivatized forms of normal Tau." Science **251**: 675-8.

- Leitzmann, M. F., Stampfer, M. J., Wu, K., Colditz, G. A., Willett, W. C., Giovannucci, E. L. (2003). "Zinc supplement use and risk of prostate cancer." J Natl Cancer Inst **95**: 1004-7.
- Li, H, DeRosier, D. J, Nicholson, W. V., Nogales, E., Downing, K. H. (2002). "Microtubule structure at 8 Å resolution." Structure **10**: 1317-28.
- Liang, J. Y., Liu, Y. Y., Zou, J., Franklin, R. B., Costello, L. C., Feng, P. (1999). "Inhibitory effect of zinc on human prostatic carcinoma cell growth." Prostate **40**: 200-7.
- Liao, G., Gundersen, G.G. (1998). "Kinesin is a candidate for cross-bridging microtubules and intermediate filaments. Selective binding of kinesin to deetyrosinated tubulin and vimentin." J Biol Chem **273**: 9797–803
- Lindahl, T., Landberg, G., Ahlgren, J., Nordgren, H., Norberg, T., Klaar, S., Holmberg, L., Bergh, J. (2004). "Overexpression of cyclin E protein is associated with specific mutation types in the p53 gene and poor survival in human breast cancer." Carcin **25**: 375-80.
- Lindwall, G., Cole, R. D. (1984). "Phosphorylation affects the ability of tau protein to promote microtubule assembly." J Biol Chem **259**: 5301-5.
- Liu, Y., Franklin, R. B., Costello, L. C. (1997). "Prolactin and testosterone regulation of mitochondrial zinc in prostate epithelial cells." Prostate **30**: 26-32.
- Lotharius J, Brundin P. (2002). "Pathogenesis of Parkinson's disease: dopamine, vesicles and alpha-synuclein." Nat Rev Neurosci **3**: 932-42.
- Löwe, J., Li, H., Downing, K. H., Nogales, E. (2001). "Refined structure of alpha beta-tubulin at 3.5Å resolution." J Mol Biol **313**: 1045-57.
- Lu, Q., Ludueña, R. F. (1994). "In vitro analysis of microtubule assembly of isotypically pure tubulin dimers. Intrinsic differences in the assembly properties of  $\alpha\beta$  II,  $\alpha\beta$ III, and  $\alpha\beta$ IV tubulin dimers in the absence of microtubule-associated proteins." J Biol Chem **269**: 2041–7.
- Lucking, C. B., Durr, A., Bonifati, V., Vaughan, J., De Michele, G., Gasser, T., Harhangi, B. S., Meco, G., Deneffe, P., Wood, N. W., Agid, Y., Brice, A. (2000). "Association between early-onset Parkinson's disease and mutations in the parkin gene." N Engl J Med **342**: 1560-7.
- Ludtke, S. J., Baldwin, P. R., Chiu, W. (1999). "EMAN: semiautomated software for high-resolution single-particle reconstructions." J Struct Biol **128**: 82–97.
- Ludueña, R. E., Banjeree, A. (2008). "The Isoypes of Tubulin: Distribution and Functional Significance" In *The role of microtubules in cell biology, neurobiology, and oncology.* ed. Fojo T. Totowa: Humana Press. pp.123-174.

- Mackenzie, G. G., Keen, C. L., Oteiza, P. I. (2002). "Zinc status of human IMR-32 neuroblastoma cells influences their susceptibility to iron-induced oxidative stress." Dev Neurosci **24**: 125-33.
- Makrides, V., Massie, M. R., Feinstein, S. C., Lew, J. (2004). "Evidence for two distinct binding sites for tau on microtubules." Proc Natl Acad Sci USA **17**: 6746-51.
- Mandelkow, E. M., Mandelkow, E., Milligan, R. A. (1991). "Microtubule dynamics and microtubule caps: a time-resolved cryo-electron microscopy study." J Cell Biol **114**: 977-991.
- Mandelkow, E., Mandelkow, E. M. (1995). "Microtubules and microtubule-associated proteins." Curr Opin Cell Biol **7**: 72-81.
- Marklund, U., Larsson, N., Gradin, H. M., Brattsand, G., Gullberg, M. (1996). "Oncoprotein 18 is a phosphorylation-responsive regulator of microtubule dynamics." EMBO J **15**: 5290-8.
- Mastropaolo, D., Camerman, A., Luo, A., Brayer, G. D., Camerman, N. (1995). "Crystal and molecular structure of paclitaxel (taxol)." Proc Natl Acad Sci USA **92**: 6920-24.
- McNally, F.J. and Vale, R. D. (1993). "Identification of katanin, an ATPase that severs and disassembles stable microtubules." Cell **75**: 419-29.
- Mitchison, T., Kirschner, M. W. (1984). "Dynamic instability of microtubule growth." Nature **312**: 237-42.
- Mizuno Y, Ohta S, Tanaka M, Takamiya S, Suzuki K, Sato T, Oya H, Ozawa T, Kagawa Y. (1989). "Deficiencies in complex I subunits of the respiratory chain in Parkinson's disease." Biochem Biophys Res Commun **163**: 1450-5.
- Mori, K. (2000). "Tripartite management of unfolded proteins in the endoplasmic reticulum." Cell **101**: 451-4.
- Moshfegh, A., Goldman, J., Cleveland, L. (2005). "What we eat in America, NHANES 2001-2002: Usual nutrient intakes from food compared to dietary reference intakes." U.S. Department of Agriculture, Agricultural Research Service Washington, DC.
- Mukhopadhyay, D., Riezman, H. (2007). "Proteasome-independent functions of ubiquitin in endocytosis and signaling." Science **315**: 201-5.
- Murphy, D. B. and Borisy, G. G. (1975). "Association of high molecular weight proteins with microtubules and their role in microtubule assembly in vitro." Proc Natl Acad Sci USA **72**: 2696-700.

- Murphy, D. D., Rueter, S. M., Trojanowski, J. Q., Lee, V. M. (2000). "Synucleins are developmentally expressed, and alpha-synuclein regulates the size of the presynaptic vesicular pool in primary hippocampal neurons." J Neurosci **20**: 3214-20.
- Narendra, D., Tanaka, A., Suen, D. F., Youle, R. J. (2008). "Parkin is recruited selectively to impaired mitochondria and promotes their autophagy." J Cell Biol **183**: 795-803
- Nettles, J. H., Li, H., Cornett, B., Krahn, J. M., Snyder, J. P., Downing, K. H. (2004). "The binding mode of epothilone on  $\alpha,\beta$ -tubulin by electron crystallography." Science **305**: 866-9.
- Nicolaou, K. C., Yang, Z., Liu, J. J., Ueno, H., Nantermet, P. G., Guy, R. K., Claiborne, C. F., Renaud, J., Couladouros, E. A., Paulvannan, K., et al. (1994). "Total synthesis of taxol." Nature **367**: 630-4.
- Nogales, E., Wolf, S. G., Downing, K. H. (1998). "Structure of the  $\alpha\beta$  tubulin dimer by electron crystallography." Nature **391**: 199-203.
- Nogales, E., Whittaker, M., Milligan, R. A., Downing, K. H. (1999). "High resolution model of the microtubule." Cell **96**: 79-88.
- Ogura, T., Iwasaki, K., Sato, C. (2003). "Topology representing network enables highly accurate classification of protein images taken by cryo electron-microscope without masking." J Struct Biol **143**: 185-200.
- Oteiza, P. I., Hurley, L.S., Lonnerdal, B., and Keen, C.L. (1990). "Effects of marginal zinc deficiency on microtubule polymerization in the developing rat brain." Biol Trace Elem Res **24**: 13-23.
- Oteiza, P. I., Clegg, M. S., Zago, M. P., Keen, C. L. (2000). "Zinc deficiency induces oxidative stress and AP-1 activation in 3T3 cells." Free Radic Biol Med **28**: 1091-9.
- Paluh, J. L., Killilea, A. N., Detrich, H. W. 3rd, Downing, K. H. (2004). "Meiosis-specific failure of cell cycle progression in fission yeast by mutation of a conserved beta-tubulin residue." Mol Biol Cell **15**: 1160-71.
- Panda, D., Miller, H. P., Banerjee, A., Luduena, R. F. and Wilson, L. (1994). "Microtubule dynamics in vitro are regulated by the tubulin isotype composition." Proc Natl Acad Sci USA **91**: 11358-62.
- Peng, H., Begg, G. E., Schultz, D. C., Friedman, J. R., Jensen, D. E., Speicher, D. W., Rauscher, F. J. 3<sup>rd</sup>. (2000). "Reconstitution of the KRAB-KAP-1 repressor complex: a model system for defining the molecular anatomy of RING-B box-coiled-coil domain-mediated protein-protein interactions." J Mol Biol **295**: 1139-62.
- Perez-Stable, C. (2006). "2-Methoxyestradiol and paclitaxel have similar effects on the cell cycle and induction of apoptosis in prostate cancer cells." Cancer Lett **231**: 49-64.

Periquet, M., Lücking, C., Vaughan, J., Bonifati, V., Dürr, A., De Michele, G., Horstink, M., Farrer, M., Illarioshkin, S. N., Pollak, P., Borg, M., Brefel-Courbon, C., Deneffe, P., Meco, G., Gasser, T., Breteler, M. M., Wood, N., Agid, Y., Brice, A. (2001). "Origin of the mutations in the parkin gene in Europe: exon rearrangements are independent recurrent events, whereas point mutations may result from Founder effects." Am J Hum Genet **68**: 617-26.

Peris, L., Thery, M., Fauré, J., Saoudi, Y., Lafanechère, L., Chilton, J. K., Gordon-Weeks, P., Galjart, N., Bornens, M., Wordeman, L., Wehland, J., Andrieux, A., Job, D. (2006). "Tubulin tyrosination is a major factor affecting the recruitment of CAP-Gly proteins at microtubule plus ends." J Cell Biol **174**: 839-49.

Pettersen, E. F., Goddard, T. D., Huang, C. C., Couch, G. S., Greenblatt, D. M., Meng, E. C., Ferrin, T. E. (2004). "UCSF Chimera--a visualization system for exploratory research and analysis." J Comput Chem **25**: 1605-12.

Pilz, R. B., Willis, R. C., Seegmiller, J. E. (1982). "Regulation of human lymphoblast plasma membrane 5'-nucleotidase by zinc." J Biol Chem **257**: 13544-9.

Poruchynsky, M. S., Giannakakou, P., Ward, Y., Bulinski, J. C., Telford, W. G., Robey, R. W., Fojo, T. (2001). "Accompanying protein alterations in malignant cells with a microtubule-polymerizing drug-resistance phenotype and a primary resistance mechanism." Biochem Pharmacol **62**:1469-80.

Prasad, A. S., Kucuk, O. (2002). "Zinc in cancer prevention." Cancer Metastasis Rev **2**: 291-5.

Pryer, N. K., Walker, R. A., Skeen, V. P., Bourns, B. D., Soboeiro, M. F., Salmon, E. D. (1992). "Brain microtubule-associated proteins modulate microtubule dynamic instability in vitro." J Cell Sci **103**: 965-76.

Pryor, D. E., O'Brate, A., Bilcer, G., Díaz, J. F., Wang, Y., Wang, Y., Kabaki, M., Jung, M. K., Andreu, J. M., Ghosh, A. K., Giannakakou, P., Hamel, E. (2002). "The microtubule stabilizing agent laulimalide does not bind in the taxoid site, kills cells resistant to paclitaxel and epothilones, and may not require its epoxide moiety for activity." Biochem **41**: 9109-15.

Qadan, L. R., Perez-Stable, C. M., Anderson, C., D'Ippolito, G., Herron, A., Howard, G. A., and Roos, B. A. (2001). "2-Methoxyestradiol induces G2/M arrest and apoptosis in prostate cancer." Biochem Biophys Res Comm **285**: 1259-66.

Ramey, V. H., Wang, H. W., Nogales, E. (2009). "Ab initio reconstruction of helical samples with heterogeneity, disorder and coexisting symmetries." J Struct Biol; **167**: 87-105.

Ranganathan, S., Dexter, D. W., Benetatos, C. A., Hudes, G. R. (1998). "Cloning and sequencing of human  $\beta$ III- tubulin cDNA: induction of  $\beta$ III isotype in human prostate carcinoma cells by acute exposure to antimicrotubule agents." Biochim Biophys Acta **1395**: 237-45.

- Rankin, C. A., Joazeiro, C. A., Floor, E., Hunter, T. (2001). "E3 ubiquitin-protein ligase activity of Parkin is dependent on cooperative interaction of RING finger (TRIAD) elements." J Biomed Sci **8**: 421-9.
- Rao, S., Aberg, F., Nieves, E., Horwitz, S. B., Orr, G.A. (2001). "Identification by mass spectrometry of a new alpha-tubulin isotype expressed in human breast and lung carcinoma cell lines." Biochem **40**: 2096-103.
- Ravelli, R. B., Gigant, B., Curmi, P. A., Jourdain, I., Lachkar, S., Sobel, A., Knossow, M. (2004). "Insight into tubulin regulation from a complex with colchicine and a stathmin-like domain." Nature **428**: 198-202.
- Redeker, V., Frankfurter, A., Parker, S. K., Rossier, J., Detrich, H. W. 3rd. (2004). "Posttranslational modification of brain tubulins from the Antarctic fish *Notothenia coriiceps*: reduced C-terminal glutamylation correlates with efficient microtubule assembly at low temperature." Biochem **43**: 12265-74.
- Ren, Y., Zhao, J., Feng, J. (2003). "Parkin binds to alpha/beta tubulin and increases their ubiquitination and degradation." J Neuroscience **23**: 3316-24.
- Reyes-Turcu, F. E., Ventii, K. H., Wilkinson, K. D. (2009). "Regulation and cellular roles of ubiquitin-specific deubiquitinating enzymes." Annu Rev Biochem **78**: 363-97.
- Rogers, S., Wells, R., Rechsteiner, M. (1986). "Amino acid sequences common to rapidly degraded proteins: the PEST hypothesis." Science **234**: 364-8.
- Safadi, S. S., Shaw, G. S. (2007). "A disease state mutation unfolds the parkin ubiquitin-like domain." Biochem **46**: 14162-9.
- Sakata, E., Yamaguchi, Y., Kurimoto, E., Kikuchi, J., Yokoyama, S., Yamada, S., Kawahara, H., Yokosawa, H., Hattori, N., Mizuno, Y., Tanaka, K., Kato, K. (2003). "Parkin binds the Rpn10 subunit of 26S proteasomes through its ubiquitin-like domain." EMBO Rep **4**: 301-6.
- Saxton, W. M., Stemple, D. L., Leslie, R. J., Salmon, E. D., Zavortink, M., McIntosh, J. R. (1984). "Tubulin dynamics in cultured mammalian cells." J Cell Biol **99**: 2175-86.
- Schiff, P. B., Fant, J., Horowitz, S. B. (1979). "Promotion of microtubule assembly in vitro by Taxol." Nature **277**: 665-7.
- Schweers, O., Schönbrunn-Hanebeck, E., Marx, A., Mandelkow, E. (1994). "Structural studies of tau protein and Alzheimer paired helical filaments show no evidence for beta-structure." J Biol Chem **269**: 24290-7.
- Serrano, L. J., Torre, R., Maccioni, R., Avila, J. (1984). "Involvement of the carboxy-terminal domain of tubulin in the regulation of its assembly." Proc Natl Acad Sci USA **81**: 5989-93.



Shimura, H., Schlossmacher, M. G., Hattori, N., Frosch, M. P., Trockenbacher, A., Schneider, R., Mizuno, Y., Kosik, K. S., Selkoe, D. J. (2001). "Ubiquitination of a new form of alpha-synuclein by parkin from human brain: implications for Parkinson's disease." Science **293**: 263–9.

Sindelar, C. V., Downing, K. H. (2007). "The beginning of kinesin's force-generating cycle visualized at 9-A resolution." J Cell Biol **177**: 377-85.

Sloboda, R. D., Dentler, W. L., and Rosenbaum, J. L. (1976). "Microtubule-associated proteins and the stimulation of tubulin assembly in vitro." Biochem **15**: 4497-505.

Snyder, J. P., Nettles, J. H., Cornett, B., Downing, K. H., Nogales, E. (2001). "The binding conformation of Taxol in beta tubulin; A model based on the electron crystallographic density." Proc Natl Acad Sci USA **98**: 5312-17.

Staropoli, J. F., McDermott, C., Martinat, C., Schulman, B., Demireva, E., Abeliovich, A. (2003). "Parkin is a component of an SCF-like ubiquitin ligase complex and protects postmitotic neurons from kainate excitotoxicity." Neuron **37**: 735–49.

Stokes, A. H., Hastings, T. G., Vrana, K. E. (1999). "Cytotoxic and genotoxic potential of dopamine." J Neurosci Res **55**: 659-65.

Sullivan, K. F. (1988). "Structure and utilization of tubulin isotypes." Annu Rev Cell Biol **4**: 687-716.

Sullivan, K. F. and Cleveland, D. W. (1986). "Identification of conserved isotype- defining variable region sequences for four vertebrate  $\beta$  tubulin polypeptide classes." Proc Natl Acad Sci USA **83**: 4327-31.

Tanaka, K., Suzuki, T., Chiba, T., Shimura, H., Hattori, N., Mizuno, Y. (2001). "Parkin is linked to the ubiquitin pathway." J Mol Med **79**: 482-94.

Tate, D. J. Jr, Miceli, M. V., Newsome, D. A. (1999). "Zinc protects against oxidative damage in cultured human retinal pigment epithelial cells." Free Radic Biol Med **26**: 704-13.

Thazhath, R., Liu, C., Gaertig, J. (2002) "Polyglycylation domain of beta-tubulin maintains axonemal architecture and affects cytokinesis in Tetrahymena." Nat Cell Biol **4**: 256–9.

Thermo Scientific. (2009). "Answers to frequently asked questions (FAQs) about Immobilized TCEP Disulfide Reducing Gel." July 12, 2009  
<http://www.piercenet.com/resources/browse.cfm?fldID=6EA1E2E1-6C4A-40A8-9AC3-F121DB466C2E>.

Tomoo, K., Mukai, Y., In, Y., Miyagawa, H., Kitamura, K., Yamano, A., Shindo, H., Ishida, T. (2008). "Crystal structure and molecular dynamics simulation of ubiquitin-like domain of murine parkin." Biochim Biophys Acta **1784**: 1059-67.

- Tran, P.T., Joshi, P., Salmon, E.D. (1997). "How tubulin subunits are lost from the shortening ends of microtubules." J Struct Biol **118**: 107-18.
- Trinczek, B., Ebnet, A., Mandelkow, E. M., Mandelkow, E. (1999). "Tau regulates the attachment/detachment but not the speed of motors in microtubule-dependent transport of single vesicles and organelles." J Cell Sci **112**: 2355-67.
- Untergasser, G., Rumpold, H., Plas, E., Witkowski, M., Pfister, G., Berger, P. (2000). "High levels of zinc ions induce loss of mitochondrial potential and degradation of antiapoptotic Bcl-2 protein in in vitro cultivated human prostate epithelial cells." Biochem Biophys Res Commun **279**: 607-14.
- Uzzo, R. G., Leavis, P., Hatch, W., Gabai, V. L., Dulin, N., Zwartau, N., and Kolenko, V. M. (2002). "Zinc inhibits nuclear factor-kappaB activation and sensitizes prostate cancer cells to cytotoxic agents." Clinical Cancer Research **8**: 3579-83.
- Uzzo, R. G., Crispen, P. L., Golovine, K., Makhov, P., Horwitz, E. M., Kolenko, V. M. (2006). "Diverse effects of zinc on NF-kappaB and AP-1 transcription factors: implications for prostate cancer progression." Carcinogenesis **27**: 1980-90.
- Vale, R. D., Milligan, R.A. (2000). "The way things move: looking under the hood of molecular motor proteins." Science **288**: 88-95.
- van Heel, M., Harauz, G., Orlova, E. V., Schmidt, R., Schatz, M. (1996). "A new generation of the IMAGIC image processing system." J Struct Biol **119**: 17-24.
- Vaughn, D. J., Brown, A. W. Jr, Harker, W.G., Huh, S., Miller, L., Rinaldi, D., Kabbinavar, F. (2004). "Multicenter Phase II study of estramustine phosphate plus weekly paclitaxel in patients with androgen-independent prostate carcinoma." Cancer **100**: 746-50.
- Ventii, K. H., Wilkinson, K. D. (2008). "Protein partners of deubiquitinating enzymes." Biochem J **414**: 161-75.
- von Bergen, M., Barghorn, S., Li, L., Marx, A., Biernat, J., Mandelkow, E. M., Mandelkow, E. (2001). J Biol Chem **276**: 48165-74
- Voter, W. A., Erickson, H. P. (1982). "Electron microscopy of MAP 2 (microtubule-associated protein 2)." J Ultrastruct Res **80**: 374-82.
- Wakimoto, P., Block, G. (2001). "Dietary intake, dietary patterns, and changes with age: an epidemiological perspective." J Gerontol A Biol Sci Med Sci **56**: 65-80.
- Walsh, C. T., Sandstead, H. H., Prasad, A. S., Newberne, P. M., Fraker, P. J. (1994). "Zinc: health effects and research priorities for the 1990s." Environ Health Perspect **102**: 5-46.

Wang, H, Nogales, E. (2005). "Nucleotide-dependent bending flexibility of tubulin regulates microtubule assembly." Nature **435**: 911-5.

Wang, X. Z., Beebe, J. R., Pwiti. L., Bielawska, A., Smyth, M. J. (1999). "Aberrant sphingolipid signaling is involved in the resistance of prostate cancer cell lines to chemotherapy." Cancer Res **59**: 5842-8.

Wang, H., Liu, B., Zhang, C., Peng, G., Liu, M., Li, D., Gu, F., Chen, Q., Dong, J., Fu, L., Zhou, J. (2009). "Parkin regulates paclitaxel sensitivity in breast cancer via a microtubule-dependent mechanism." J Pathol **218**: 76-85.

Weingarten, M., Lockwood, A., Hwo, S., and Kirschner, M. (1975). "A protein factor essential for microtubule assembly." Proc Natl Acad Sci USA **72**: 1858-62.

Westermann, S., Weber, K. (2003). "Post-translational modifications regulate microtubule function." Nat Rev Mol Cell Biol **4**: 938-47.

Wong, E. S., Tan, J. M., Wang, C., Zhang, Z., Tay, S. P., Zaiden, N., Ko, H. S., Dawson, V. L., Dawson, T. M., Lim, K. L. (2007). "Relative sensitivity of parkin and other cysteine-containing enzymes to stress-induced solubility alterations." J Biol Chem **282**: 12310-8.

Xia, L., Hai, B., Gao, Y., Burnette, D., Thazhath, R., Duan, J., Bre, M. H., Levilliers, N., Gorovsky, M. A., Gaertig, J. (2000). "Polyglycylation of tubulin is essential and affects cell motility and division in *Tetrahymena thermophila*." J Cell Biol **149**: 1097-1106.

Xiao, H., Verdier-Pinard, P., Fernandez-Fuentes, N., Burd, B., Angeletti, R., Fiser, A., Horwitz, S. B., Orr, G. A. (2006). "Insights into the mechanism of microtubule stabilization by Taxol." Proc Natl Acad Sci USA **103**: 10166-73.

Yamamoto, A., Friedlein, A., Imai, Y., Takahashi, R., Kahle, P. J., Haass, C. (2005). "Parkin phosphorylation and modulation of its E3 ubiquitin ligase activity." J Biol Chem **280**: 3390-9.

Yang, F., Jiang, Q., Zhao, J., Ren, Y., Sutton, M. D., Feng, J. (2005). "Parkin stabilizes microtubules through strong binding mediated by three independent domains." J Biol Chem **280**: 17154-62.

Yonekura, K., Toyoshima, C. (2000). "Structure determination of tubular crystals of membrane proteins. II. Averaging of tubular crystals of different helical classes." Ultramicros **84**: 15-28.

Zago, M. P., Mackenzie, G. G., Adamo, A. M., Keen, C. L., Oteiza, P. I. (2005). "Differential modulation of MAP kinases by zinc deficiency in IMR-32 cells: role of H<sub>2</sub>O<sub>2</sub>." Antioxid Redox Signal **7**: 1773-82.

Zhang, Y., Gao, J., Chung, K. K., Huang, H., Dawson, V. L., Dawson, T. M. (2000). "Parkin functions as an E2-dependent ubiquitin-protein ligase and promotes degradation of the synaptic vesicle-associated protein CDCrel-1." Proc Natl Acad Sci USA **97**: 13354-9.

Zheng, N., Wang, P., Jeffrey, P. D., Pavletich, N. P. (2000). "Structure of a c-Cbl-UbcH7 complex: RING domain function in ubiquitin-protein ligases." Cell **102**: 533-9.

Zhuang, S. H., Burnstein, K. L. (1998). "Antiproliferative effect of 1alpha,25-dihydroxyvitamin D3 in human prostate cancer cell line LNCaP involves reduction of cyclin-dependent kinase 2 activity and persistent G1 accumulation." Endocrinology **139**: 1197-207.